Novel Techniques for Engineering Neural Tissue Using Human Induced Pluripotent Stem Cells

by
Laura De la Vega Reyes
B.S., Monterrey Institute of Technology and Higher Education, Guadalajara, Mexico, 2015

A Dissertation Submitted in Partial Fulfillment
of the Requirements for the Degree of

DOCTOR OF PHILOSOPHY

in the Department of Mechanical Engineering

Supervisory committee

Novel Techniques for Engineering Neural Tissue Using Human Induced Pluripotent Stem Cells

by

Laura De la Vega Reyes
B.S., Monterrey Institute of Technology and Higher Education, Guadalajara, Mexico, 2015

Supervisory committee

Dr. Stephanie Michelle Willerth, Supervisor
Department of Mechanical Engineering

Dr. Mohsen Akbari, Departmental Member
Department of Mechanical Engineering

Dr. Alexandre Brolo**,** Non-Departmental Member
Department of Chemistry

Abstract

Tissue engineering (TE) uses a combination of biomaterial scaffolds, cells, and drug delivery systems (DDS) to create tissues that resemble the human physiology. Such engineered tissues could be used to treat, repair, replace, and augment damaged tissues or organs, for disease modeling, and drug screening purposes. This work describes the development and use of novel strategies for engineering neural tissue using a combination of drug delivery systems (DDS), human induced pluripotent stem cells (hiPSCs), and bioprinting technologies for the generation of a drug screening tool to be used in the process of drug discovery and development. The DDS consisted of purmorphamine (puro) loaded microspheres that were fabricated using an oil-in-water single emulsion with 84% encapsulation efficiency and showed the slow release of puro for up to 46 days *in vitro.* Puro and retinoic acid (RA)-loaded microspheres were combined with hiPSCs-derived neural aggregates (NAs) that differentiated into neural tissues expressing βT-III and showed increased neural extension. hiPCS-derived neural progenitor cells (NPCs) were bioprinted on a layer-by-layer using a fibrin based-bioink and extrusion based- bioprinting. The bioprinted structures showed >81% cellular viability after 7 days of culture *in vitro* and the expression of the mature motor neuron (MN) markers HB9 and CHAT. Lastly, hiPCS-derived NPCs were bioprinted in combination with puro and RA-loaded microspheres and cultured for 45 days *in vitro*. The microspheres slowly released the drug and after 30 and 45 days the tissues contained mature neurons, astrocytes and oligodendrocytes expressing CHAT, GFAP, and O4, respectively. Changes in membrane potential indicated tissue responsiveness to different types of treatments such as acetylcholine and gamma-aminobutyric acid (GABA). In the future the bioprinted tissues

could contain localized regions of varied drug releasing microspheres using a concentration gradient to promote differentiation into specific cell types in order to create more complex tissues. Moreover, these tissues will benefit from the presence of a neurovascular unit (NVU). Upon validation, the engineered tissues could be used as preclinical tools to test potential drugs and be used for personalized medicine by using patient specific hiPSCs.

Table of contents

List of tables

List of figures

List of abbreviations

TE- tissue engineering
CNS- central nervous system
PNS- peripheral nervous system
SC- Spinal Cord
BBB- blood-brain barrier
ECM- extracellular matrix
NVU- neurovascular unit
ESC- embryonic stem cells
iPSCs- induced pluripotent stem cells
AD- Alzheimer's disease
PD- Parkinson's disease
ALS- Amyotrophic lateral sclerosis
TBI- traumatic brain injury
SCI- spinal cord injury
MN- motor neurons
2D-2-dimensional
NSC- neural stem cells
NPC- neural progenitor cells
OPC- oligodendrocyte progenitor cells
OEC- olfactory ensheathing cells
3D-3-dimensional
MRI-magnetic resonance imaging
hiPSCs- human induced pluripotent stem cells
OCT4- octamer binding transcription factor 4
SOX2- sex determining region Y-box2
KLF4- Kruppel-like factor 4
C-MYC- myc proto-oncogene protein homolog
NAS- neural aggregates
NIM- neural induction media
SMAD- mothers against decapentaplegic protein
BMPs- bone morphogenic proteins
TGFβ- transforming growth factor beta
LDN-LDN193189
SB- SB431542
GABA-gamma-Aminobutyric acid
SHH- protein sonic hedgehog
PTCH1- patched homolog 1
SMO- smoothened
Puro- purmorphamine
RA- retinoic acid
HOX-homeobox
PLGA- poly(lactic-co-glycolic acid)
PEG- poly(ethylene glycol)
PCL- polycaprolactone
Ca^{2+}-calcium ions
VEGF- vascular endothelial growth factor
GP- glycerol phosphate
βT-III- beta-tubulin class III
GAD- glutamic acid decarboxylase
CAD- computer-aid design
LOP- Lab-on-a-printer
PDMS- polydimethylsiloxane
LLLT-low level light therapy
CHIR- CHIR99021
GFAP- glial fibrillary acidic protein
MAP2-microtubule associated protein
CHAT-choline acetyltransferase
DDS- drug delivery systems
C-AMP-cyclic adenosine monophosphate
BP- Brainphys Neuronal Medium
CpdE- Compound E
GDNF-glial derived neurotrophic factor
IGF-1- insulin-like growth factor
AA-L-ascorbic acid
BDNF- brain-derived neurotrophic factor
PSA- penicillin-streptomycin-amphotericin B
NBM- Neurobasal™ Medium
SMNS-spinal motor neurons
SSEA-1 stage specific embryonic antigen-1
OLIG2- Oligodendrocyte transcription factor 2
HB9- homeobox protein 9
ISL-1 Islet-1
PE- Phycoerythrin
PerCP- Peridinin Chlorophyll Protein complex
ICC-immunocytochemistry

PBS-phosphate buffered saline
NGS-normal goat serum
EE- encapsulation efficiency
SSEA-4- stage specific embryonic antigen-4
PAX6- paired box protein-6
SEM- scanning electron microscope
HPLC- high-performance liquid chromatography
CAN- acetonitrile
DAD- diode-array detector
ID- internal diameter
TFA- Trifluoroacetic acid
Sy38-synaptophysin
NeuN- neuronal nuclei protein
DAPI- (4′,6-diamidino-2-phenylindole)
NF-Kβ- (nuclear factor kappa-light-chain-enhancer of activated B cells
NPM- Neural Progenitor Medium
PLO- poly-L-ornithine
FBS- fetal bovine serum
EDTA- Ethylenediaminetetraacetic acid
CAR T-cell- chimeric antigen receptor T- cell
PFA-paraformaldehyde

Acknowledgements

I am profoundly grateful to my supervisor Dr. Stephanie Willerth for giving me the opportunity to grow as a scientist and find my passion for tissue engineering. It has been a great honour being her student and having an excellent role model who has become a mentor to me. Thank you for the countless opportunities to expand my research and knowledge, continuous feedback, encouragement, and more importantly for her trust. I would also like to thank my committee members for their valuable feedback and advice during my doctoral degree and for the completion of this dissertation.

To all the members of the Willerth lab who have encouraged and helped me along the way. Special thanks Ms. Laila Abelseth for her advice, support, and feedback. To Ms. Ruchi Sharma, Ms. Tara Styan, Mr. Chris Lee, Ms. Meghan Robinson, Mr. Andrew Agbay, and all the co-op and MITACS students for being part of and helping me along this journey. It's been a privilege to learn, teach, and make new discoveries together.

I would like to recognize MITACS for giving me a fellowship to pursue my PhD. To the Canadian Biomaterials Society, ICORD, and the Stem Cell Network for their funding and many opportunities that allowed me to build up on my skills and training. To Ori Granot for his assistance with the HPLC, CAMTEC staff, for their instruction in many of the instruments used. Juan Triviño-Paredes for his assistance with confocal imaging and, Aspect Biosystems for their continuous feedback and guidance in bioprinting.

Lastly, I would like to thank my loving husband and my family for their endless support, encouragement, and patience throughout the duration of this degree. Thank you for being my motivation.

Laura de la Vega Reyes

University of Victoria

November, 2019

Dedication

I dedicate this dissertation to my husband, my parents, and grandparents. I also dedicate this to all the people suffering from a spinal cord injury. I am hoping this work will contribute to the development of new treatments.

Chapter 1 Introduction[a]

Tissue engineering (TE) - an integrative, multidisciplinary field - develops biological substitutes that restore, replace or regenerate defective tissues by combining cells, biomaterial scaffolds, and drug delivery systems (DDS) [1]. These engineered tissues can also be used for disease modeling and as a tool for drug screening and for elucidating the biological mechanisms. The goal of TE is to assemble functional constructs that maintain or improve damaged tissues or whole organs [2]. Such engineered tissues could decrease the demand for organ replacement and significantly fast-track the discovery and manufacturing new drugs for disease and injury. Examples of TE include artificial skin, muscle, neural tissue [3].

Neural tissue is found in the central nervous system (CNS) and the peripheral nervous system (PNS). It is comprised mostly of neurons and glial cells and serves the unique function of integration and communication of electrical signals throughout the body [4]. Neurons, highly specialized nerve cells, generate and conduct nerve impulses known as action potentials across connected cells. Glial cells are comparatively more abundant non-neuronal cells, and they include astrocytes, oligodendrocytes, ependymal cells, microglia, and Schwann cells **(Figure 1.1)**. They are nonconductive and serve supporting functions for neurons such as elimination of debris, physical support, and electrical insulation [5]. The CNS generally lacks regenerative capacity, while the PNS has a higher regenerative capacity, making natural recovery difficult for neural tissue [6]. Thus, successful neural TE strategies would generate engineered living tissues that could integrate

a The following chapter contains excerpts from: De la Vega L, Lee C, Sharma R, Amereh M, Willerth SM. **3D bioprinting models of neural tissues: The current state of the field and future directions**. Brain Research Bulletin. 2019;150:240-249.

with the diseased or damaged nervous system to promote regeneration [7]. However, engineering neural tissue remains challenging due to the complex architecture of the brain, spinal cord (SC), and peripheral nerves [8]. In particular, the blood-brain barrier (BBB) – the semipermeable interface between the CNS and circulating blood – works with the neural tissue and the natural extracellular matrix (ECM) to form the neurovascular unit (NVU) – a complex interface vital for brain homeostasis and, subsequently, brain health [9,10]. As such, engineered neural tissue can range from single cells constructs, that focus on replicating cell function, to intricate multicomponent models that attempt to recapitulate the most complex aspects of natural neural tissue.

The selection of cells serves as an important parameter when engineering tissues. Most TE strategies use one of the following types of cells: 1) primary cells, 2) immortalized cells, or 3) stem cells. Primary cells are isolated directly from human tissues. While these cells can be cultured *in vitro*, the number of times they can be passaged is often limited, capping the number of cells that can be obtained. Immortalized cells are genetically modified to enable extended passaging, but often are not suitable for clinical applications as the immortalization procedure changes the properties of the cell. The third category of cells – stem cells - have significant potential for TE as all stem cells possess two key properties: they can 1) replicate indefinitely unlike primary cells and 2) develop into different cell types [11]. Stem cells can be derived from tissues, both fetal and adult, through embryos or by reprogramming other mature cell types back into a stem cell-like state respectively. While tissue specific stem cells usually only produce the cells found in their tissue of origin, both embryonic stem cells (ESCs) and induced pluripotent stem cells (iPSCs) possess the property of pluripotency where they can generate any type of cell in the body. Thus, these cells serve as valuable tools for TE. ESCs are derived from the inner cell mass of the blastocyst while iPSCs are adult cells reprogrammed back into pluripotent state. While there are

some ethical concerns with using ESC lines, iPSCs are less controversial and can also generate patient specific stem lines, which is an important consideration for clinical applications. Disease specific iPSC lines can recapitulate the disease phenotypes in a dish, making them a powerful tool for understanding neurodegenerative diseases [12]. Accordingly, cell therapies using iPSCs to treat nervous system disorders remains an area with great potential [13,14]. Neural stem cells (NSCs), an example of tissue specific stem cells, can be used to generate engineered neural tissues as these cells can differentiate in the mature cells of the CNS [15].

Another important consideration when engineering neural tissue is the biomaterial scaffold, which needs to serve as a substitute of the ECM and support the cells through differentiation and maturation. Therefore scaffolds used in TE must meet several requirements in order for the cells to perform their specific function [16]. Scaffolds must be biocompatible, biodegradable and non-immunogenic, and possess optimal mechanical properties as well as adequate porosity and morphology for gas and nutrient transport [17].

1.1. Disease modeling and drug screening tools

This research was focused on the engineering of neural tissues, both the brain and the SC tissues in the CNS. The CNS receives and processes all the information that comes from the external environment as well as inside of the body and controls responses [18]. The need for engineering neural tissues arises from the limited understanding of the complex environment of the CNS and associated diseases, requiring models to investigate advanced approaches to heal and repair after injuries or neurodegeneration – the progressive loss of structure and function of the cells in our brain [19]. The CNS possesses a very low regeneration capacity and therefore, TE tools are needed to create models that can emulate the natural environment of the brain and SC.

Electrospun guidance channels, bridging scaffolds, DDS, hydrogels, 3D bioprinting are amongst the most popular TE approaches for repairing and mimicking the CNS environment [20-26] [22,25,27,28].

Engineered neural tissues can also be used as drug screening tools for potential therapeutics. Many diseases and disorders affecting the CNS are uncurable or lack long-term treatment options. Some of the neurodegenerative diseases and disorders, which collectively affect over 55-million people in North America, include Alzheimer's disease (AD), Parkinson's disease (PD), Amyotrophic lateral sclerosis (ALS), traumatic brain injury (TBI), stroke, and spinal cord injury (SCI) [29]. SCI is a highly debilitating disorder that occurs most frequently after falls, car accidents, and sports injuries [30]. The SC is the caudal component of the CNS that is in charge of transmitting signals between the brain and the body [18] **(Figure 1.1)**. Neurons in the SC serve two purposes; (i) relay cutaneous sensory input to the brain (located in the dorsal half of the SC) and (ii) transform sensory input into motor output (located in the ventral half of the SC). The cells that control the motor output are called motor neurons (MNs) [18]. When a SCI occurs, the tissue is compressed or lacerated, causing the loss of neuronal cells and disruption of the ascending and descending tracts running through the SC [31]. In addition, inflammatory events and secretion of molecules can lead to the creation of a hostile environment, inhospitable for healthy cells [20,24]. In spite of the many years and millions of dollars spent in research focused on the repair of the injured SC, there is no cure for SCI. A great barrier for the existence of potential treatments for SCI are the differences in types of injuries, which makes it challenging to raise funding for research. Other obstacles include the time, cost and rate of failure of clinical trials. The estimated time from the scientific discovery to the approval of a new drug treatment is about 20 years, and each clinical trial costs from 1.3 to 1.7 billion dollars [32]. Success rate of these trials is very low (8%), which brings significant implications for public health and drug discoveries [33]. Current strategies for pre-

clinical drug testing include the use of animal models, 2-dimensional (2D) cell monolayer cultures or cadaveric organ slices [34,35]. Cadaveric organ slices are a great bridge between animal models and human outcomes as they possess structural and functional features of *in vivo* tissues however, availability is limited [35]. In addition, 2D monolayer cultures and animal models do not offer a clear prediction of *in vivo* human responses. This is because 2D monolayers are attached to a plastic hard surface where the cells are forced to proliferate and grow one next to the other and the cell-ECM interactions, morphology, polarity, are disturbed as opposed to a soft and 3D substrate where they can interact from multiple points of contact, as observed in a native environment [36]. Furthermore, while strict laboratory conditions can be regulated for animal models such as diet, routine, light exposure, and temperature, there are still many variables that cannot be controlled or predicted by an individual [34]. Notwithstanding, given that animal models are multi-organ and contain an immune system, they serve as a useful tool for evaluating the overall response of certain treatments and understand pharmacodynamics. The use of a humanized 3D model can complement this information and provide a reliable hypothesis of the effects of a potential drug in humans.

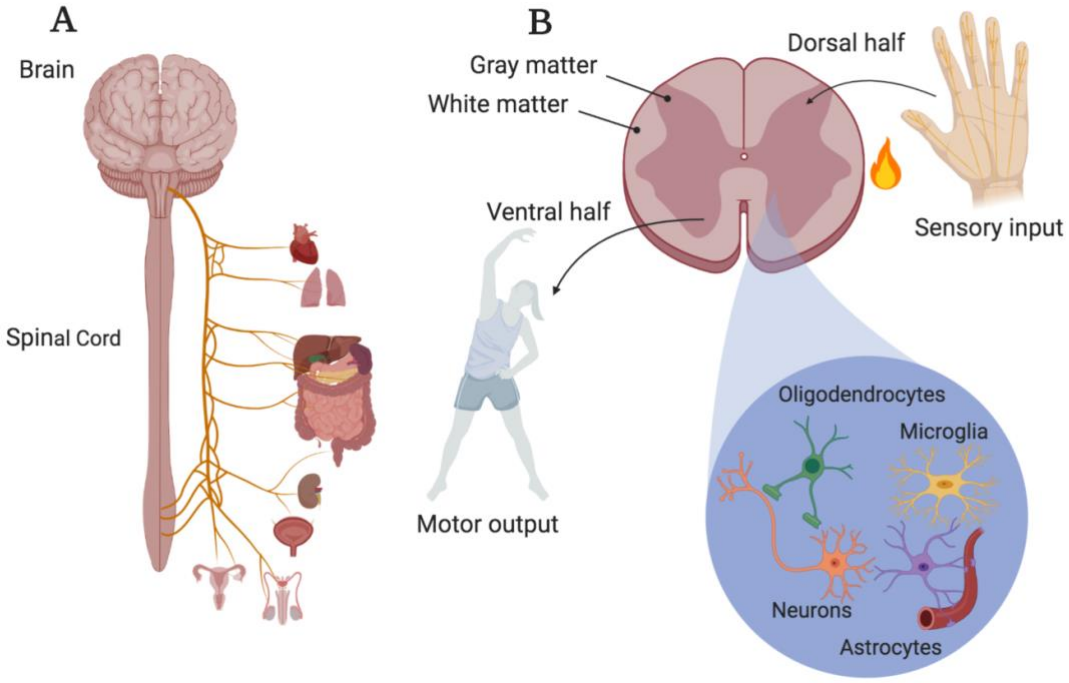

Figure 1.1. Functions of the Central Nervous System (CNS) and spinal cord (SC) anatomy.
a) The CNS is composed of the brain and SC, together they control the activities and function of the body. b) cross-section of the SC, the dorsal half controls sensory input while the ventral half controls voluntary movement. Cells present in the CNS include neurons, astrocytes, oligodendrocytes, and microglia. Figure created with biorender.com.

1.2. Ongoing research for treating SCI

There is no current cure for a SCI, and most of the approaches for treating this injury are focused on reduction of pain and inflammation or prevention of a secondary injury – an injury which occurs from minutes to weeks after the primary injury [22]. The secondary injury is characterized by a series of events that involve inflammation, ischemia, apoptosis, free radical production, and demyelination [22,37]. These events lead to the formation of a scar that acts as a chemical and physical barrier for regeneration. Treatments following a SCI include surgical approaches, such as decompression laminectomy in order to remove fluid or tissue being

compressed against the SC, or traction which is the alignment of the SC [38]. Ongoing clinical trials are categorized into (i) neuroprotective approaches, which are focused on understanding the patho-mechanism followed after a SCI, or (ii) neuro-regenerative approaches that are centralized on enhancing endogenous repair and alteration of the congenital barrier [39]. Strategies focused on neuroprotection for SCI are shown in (**Table 6.1- Appendix A)** [39]. Most of these studies have shown significant spontaneous improvements in animals but they have not been shown to bring recovery to a normal state [40]. Furthermore, translation from animal models remains imprecise when talking about a functional recovery in a clinical setting [40]. Moreover, the use of animal models requires a large amount of expertise and is very costly [41].

In addition to diet and physical rehabilitation, cell transplantation has received a lot of focus for neuro-regeneration purposes. Many cell candidates have been studied like Schwann cells, NSCs, neural progenitor cells (NPCs), oligodendrocyte progenitor cells (OPCs), olfactory ensheathing cells (OECs) and mesenchymal stem cells (MSCs) (**Table 6.2- Appendix A**) [40]. This research has evolved within the past decade and early phase clinical trials have shown its feasibility [40]. However, long-term patient safety still remains questionable given inequality between the extensive research related to the potential of cellular therapies but limited research associated with the mechanisms that promote repair and functional improvements [40].

Tetzlaff *et al.* reviewed five mechanisms for cell transplantation that can promote recovery through neuroprotection, immunomodulation, axon sprouting and/or regeneration, neuronal relay formation and myelin degradation (**Table 6.2- Appendix 1)** [40]. In a clinical trial run by Asterias Biotherapeutics called SCiStar-Phase I/IIa, OPCs derived from human ESCs were transplanted into patients with cervical SCI. After 90 days of transplantation, the patients shower motor

improvement [42]. The 25 patients completed the 12-month follow-up in which magnetic resonance imaging (MRI) scans showed consistent engraftment of cells at the injury site, 95 % of the patients showed improved motor on at least one level on at least one side, no evidence of adverse effects, and no evidence of decreased motor function [43,44].

Despite this neuro-regenerative approach showing promising results, there are still a lot of caveats for making such treatment available to the general public such as costs of production and medical care, large-scale production of the OPCs, quality control, regulation, etc. Due to prolonged production time and expensive cost of cell therapies, the financial cost of development is one of the major hurdles associated with such therapies. Other obstacles are the regulatory affairs and the rise in the aging population, the latter resulting in increased health care costs and the need for such therapies [45]. As for the neuroprotective approaches, long-term evaluations often lack proof of efficacy, recovery, or safety. These phenomena can be attributed to the lack of pre-clinical model alignment with a real clinical perspective. Areas where risky complications developed in humans might not always be reflected in animal models during pre-clinical trials [40].

For these reasons, the creation of humanized 3D models, that better replicate human physiology, is needed in order to create safer treatments, because testing will elicit similar responses between the models and the human body. Such models could be used in early stages of scientific development and pre-clinical trials as a way to accept or dismiss potential therapeutics. The development of a robust and reproducible drug screening tool could also prove beneficial in reducing the financial burden of clinical trials and the time spent testing with pre-clinical models. Furthermore, the development of a drug to treat a specific condition and the analysis of its effects could produce more immediate results due to the shorter regulatory pathway and lower cost of

clinical trials compared to cellular transplantation [46]. For instance, the chimeric antigen receptor (CAR) T-cell therapy, in which the patient's own immune system destroys tumor cells, has been approved by the Food and Drug Administration (FDA) for diffuse large B-cell lymphoma (DLBCL) after 50 years of research [46]. Patients who have had this therapy administered showed no further lymphoma recurrences as of yet, however further relapse and potential late toxicities of CAR T-cell might emerge. Notwithstanding, this product is one of the most expensive existent therapies ranging from $373,000-475,000 and some governments are already opposing the use of such therapies due to the elevated healthcare costs [46,47].

1.3. Relevant components used for the generation of neural tissues

1.3.1. Pluripotent stem cells

A popular type of stem cells used in TE in the past decade are human induced pluripotent stem cells (hiPSCs). These cells were first discovered by Yamanaka *et al*, in 2007 by reprogramming somatic cells through the expression of four important transcription factors: octamer binding transcription factor 4 (OCT4), sex determining region Y-box2 (SOX2), Kruppel-like factor 4 (KLF4), and myc proto-oncogene protein homolog (C-MYC) [48]. The first two transcription factors are essential for reprogramming, whereas KLF4, and C-MYC induce proliferation and colony formation [49].

The reprogramming of somatic cells can occur using retrovirus transduction, the use of transient gene expression vectors for gene delivery, protein transduction, or activation of endogenous pluripotent regulators by using small molecules [49]. hiPSCs have the same capabilities as ESCs, such as self-renewal and pluripotency, the ability to differentiate into any type of cell

found in the body. Under the right conditions, hiPSCs can be directed into any of the three germ layers; endoderm, mesoderm, and ectoderm. The ectoderm is the germ layer in which neural cells are emerged from and therefore hiPSCs can be used to generate the cells present in the CNS. The discovery of hiPSCs opened endless possibilities for applications in the field of TE such as cell-replacement therapies, patient-specific stem cell lines and disease modeling, as well as drug screening [49,50].

1.3.2. Differentiation of hiPSC-derived neural progenitor cells

hiPSCs can be differentiated into NPCs by culturing them in monolayer or by creating an environment that resembles early development [13,51,52]. The formation of spherical cell aggregates, called neural aggregates (NAs), allows for the formation of cell-cell interactions and intracellular signaling that the cells need to survive and begin to differentiate [53-55]. The formation of these 3D structures is achieved by the aggregation of cells on a non-adhesive AggreWell™800, a plate with an array of microwells with an inverted pyramidal-shaped bottom **(Figure 1.2)** [56-58]. The NAs are then incubated for 3-7 days in the presence of neural induction media (NIM). Directed differentiation into a specific germ layer can be achieved by the addition of physical cues or chemical cues in the culture media that will activate specific pathways of differentiation [53,55]. These cues include cell-cell interactions, cell-growth factor interactions, and the cell's interactions with the ECM [59]. Following the formation of NAs, neural induction is continued by the enzyme-free selection of neural rosettes where the neural rosette clusters are detached from the NAs [60,61]. Neural rosettes are an arrangement of cells that express many of proteins present in the neuroepithelial cells in the neural tube [62]. Differentiation of NPCs from hiPSCs can be achieved by culturing in Neural Induction Media (NIM) as it contains molecules that inhibit the small mothers against decapentaplegic protein (SMAD), which mediates multiple signaling pathways including the bone

morphogenic proteins (BMPs) and transforming growth factor beta (TGFβ) related proteins [18]. BMPs are involved in cell growth, apoptosis, morphogenesis, development and immune responses [63]. They act through kinase receptors on ectodermal cells which leads to the suppression of neural differentiation and promotes epidermal differentiation. The inhibition of the protein expression levels for these factors can be achieved by the presence of proteins like noggin, chordin, follistatin or small molecules like LDN193189 (LDN) and SB431542 (SB) [18,61] **(Figure 1.2)**.

Once the BMPs are inhibited, differentiation into the neural lineage (formation of neural rosettes) is directed due to the blocking of the mesoderm and endoderm pathways [61]. NPCs then have multipotency and can be differentiated into the different lineages of the CNS such as neurons or glial cells (astrocytes and oligodendrocytes) [59]. Neurons vary in location in the CNS and morphology. Moreover, depending on their finite differentiated state, they can release specific neurotransmitters that allow them to perform different actions. For example, MNs are present mainly in ventral half of the SC and they carry commands from the brain or SC to the rest of our body, causing muscles to contract and generate movement [18]. MNs can perform this action by the transmission of synaptic signals by the release of the neurotransmitter acetylcholine. Neurons can be named by the type of neurotransmitter that they release, e.g. cholinergic, dopaminergic, gamma-Aminobutyric acid (GABAergic) neurons. Therefore, MNs are also known as cholinergic neurons.

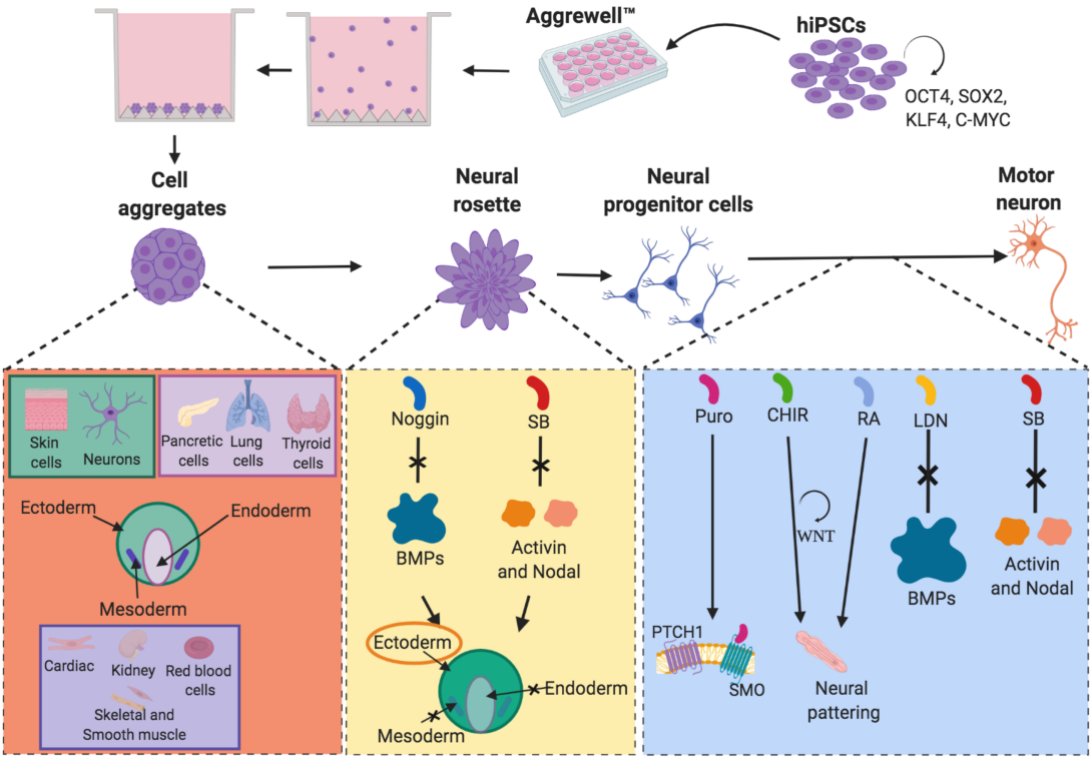

Figure 1.2 Differentiation of hiPSCs into Motor Neurons (MNs) via cell aggregate formation.
hiPSCs can be differentiated by forming cell aggregates that have the capability to differentiate into any of the three germ layers. In order to induce neural differentiation, the cell aggregates must be exposed to different morphogens that promote induction into NAS, followed by the formation of neural rosettes and neural progenitor cells (NPCs). MN differentiation can be achieved by the addition of a cocktail of small molecules. Figure created with biorender.com.

1.3.3. Differentiation of hiPSC-derived neural progenitor cells into motor neurons

During neurodevelopment, the identity and position of the developing MNs depends on the activity of the protein sonic hedgehog (SHH). This protein controls aspects of embryonic development and is secreted by the notochord, which is a mesoderm tissue that influences the dorsoventral pattering of the neural tube [18]. SHH acts as a morphogen that directs the cell fate of neuronal cells depending on the concentration. SHH performs its activity by interacting with a

complex of twelve transmembrane receptors called patched homolog 1 (PTCH1) and a signal-transducing subunit called smoothened (SMO) [64]. When SHH binds to PTCH1, the inhibition of SMO stops, leading to the activation of the *SHH* genes and the activation of transcription factors and protein kinases involved in the differentiation of MNs [18,64]. As an alternative to using the protein SHH, the hydrophobic-small molecule purmorphamine (puro) can be used to promote differentiation of hiPSCs into neural cells[64-67]. Puro is a purine derivative- SMO agonist that activates the SHH pathway (**Figure 1.2-1.3)** [64]. Small molecules are drugs that have low molecular weight – below 1000Da – that have been fabricated using chemical synthesis as opposed to proteins, peptides, nucleotides, etc. which are produced through biological processes [68]. Small molecules have been widely used for the maintenance, production, and differentiation of PSCs. Their effect in biological systems can be modulated by varying the concentration. In addition, they are inexpensive compared to proteins and peptides and they are easy to store which makes them great tools for research purposes and usage in DDS [68].

Another small molecule important during neurodevelopment is the derivative of vitamin A: retinoic acid (RA), which acts as a BMP inhibitor (**Figure 1.2-1.3)** [68]. RA is produced prenatally and postnatally in the CNS at specific times. It acts specifically on the homeobox (*HOX*) genes which is essential in organogenesis and neural development [69]. When the neural tube has acquired a rostro-caudal form, the mesoderm and endoderm secrete additional signals to further define the pattern of the neural tube. The secretion of RA occurs closer to the caudal levels, establishing the subdomains of the hindbrain and SC [18]. RA enters the nucleus of the cells and it binds to target genes via nuclear receptors [70].

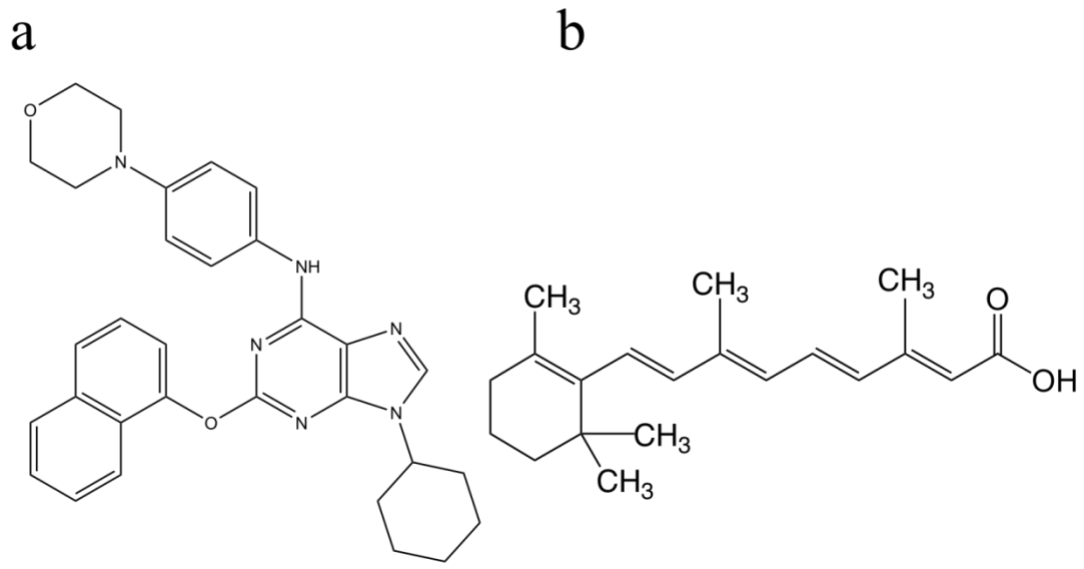

Figure 1.3 Chemical structures of (a)Purmorphamine (puro), and (b) Retinoic acid (RA).

1.4. Biomaterials used to build neural tissues

In addition to hiPSCs and morphogen exposure, the fabrication of tissues also depends on the adequate environment surrounding the cells. This environment can be provided by scaffolds made of biocompatible and biodegradable materials, also known as biomaterials. Scaffolds must be analogous to the ECM to provide temporary support for the cells to proliferate, grow, differentiate, and maintain tissue structure [71]. A common tool in the field of TE is the use of hydrogels, which are polymeric materials that swell extensively in the presence of water [25]. Hydrogels can be obtained from a variety of natural polymers and polysaccharides such as hyaluronan, alginate, chitosan, agarose, fibrin, collagen [25]. These materials have been widely used in the field of TE for the fabrication of soft tissues such as the brain and SC which have a compressive moduli of ~2000 Pa, which highlights the capability of these tissues to withstand loads of stress per unit area or change in volume [25]. Mimicking the mechanical properties of the

native tissues will have a great impact on the proliferation and differentiation of the cells as different regions of the brain or SC have varied stiffness such as the white and grey matter [25,72]. A study performed by Leipzig *et al.,* observed that substrate stiffness has an effect in NPC behavior [73]. Substrates with an elastic modulus of <10kPa favored NPC proliferation, while softer scaffolds with an elastic modulus of <1kPa led to neural differentiation. Stiffer scaffolds with elastic modulus of 1-3.5kPa led to astrocyte differentiation, while scaffolds with an elastic modulus of >7kPa favored oligodendrocyte differentiation [73].

Cell-binding domains, stiffness similar to that of the natural tissue, and pore size are among the properties that make a hydrogel suitable to sustain a specific type of tissue. Hydrogel mechanical properties and pore size can be modulated and used to form micro- and macro-architectures which are extremely important in the generation of neural tissues [74,75]. These features are relevant in the generation of SC tissues which have an overall tubular-shape, but the microstructures are composed of the white matter, that contains the aligned axon tracts, and grey matter, that contains the cell bodies of MNs and interneurons [18,25]. Moreover, many hydrogels have also shown to direct neural behavior, increase cell viability, and promote cellular differentiation [74]. These responses happen as a result of the nature of many natural biomaterials that contain cell-binding domains such as the RGD motif (arginine, glycine, aspartate) peptide that allow cell adhesion to the ECM protein laminin that allow cell-adhesion and survival [76]. Hydrogels that do not contain these peptide motifs can be modified to incorporate bioactive domains of ECM proteins such as fibronectin, vitronectin, or laminin to create biomimetic materials that allow cell adhesion and survival [77,78].

A study performed by Abelseth *et al.,* from the Willerth laboratory used various natural biomaterials for the creation of a bioink that could support the proliferation and differentiation of hiPSCs derived neural tissues [79]. In this study, a fibrin based bionk was fabricated in combination with the polysaccharides- alginate and chitosan where hiPSCs-derived NAs were bioprinted and cultured *in vitro* for 30 days. The NAs showed high levels of cell viability, differentiation into neural tissues as observed by the expression of the marker βT-III and neurite extension [79]. Given the development and successful results of this fibrin based-bioink to support neural tissues in a 3D environment, the further sections will focus on revising the nature and properties of fibrin, alginate, and chitosan.

1.4.1. Fibrin

Biologically-derived proteins can serve as scaffolds for TE and formation of hydrogels [80]. Fibrin is a natural protein that serves as an important component in the wound healing process. The formation of fibrin networks (gel) and platelets are key components to maintain hemostasis and thrombosis (vascular occlusion) during the coagulation cascade that occurs at an injury site [81]. The serine protease enzyme thrombin cleaves the glycoprotein fibrinogen to initiate fibrin polymerization [81]. Thrombin is a product of the enzymatic cleavage of prothrombin by the activated factor (Xa). After the fibrinogen is cleaved, the next step is the self-assembly of fibrin monomers into two stranded oligomers, each of 20-25 monomers. These oligomers aggregate laterally to form protofibrils. Lastly, the protofibrils aggregate forming a fibrin network [81]. Another component involved in the polymerization and stability of fibrin are the calcium ions (Ca^{2+}). Fibrin contains high affinity binding sites for Ca^{2+} and its binding is necessary for the formation of

protofibrils as it increases the extent of lateral aggregation and promotes formation of thicker fibers **(Figure 1.4)** [81].

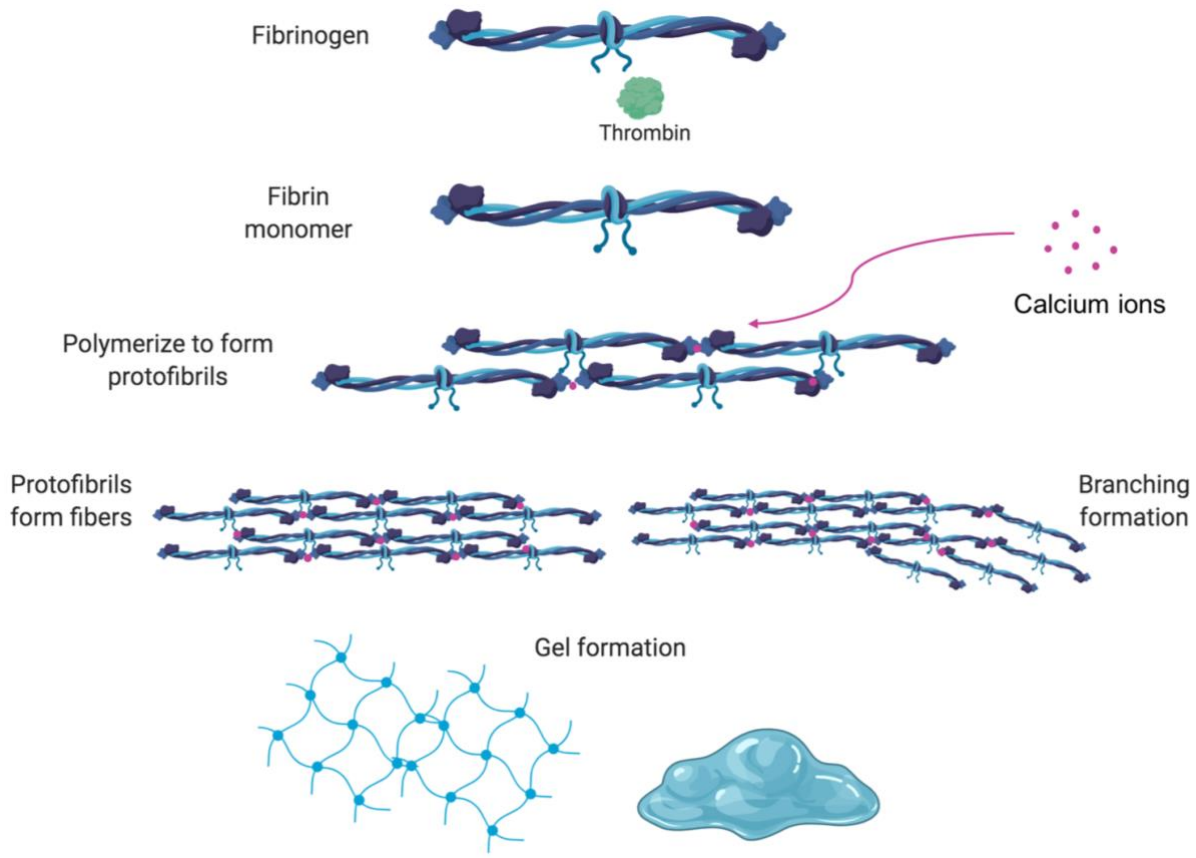

Figure 1.4 Schematic representation of fibrin formation.
Figure created with biorender.com.

Fibrin has been widely used in TE for both *in vitro* and *in vivo* applications [82]. Fibrin hydrogels have been used for bone grafts [83], NSC culture [84], and vascularized tissue production [85]. Willerth *et al.* successfully cultured ESC derived NPCs seeded in fibrin scaffolds in order to determine the ideal concentrations of growth factors needed for survival and differentiation [84]. Lee *et al.* used collagen and vascular endothelial growth factor (VEGF)-releasing fibrin scaffolds to

bioprint NSCs [86]. In addition, fibrin has also been used as a bioink to 3D print different type of tissues, like microvasculature constructs where endothelial cells showed angiogenesis [85]. Fibrin gels provide a good environment for cell survival and differentiation as it contains several RGD motifs where the cells can attach and survive [76]. However, scaffold printability and degradation are major concerns when growing neural tissue due to the long periods of time required for its differentiation and maturation. Previously, Robinson *et al,* demonstrated that the molecule genipin manipulates the mechanical properties of fibrin scaffolds by increasing scaffold stability, while polymerizing and decreasing the degradation rate of fibrin [87]. Genipin is a plant-derived blue-colored cross-linking agent extracted from the fruits of *Genipa Americana* and *Gardenia jasminoides Ellis* found in tropical areas from Mexico and the Caribbean[88]. Genipin stabilizes biopolymers by forming covalent bonds with the primary amine groups [87,88]. It has also been used in studies to crosslink gelatin, collagen, and chitosan [88].

1.4.2. Alginate

Alginate is a natural polymer obtained from brown seaweed *(Phaeophyceae)* that forms a gel in the presence of divalent cations. Is an anionic compound composed by two types of Uronic acid: the Mannuronic acid (M blocks) and Glucuronic acid (G blocks) (**Figure 1.5**). These blocks are covalently linked, and depending on their configuration the alginate presents different gelling capabilities and strength [89]. The arrangement of the M and G blocks can vary depending on the type of seaweed harvesting method, seasons of harvesting, etc. Alginate has been used in the pharmaceutical industry and also has been widely studied as a 3D scaffold to encapsulate NSCs [90]. Some of the advantages of using alginate as a hydrogel for bioprinting is that it has been demonstrated to be biocompatible with the CNS, shows low cytotoxic effects and is very low cost [90]. Furthermore, the elastic modulus of this hydrogel can be altered and the proliferation and

differentiation of encapsulated NSCs is increased with a low elastic modulus of ~180Pa in comparison with hydrogels with elastic modulus of 20,000 Pa. [75]. Alginate can also polymerize very quickly under normal conditions, which is great for bioprinting purposes as the hydrogel should be able to maintain its shape after ejection from the print nozzle. Different tissues have been successfully 3D printed with this hydrogel, such as aortic valves and cartilage tissue [91,92].

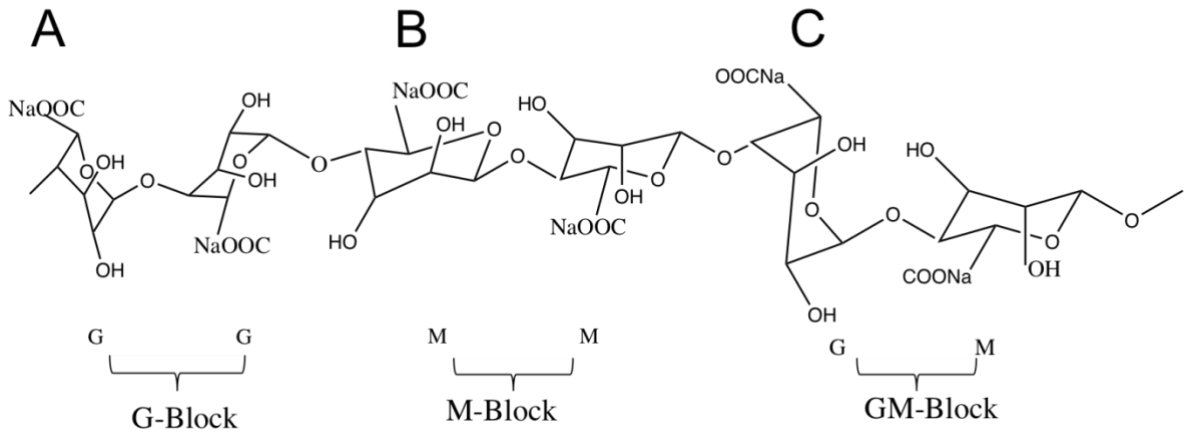

Figure 1.5 Alginate structure.
(a)and (b) show G and M blocks respectively(c) shows G and M blocks

Alginate has been used as a scaffold for mammalian cells as it possess tunable mechanical properties that can be made similar to different tissues such as smooth muscle [93,94], cartilage [95,96], bone [97,98], skeletal muscle [99], neural [90,100-103]. As previously mentioned, in the presence of divalent cations, alginate undergoes an aqueous sol-gel transformation [104]. The crosslinking of this biomaterial occurs relatively fast (less than 1 min [100]) when exposed to Ca^{2+} ions, where the carboxyl groups and the G blocks react and change the properties of the gel [89,100]. When Ca^{2+} ions are combined with alginate, they first react with repeating G units that lead to stacking and

formation of a “box”-shaped structure [104]. The remaining Ca^{2+} ions form a Ca^{2+}-alginate complex by interacting with the other G and M units. This effect happens as a result of unequal affinity of Ca^{2+} ions for G and M units. Therefore, the mechanical properties of alginate can be modulated by varying the concentrations of G and M which changes the composition and porosity of the scaffolds [104]. Alginate with higher G content will be more rigid with higher porosities, whereas higher M contents will lead to less porous scaffolds [104]. Given that alginate does not possess cell binding domains that benefit cell survival, alginate can be functionalized with peptide sequences in order to promote cell attachment and survival or combined with other materials that can support cell adhesion and survival [79,100,105]. These properties make alginate a suitable material to use in combination with fibrin to 3D print SC tissue in order to increase cell viability, differentiation and have a rapidly polymerizing hydrogel.

In a study performed by Purcell *et al,* the effects of alginate composition on cell viability and survival of NSCs were evaluated [90]. After 21 days of culture *in vitro,* murine cortical NSCs encapsulated in alginate beads survived and proliferated regardless of the composition tested. Furthermore, their results showed that beads with high L-glucuronic acid content were significantly more stable when exposed to solutions of low osmolarity [90]. Another study used alginate as a cell scaffold for a variety of cells in the CNS: astrocytes, microglia and neurons [100]. The alginate scaffold was functionalized by attaching proteins and epitopes covalently in order to promote cell attachment [100]. After 14 days, astrocyte cells were viable, and no signs of cytotoxicity was observed. Neural cells showed neural outgrowth of a couple hundred micrometers after 14 days in culture [100]. In a study performed by Xu *et al.,* glioma cells were bioprinted in a composite scaffold that contained alginate, gelatin and fibrinogen. The purpose was to study was to mimic the *in vivo* tumor environment. The expression of the neural marker NESTIN, and the malignant

brain tumor marker VEGF were observed in this model. Moreover, the 3D bioprinted brain tumor model showed to be more resistant to chemotherapy drugs [106].

1.4.3. Chitosan

Chitosan is another natural polymer obtained from shells or shellfish from food industry waste [107]. Research for the use of chitosan as a biomaterial has increased in the past 25 years. This material is obtained from chitin, which an abundant structural polysaccharide and one of the most abundant organic materials produced by biosynthesis [17,108]. Chitosan has the characteristics needed for TE applications as it is biodegradable and biocompatible, while additionally having antibacterial, antitumoral and wound-healing activity [17]. Chitosan is composed by three main functional groups; (i) an amino group at the C(2), (ii) a primary hydroxyl group at the C(3), and a secondary hydroxyl group at the C(6) positions (**Figure 1.6)**. The biological, physical and chemical properties of chitosan can be tailored through covalent and ionic modifications in these main functional groups [17].

Biomaterials made from chitosan form porous scaffolds which allows cells to proliferate and migrate inside the scaffold. Depending on the pore size and orientation of the scaffold, the mechanical properties will change [17]. It has been shown that the tensile strength of the hydrated scaffolds is reduced with higher porosity [109]. In addition, studies performed by Chen *et al.*, showed that chitosan with lower molecular weight showed less crystallinity and therefore, lower tensile strength [110]. Degradation of chitosan *in vivo* occurs via enzymatic hydrolysis, a process facilitated by enzymes where bonds in the molecule are cleaved and replaced by the addition of water [17,111]. The main enzyme involved in the degradation of chitosan is lysozyme – an enzyme present in secretions, like tears and saliva, that has antibiotic properties[112]. Lysozyme targets the acetylated residues [17,108,113]. The higher percentages of deacetylation, the lower degradation rates [17].

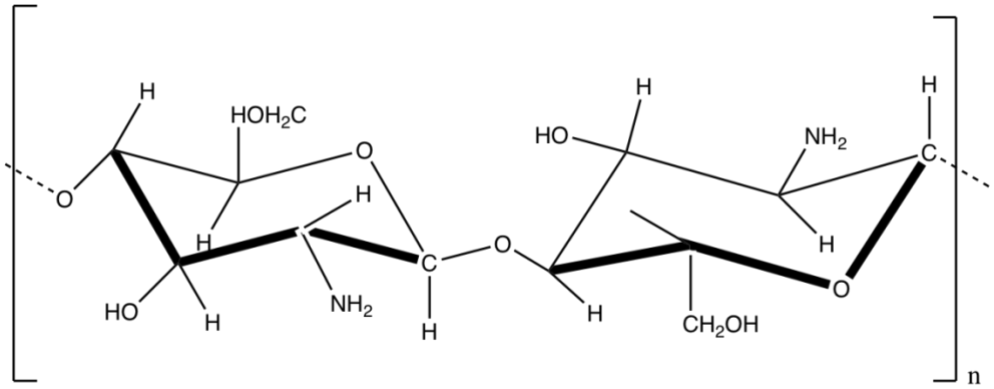

Figure 1.6 Chitosan structure.

Combinations of alginate-chitosan have been used in the field of biomaterials and drug delivery as the presence of chitosan increases the mechanical strength of alginate [104,114,115]. When alginate is combined with Ca^{2+}, a negative charged pre-gel is formed followed by the enclosing of positively charged chitosan [104]. At higher concentrations, the Ca^{2+} ions bind to the alginate preventing the enclosing of cationic molecules [104].

Chitosan forms a viscous solution when it is dissolved in acidic conditions with pH below 6.2 [88]. Raising the pH results in the formation of a gel. However, the pH of chitosan can be neutralized to physiological standards using a solution of the disodium salt-glycerol phosphate (GP), allowing it to be in liquid form below room temperature [17,116]. The GP increases the pH by acting as a neutralizer of the phosphate groups [116]. This chitosan-GP solution remains in liquid form at physiological pH of 6.8-7.2. Now, at body temperature, this solution turns into a gel, making it is ideal for encapsulating cells and proteins. This approach becomes useful for the formulation of a bioink because it can provide a higher viscosity to the composite material by forming a gel *in situ* once it has been crosslinked and the temperature has been raised.

When chitosan is crosslinked, it forms permanent covalent bonds that enhance the mechanical properties of the polymer and allow the free diffusion of water and molecules [117]. When crosslinked, chitosan forms 3D interconnected networks. The most common crosslinker for chitosan is glutaraldehyde, which is a dialdehyde. However, this chemical is neurotoxic and therefore it cannot be used as a crosslinker for a bioink [118]. As an alternative for glutaraldehyde, chitosan can be crosslinked with genipin [119]. Crosslinked chitosan with genipin can be used for the preparation of elastic and stable gels to carry cells and be used for bioprinting purposes [119].

Chitosan has been used in the field of TE with applications in skin [120], bone [107], cartilage[121], blood vessels[122], liver[123], and nerve tissue[124,125]. In a study led by Nomura, NSCs were seeded in chitosan channels to treat rats with SCI. Recovery was observed through histological analysis, which revealed long term survival, tissue bridging, and neural differentiation [28]. In another study, chitosan microspheres were crosslinked with heparin for the delivery of rat NSCs and growth factors. After 12 weeks of culture *in vitro,* cell survival and the neuronal marker NESTIN were observed [126]. Another study performed by Gu *et al.* used a combination of carboxymethyl-chitosan, alginate and agarose to bioprint functional neural mini-tissues from human NSCs [127]. After 24 days, the NSCs expressed the neuronal marker beta-tubulin class III (βT-III) and expressed the GABAergic neuron markers GABA and glutamic acid decarboxylase (GAD). In addition, the differentiated neurons formed synaptic connections, and expressed spontaneous Ca^{2+}response [127].

1.4.4. Microparticles as a DDS

DDS are commonly made of biodegradable polymers and are widely used in research and pharmaceutical fields to deliver vaccines, proteins, nucleic acids, and small molecules [128]. Depending on the need and specifications of the drug or morphogens, DDS can be designed to provide a time-specific or a continuous delivery. Additionally, DDS can protect the encapsulated

molecules from degradation and be localized at the place of interest [128]. In the field of neural TE, the use of DDS has shown to be an efficient method to differentiate stem cells into the desired cell type. Moreover, the presence within the tissues overcomes barriers of diffusion and promotes homogeneous differentiation of the stem cells [58,129,130]. The source and types of cells, nature and mechanical structure of the biomaterial, and combination of drugs needed vary immensely depending on the tissue of interest [16,131].

Nano- or micro- particles are particles of the nanometer ($1x10^{-9}$ meter) and micrometer ($1x10^{-6}$ meter) sizes fabricated from various materials and possess multiple shapes. Their use has many applications for the delivery of water soluble or insoluble drugs like proteins, small molecules, nucleic acids, antibiotics, and vaccines [132-134]. Their main objective is to improve biological stability, decrease toxic effects, mediate the distribution of the compounds, achieve a targeted and slowed release, and finally, interact with biological barriers [132,135]. Other types of DDS include the use of liposomes, proliposomes, gels, prodrugs, cyclodextrins [135]. Drug-loaded microspheres for use in hiPSC differentiation can be fabricated with the use of biodegradable polymers like PLGA or PCL [129]. As the polymer degrades, the drug or soluble factor needed for the cells to differentiate into a specific cell type will be released over time in a controlled rate.

PCL is a biodegradable polymer useful for long-term implantable devices due to its slow degradation. A hydrolysis reaction of its ester bonds is what catalyzes its degradation, making it a good option of controlled release inside the body [133]. It's also inexpensive, has good solubility, and a low melting point adding to its attractiveness for use in biomaterial applications. It has been demonstrated as a potential microsphere-based DDS and shows a promising alternative for future pharmaceutical purposes [129]. Different drugs have been successfully encapsulated in this polymer

such as: tamoxifen – used for breast cancer treatment, clonazepam – used to prevent seizures, and insulin [133].

1.5. 3D bioprinting

Bioprinting is the process of fabricating 3D biological tissues, organs and cell constructs using a combination of biomaterials and 3D printing technology using the specifications created in a computer-aid design (CAD) file [91]. 3D bioprinting is an emerging TE strategy that allows for a faster and reproducible generation of tissues *in vitro* [136,137]. The process of bioprinting consists of i) cells, ii) "bioink" which acts as mechanical and biochemical support of the tissue, often iii) drug delivery systems, and iv) CAD file [136,138]. In contrast with conventional TE strategies, the 3D printing process offers several advantages including lower amounts of labor in the assembly and combination of the raw material components, high-throughput, and creation of specific cell pattering and micro-architectures [136,137,139].

Inkjet, extrusion, and laser-assisted, are the main strategies for bioprinting tissues [136,139]. However, one of the major challenges faced when using these technologies is the amount of shear stress the cells receive as they are extruded, which leads to low cell viability and lack of long term-functionally of the tissues [140-143]. A novel bioprinting method that combines an inkjet dispensing bioprinter (RX1) and a microfluidic device called Lab-on-a-printer (LOP™) was developed by Aspect Biosystems (**Figure 1.7)** [144,145]. The RX1™ allows for the rapid bioprinting of physiological relevant tissues in a high-throughput and reproducible manner. The use of an inkjet dispenser allows the user to create programmable patterns to be printed defining the micro-architecture of the tissue. With the LOP™ technology, all the materials required to produce the construct, e.g. scaffold material, multiple cell types, and crosslinker, are introduced to the

microfluidic system and allowed to interact prior to the ejection from a single nozzle. The precise regulation of fiber composition and print speed is another advantage of the single nozzle, as it allows for more control over the printing job [144]. Hydrogel fibers of a defined diameter can be generated, and specific components such as more than one type of cells, different materials and drug delivery systems can be deposited in different locations to fabricate functional tissues [144].

One of the major differences with other bioprinting technologies is that during the bioprinting process with the LOP™ technology, the cells are protected from shear-stress. This happens as a result of sheathing the bioink with a cross-linking agent that triggers the formation of a gel which creates cell-loaded fibers. For these reasons, the combination of the RX1™ and LOP™ technologies creates a good system for bioprinting neural tissue as neural cells tend to be very sensitive and once they are differentiated, they become post-mitotic and are no longer capable of undergoing mitosis [146]. Therefore, ensuring a high number of viable bioprinted NPCs is essential for the survival and differentiation of neural tissues.

Another compelling feature of the RX1 bioprinter is the use of disposable polydimethylsiloxane (PDMS) modules that are easily switched when using different components to avoid cross-contamination [144]. Moreover, the RX1™ will print the tissue in a layer-by-layer manner, where the positioning of biological materials and biochemical components are evenly placed throughout the cells and the 3D structure **(Figure 1.7)** [147]. This approach will allow manufacturing of structures with micro-architectures and specific designs to promote neuronal differentiation and axonal extension. After successful generation of 3D printed tissue, further maturation and *in vitro* evaluation will be required in order to be used for further research such as drug screening [147].

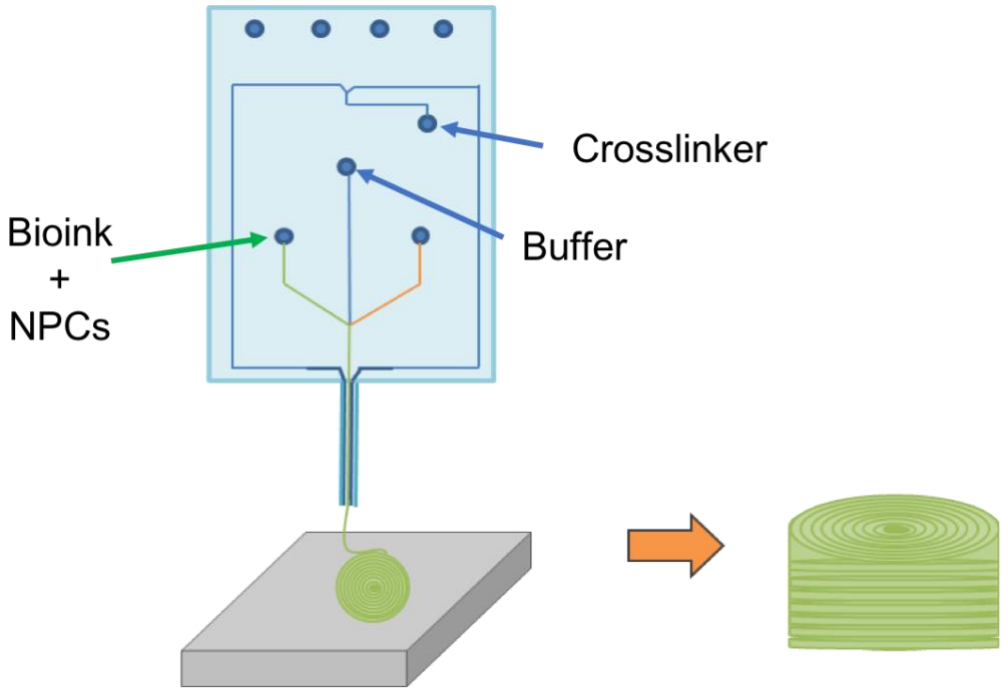

Figure 1.7 Schematic representation of the 3D bioprinting process using the LOP™. [b]

1.5.1. Use of stem cells when bioprinting neural tissues

The relevance of using stem cells to bioprint tissues relies on their capability to self-renew and, depending on their potency, to differentiate into any of the three germ layers (endoderm, mesoderm and ectoderm). In addition to the development of patient -specific cell lines. In this way, the tissues can be differentiated to further assess their functionality and can be used for personalized disease modelling and drug screening. Models simulating healthy or diseased tissues can be created by 3D bioprinting constructs using stem cells [136]. Researchers have successfully

b Figure from: de la Vega L, Rosas Gomez D, Abelseth E, Abelseth L, Alisson da Silva V, Willerth SM. **3D bioprinting human induced pluripotent stem cell-derived neural tissues using a novel Lab-on-a-Printer technology**. Applied Science 2018 In press.

bioprinted tissues like cartilage, bone, cardiac, liver, vascular and neural tissue [136]. A group led by Gu *et al.* bioprinted NSCs that differentiated into neural GABAergic neurons and glial cells in a bioink composed of alginate, agarose, and chitosan [127]. Shu *et al.,* bioprinted neural tissue by using mouse NSCs with a thermo-responsive bioink. The observed cell viability was 50% 24-hours post-printing. The bioprinted constructs showed recovery in a zebrafish model with TBI [148]. Another group tried different approaches and bioinks like the combination of collagen to bioprint neurons and astrocytes in a layer-by-layer manner[149]. Stereolithography, low level light therapy (LLLT), and electrospun fibers are other 3D printing strategies that have been used to create neural tissue [150,151].

1.6. Research aims

As mentioned, many of the studies that focused on neuroprotection or regeneration of neural tissue following a SCI are inconclusive, lack significant improvement or demonstrate significant financial or regulatory challenges [40,152-155]. There is a significant need of a drug screening tool to test potential drugs for disorders in the CNS to accelerate of the process of drug development. Therefore, this research is focused on the development of a drug screening platform for SCI. Given that one of the major disruptions when a SCI occurs is the damage of the MN tracts that transmit signals from the brain to the rest of the body, this research will focus on the differentiation of hiPSC-derived NPCs into MNs.

A number of protocols have shown the differentiation of hiPSCs and NPCs into MNs by the addition of the small molecules puro/SHH, RA, CHIR99021 (CHIR), SB, and LDN [60,65,66,156]. Most of these studies are performed in monoculture or in co-culture with other types of cells [66].

However, these differentiation protocols lack a 3D environment to produce relevant physiological tissues *in vitro.* With the added benefits of reducing time, costs, and the use of animal models to predict human physiology, 3D bioprinted neural tissues could more accurately reflect human physiology and help to improve the pipeline of drug testing for neurological diseases and disorders [157]. This research determined the conditions necessary for bioprinting neural tissue that resemble the SC to be used as a platform for drug screening. The proposed work will be performed by combining hiPSC-derived NPCs, a fibrin-based bioink, and small molecules to promote neuronal differentiation into MNs. This work will also be tested with puro and RA releasing microspheres to demonstrate that DDS can be used in combination with 3D bioprinting and serve as tools for differentiation *in situ*. The resulted constructs will be characterized to evaluate their neuronal morphologies, protein markers. Neuronal activity will also be evaluated based on their membrane potential.

1.6.1. Research aim 1

We hypothesized that the encapsulated small molecules puro and RA in drug-loaded microspheres can promote neural differentiation of hiPSCs-derived NAs.

Objective 1: To demonstrate encapsulation and the controlled release of puro in PCL loaded microspheres.

Objective 2: To demonstrate that the incorporation of both puro and RA microspheres embedded in NA promotes neural differentiation.

In chapter two, it was studied how neural tissues can be engineered from hiPSCs and drug-loaded microspheres as an efficient method in comparison with conventional tissue culture

techniques. We demonstrate that puro can be encapsulated in PCL microspheres using a single emulsion oil-in-water and determination of encapsulation efficiency and controlled release for 46 days. Furthermore, we observed that after 35 days, the NAs showed morphologies characteristic of MNs with extensive neurite outgrowth and the expression of MNs markers HB9, ISL-1. Expression of the cholinergic neuron marker-choline acetyl transferase (CHAT) was observed after 60 days of culture *in vitro*, proving their maturation [37].

1.6.2. Research aim 2

We hypothesize that neural tissues can be engineered using hydrogels and bioprinting technologies using hiPSC-derived NPCs that will survive and further differentiate and mature into neuronal subtypes.

Objective 1: To demonstrate that hiPSC-derived NPCs can be bioprinted using the fibrin based bioink, RX1 and LOP™ technologies.

Objective 2: To demonstrate that the bioprinted tissues can survive, differentiate, and mature into neuronal subtypes.

In chapter three we investigated the use of hiPSC-derived NPCs for bioprinting neural tissues using a novel bioink composed of the natural biomaterials: fibrin, alginate, and chitosan using the RX1 and LOP™ technologies. Structures with defined macro-architecture (cylinders of 1cm dimeter) and micro-architectures (~175 μm fiber diameter) were bioprinted. The bioprinted tissues were treated with a cocktail of small molecules to promote neuronal maturation. Cell viability was analyzed after 7 days of being bioprinted in which all groups showed above 80% viability. After 30 days of culture, the differentiated hiPSC-derived NPCs showed the expression

of CHAT, the newly generated neuron marker βT-III, and the glial fibrillary acidic protein (GFAP)-an astrocyte marker proving their differentiation maturation after being bioprinted.

1.6.3. Research aim 3

We hypothesize that hiPSC-derived NPCs can effectively be differentiated into neural tissues using drug releasing microspheres and bioprinting technologies.

Objective 1: To demonstrate that drug and fluorescent releasing microspheres can effectively be bioprinted using the fibrin based bioink, RX1 and LOP™ technologies.

Objective 2: To demonstrate that bioprinted hiPSC-derived NPCs can be differentiated *in situ* after being bioprinted.

In chapter four we investigated the incorporation of puro and RA releasing microspheres in combination with the fibrin-based bioink to differentiate hiPSC-derived NPCs when being bioprinted using the RX1 and LOP™ technologies. The neural tissues were bioprinted in a cylindrical structure of 13 mm diameter and height of 2.7 mm. Fluorescent microspheres were also bioprinted under the same conditions in order to analyze the microsphere distribution within the construct. The bioprinted neural tissues were cultured for up 45 days where they showed the expression of the microtubule associated protein 2 (MAP2), and CHAT -indicating differentiation and maturation into MNS, as well as the expression of GFAP, the oligodendrocyte marker O4 and myelin-indicating the presence of astrocytes and myelinating oligodendrocytes.

Moreover, in chapter five, discussion and conclusions for each chapter are presented, as well as a general overview and future work. Future work related to the current project are discussed in detail.

Chapter 2 Engineering Neural Tissue from Human Pluripotent Stem Cells Using Novel Small Molecule Releasing Microspheres [c]

Laura De la Vega [1], Karina Karmirian [2], Stephanie Michelle Willerth [3*]

[1] Department of Mechanical Engineering, University of Victoria, Victoria, BC, Canada.
[2] Biomedical Sciences Institute, Federal University of Rio de Janeiro, RJ, Brazil.
[3] Division of Medical Sciences, University of Victoria, Victoria, BC, Canada.

Key words:

Controlled release, drug delivery, motor neurons, purmorphamine, retinoic acid.

Author contributions

De la Vega L. performed most of experimental work, design, analysis, and wrote the manuscript draft. Karmirian K. helped to perform experiments, analysis and assisted on writing the initial manuscript. Willerth S.M. provided input to experimental design and provided feedback and editing on the manuscript.

c The following chapter is from: De la Vega L, Karmirian K, Willerth SM. **Engineering Neural Tissue from Human Pluripotent Stem Cells Using Novel Small Molecule Releasing Microspheres.** Advanced Biosystems. 2018;0(0):1800133.

2.1. Abstract

Here a novel technique for engineering neural tissue consisting of motor neurons by combining human-induced pluripotent stem cells (hiPSCs) with small molecules releasing microspheres is demonstrated. First, the small molecule purmorphamine (puro) is successfully encapsulated into poly ε-caprolactone (PCL) microspheres using a single emulsion oil-in-water (o/w) method for the first time with an efficiency of (84% ± 2.12%). These microspheres release 91% ± 1.7% of the encapsulated puro in a controlled fashion over 46 days. Puro microspheres, along with previously characterized retinoic acid (RA) releasing microspheres, are then incorporated into hiPSC aggregates to engineer neural tissue. The combination of puro and RA microspheres promotes hiPSC differentiation as indicated by the expression of multiple neural markers, including the neuronal marker β-tubulin III (βT-III), and the transcription factor Olig2 (7.69 ± 8.38%) on day 28. These tissues express the motor neuron marker HB9 (24.85 ± 4.51%) on day 35, and the mature motor neuron marker ChaT (12.35 ± 4.17%) on day 60. These engineered tissues can be used for regenerative medicine applications such as treating SCI, disease modeling, and drug screening.

2.2. Introduction

Adult somatic cells can be reprogrammed back into a pluripotent state by expressing a specific set of transcription factors known as Yamanaka factors, which includes Oct3/4, Sox2, Klf4, and c-Myc. [48] The resulting cells are known as human induced pluripotent stem cells (hiPSCs). [48] The discovery of hiPSCs provides intriguing possibilities for applications in regenerative medicine, TE and disease modeling. hiPSCs can self-renew and differentiate into all three germ layers like human embryonic stem cells (hESCs). However, using hiPSCs avoids the controversial ethical issues associated with human embryo derived hESCs. Furthermore, hiPSCs can be more readily used for clinical treatment, as patient-derived hiPSCs reduce the risk of immune rejection when transplanted back into the original patient. [26,158,159]

Often cell culture conditions are manipulated to direct the differentiation of hiPSCs into the desired cell phenotypes. One such established differentiation method requires the formation of hiPSC aggregates to generate specific cell lineages. [65,160-162] These aggregates self-organize into a structure, replicating the process of embryogenesis. [162] The aggregates can be treated with morphogens to promote directed differentiation towards target lineages. Thus, ensuring diffusion of morphogens throughout the aggregate is essential to producing a homogenous population of the desired mature cell lineage. However, the 3-dimensional nature of the cell aggregates limits diffusion, meaning morphogens only reach the outer layers of the cell aggregate - resulting in heterogeneous differentiation. [163,164] Achieving homogeneous differentiation *in vitro* is necessary to for many *in vivo* applications, as undifferentiated stem cells pose a risk of tumor formation. [165-167] An inside-out approach to morphogen delivery can address the issues of poor diffusion, and the resulting heterogeneous differentiation. This method requires embedding morphogen-loaded microspheres into cell aggregates, allowing for the targeted and controlled release of the required

morphogen throughout the aggregate. [168] Morphogen-loaded microspheres enable localized drug delivery in a temporally controlled manner for homogeneous and organized stem cell differentiation inside of aggregates. [169,170] Our group previously demonstrated that applying such a strategy by using retinoic acid (RA)-loaded microspheres led to high levels of neuronal differentiation for hiPSC-derived cell aggregates. [171] Such homogeneous cell populations serve as a potential platform for *in vivo* studies to promote recovery and regeneration of cells affected by neurological disorders such as SCI. [171]

The SC, the most caudal component of the CNS, receives sensory information and contains motor neurons (MNs). These cells control voluntary muscle activity by conducting information from the CNS to the rest of the body through the ventral horn of the SC. [18,172] The ascending and descending tracts of the nervous system are disrupted during traumatic SCI, causing major motor and sensory impairments to the patient. [31] In addition to cell death due to the primary injury, the resulting inflammatory response produces an unfavorable environment for regeneration and disrupts the ionic balance of the surrounding tissue, which creates a secondary and irreversible injury. [173,174] The secondary injury can occur within minutes, day or weeks, and it is characterized by events such as inflammation, ischemia, apoptosis, free radical production, and demyelination. [22,24] Furthermore, astrocytes surround the injury site, becoming reactive and forming a glial scar that serves as a physical barrier to regeneration. [31,173,175] Thus, inducing axonal sprouting remains a major challenge when repairing the injured SC. Transplanting engineered neural tissues at the site of injury can potentially improve function by bridging the injury site to re-establish connectivity. [172]

Accordingly, research has focused on deriving MNs by exposing human pluripotent stem cells (PSCs) to the morphogens RA and sonic hedgehog (SHH) as these factors pattern the SC during development. [51,65] Puro, a hydrophobic small molecule agonist of the protein smoothened (SMO), induces SHH signaling, which generates oligodendrocyte transcription factor 2 (Olig2) – expressing progenitor cells that can become post-mitotic MNs that express the protein homeobox 9 (HB9) and the transcription factor Islet1 (ISL-1). Thus, puro serves as a cost effective alternative to SHH when engineering neural tissue. [65] Also, it is less sensitive to the microsphere fabrication process where the use of organic solvents can denature proteins like SHH. Additionally, puro treatment can generate functional MNs from hiPSCs when cultured in a 3D microenvironment – making it a powerful tool for stem cell engineering. [176] However, no previous studies have characterized biomaterial-based systems for generating controlled release of puro – which we address in this work.

The purpose of this study was to generate neural tissues containing motor neurons by combining novel morphogen releasing microspheres with hiPSCs. Our drug delivery system addresses the shortcomings of currently existing protocols which rely upon frequent media changes that results in heterogenous cell populations. Although mechanical cell sorting can address the issue of heterogeneity in existing protocols, these methods require 3 to 4 additional weeks of *in vitro* culture, along with the added costs of cell sorting reagents and equipment. [65] Drug-releasing hydrogels can deliver morphogens in an autonomous fashion *in vivo*, but they only deliver morphogens to the outer layers of the cells aggregates embedded inside. [54] Building upon our previous work, we fabricated puro-releasing microspheres from poly ε-caprolactone (PCL), a synthetic low-cost hydrophobic polymer with excellent biocompatibility. [177] We showed for the first time the successful encapsulation and controlled delivery of the small-molecule puro. These

PCL-microspheres possessed an encapsulation efficiency (EE) of 84% ± 2.12% and they released 91 ± 1.7% of the encapsulated puro loaded over 46 days in a controlled fashion. Puro- and RA-loaded microspheres then were incorporated into hiPSC-derived cell aggregates to generate engineered neural tissues. Assessment of the differentiated cells was performed at 4 different time points using flow cytometry, immunocytochemistry (ICC), and measurements of neurite extension and branching. The microsphere-loaded neural tissues showed extensive and organized neurite outgrowth in comparison to positive controls in which soluble RA and puro were added directly to the media on a regular basis. Microsphere-loaded aggregates expressed higher levels of the transcription factor Olig2 (8.19%) in comparison to the positive control group (2.8%) on day 28 of culture. The microsphere-loaded aggregates expressed the MN related transcription factors HB9 (~24.8%) and ISL-1 expression (~2.6%) on day 35. Finally, these engineered neural tissues expressed choline acetyltransferase (ChAT) (~12.3%) on day 60, indicating the presence of mature MNs.

2.3. Results

2.3.1. Characterization of puro-encapsulated microspheres and their release kinetics

Scanning electron microscopy showed that puro encapsulated microspheres possessed an average diameter of 3.4 ± 1.17 μm and exhibited a smooth rounded morphology **(Figure 2.1-a)** similar to unloaded microspheres (average diameter previously reported as 2.24 ± 2.04 μm) (**Figure 2.1-b**). [58] The size distribution for the puro loaded microspheres is shown in **Figure 2.1-c**. Analysis determined that the encapsulation efficiency (EE) of Puro into the microspheres was 84 ± 2.12%. In comparison, 4 μg/mg (w/w, RA/PCL) RA-loaded microspheres were previously reported to have an average diameter of 3.59 ± 2.48 μm with an EE of 60.9 ± 1.9%. [171] 16% of the total puro was released in an initial burst of drug release on Day 1 followed by slow, continuous release over the remaining 45 days. 91 ± 1.7% of encapsulated puro was released by day 46 (**Figure 2.1- d**).

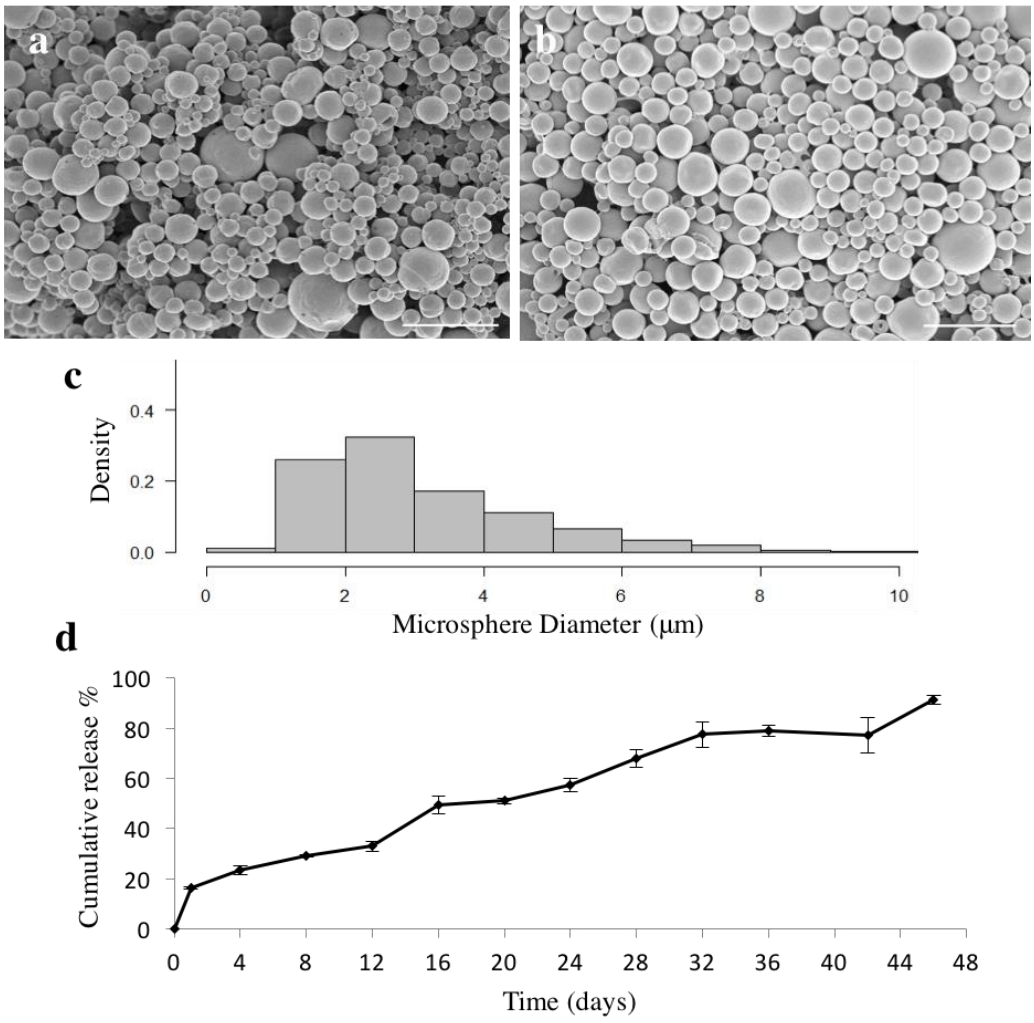

Figure 2.1 Characterization of the properties of purmorphamine loaded microspheres.

a) Scanning electron microscopy images showing shape and size of puro-loaded microspheres which have an average size of 3.4 ± 1.17 μm, n = 600, b) and blank microspheres with an average size of 2.24 ± 2.04 μm, n = 600. Scale bars are 10 μm. c) Density histogram showing the distribution of the measured microsphere diameters for purmorphamine-loaded microspheres. d) Quantification of purmorphamine release over 46 days (n = 3)– (91%) of the drug was released at the end of the time period. The data are being reported as the average with the error bars representing the standard deviation.

2.3.2. Microsphere directed differentiation of hiPSCs into functional neural tissue

Combining drug releasing microspheres with hiPSCs to generate neural tissue

A previous study treated PSCs with 0.1 µM RA beginning on day 10 followed by 1 µM puro from day 15 on. [65] Our lab tested different ratios for the combination of both drug-loaded microspheres on the differentiation of hiPSCs into MNs with a 2:1 ratio of puro/RA microspheres showing the most promising results for differentiation of hiPSCs into neurons as indicated by staining for the early neuronal marker β-tubulin III (βT-III). The positive control aggregates were initially treated with 2 µm RA and 1 µm puro for as previously reported, [65] followed by a decrease over time to simulate the amount of drug being released from the microsphere group. Each group of aggregates was represented by a letter: positive control (P), negative control consisting of untreated aggregates (N), aggregates combined with unloaded microspheres (U), and aggregates combined with puro/RA loaded microspheres (M). The appearance of microspheres was evident in the U and M groups after one day in the AggreWell™ 800 plate. Consequently, U and M aggregates were larger than N and P aggregates by day 7 **(Figure 6.1- Appendix B)**.

Figure 2.2 shows qualitative images of neurite growth and extension for all groups after 35 days. These aggregates were stained for the neuron-specific microtubule marker βT-III and then imaged using an IncuCyte® automated imaging machine. M showed extensive, organized neurites (Figure 2.2-a). Conversely, N and U showed reduced, disorganized neurite growth (**Figure 2.2-b, c**). P possessed a larger aggregate area in comparison with M, and exhibited long, organized neurites (**Figure 2.2-d**). Quantitative analysis of neurite growth and branching was performed using the NeuroTrack and Basic Analyzer configuration software on days 15, 28, and 35 on an IncuCyte ZOOM® live-cell imaging system **(Figure 2.3)**. U showed the greatest neurite growth and branching per aggregate area on day 15 in comparison with P (**Figure 2.3-a**). P and M had developed greater neurite outgrowth and branching per aggregate area than N and U by day 28 (**Figure 2.3-b**). This trend continued on day 35, where statistically significant differences in

neurite branching per aggregate area were observed between P in comparison to the U and N groups (**Figure2. 3-c**).

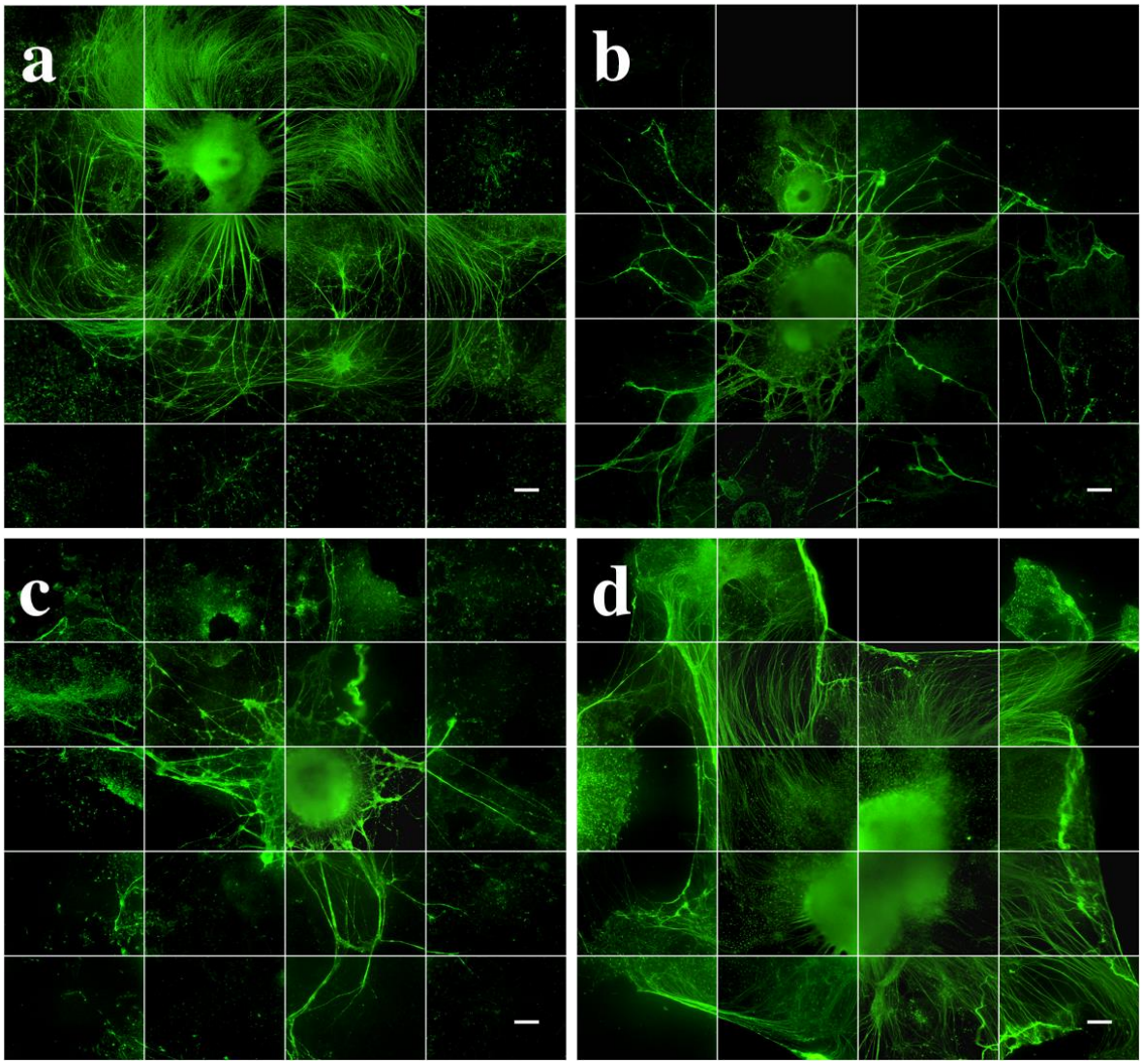

Figure 2.2 Neurite growth extension after 35 days *in vitro* for neural aggregates.
All groups (n=3, with 1-5 aggregates per well) were stained for β-tubulin III (βT-III neuronal marker, green. a) puro/RA-loaded-microspheres (M), b) unloaded microspheres (U), c) negative control (N) and d) positive control (P). Images are made into montages with Image J software from 36 images taken by an IncuCyte automated imaging machine. Scale bars represents (300 μm).

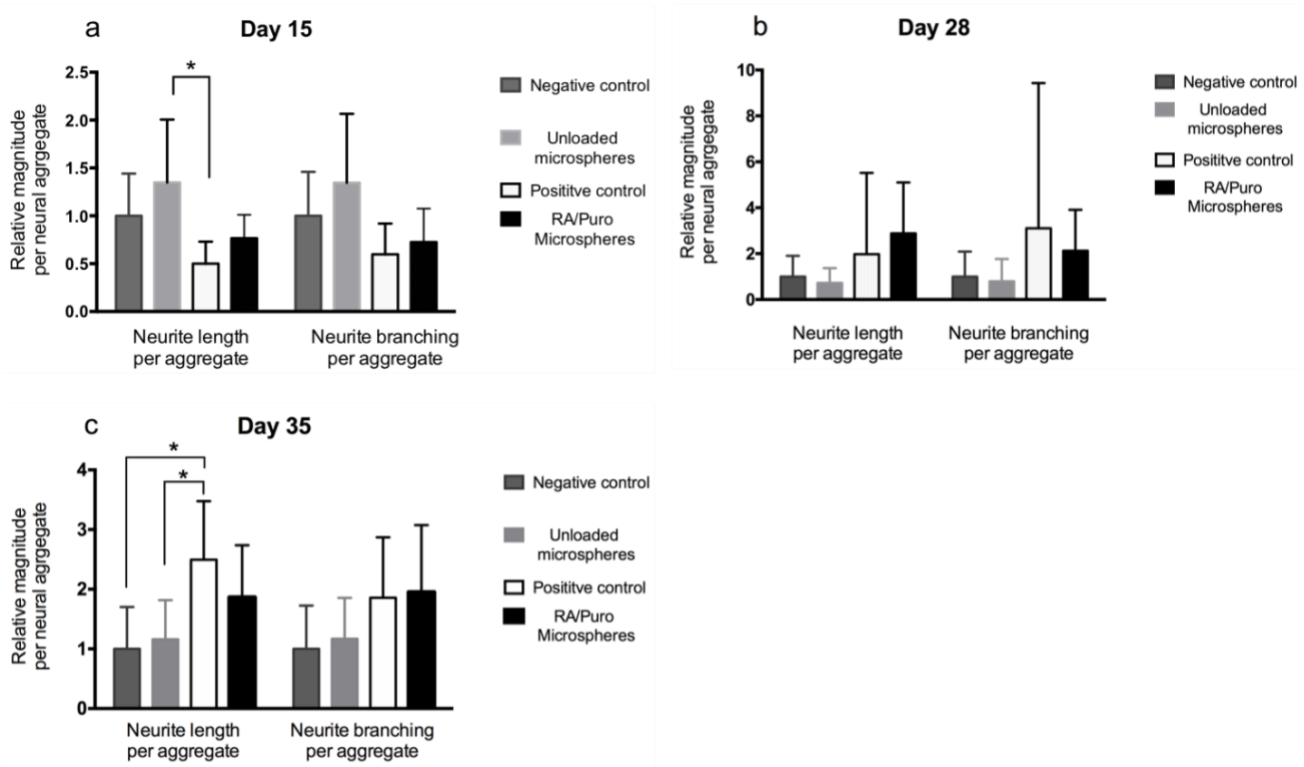

Figure 2.3 Quantitative analysis of neurite extension and branching was quantified by IncuCyte® Neurotrack software by Essen BioScience.

After a) 15, b) 28 and c) 35 days of differentiation in vitro for all groups. n=6, with each replicate consisting of 1-5 cell aggregates. Aggregates from N were used to normalize the data against U, P, and M groups. The data being reported as the average with the error bars representing the standard deviation. One-way ANOVA and Tukey post-hoc analysis was performed for statistical analysis using a confidence level of 95% ($p<0.05$). * for $p<0.05$.

2.3.3. Analysis of protein expression in Day 15 cultures

ICC was performed on all cultures at day 15 for βT-III, stage-specific embryonic antigen-4 (SSEA-4, pluripotency marker) and counterstained with 4',6-Diamidino-2 Phenylindole (DAPI, nucleic acid marker). βT-III expression was expressed in all the conditions **(Figure 2.4-b, f, j, n)**. Neurite growth and extension was prominent in P and M. SSEA-4 was expressed in N, U and M. P did not show SSEA-4 expression (**Figure 2.4-c, g, k, o**). On day 15, aggregates were also stained for the paired box protein (PAX6, neuroectoderm marker) and Nestin (neural progenitor marker) with all the conditions being negative for these markers (data not shown). Flow cytometry was performed at the same time point to quantify cell marker expression. The expression of SOX-2 (neural progenitor marker) and SSEA-4 was quantified for all conditions (**Figure 2.4- q, r**). P showed an increased expression of SOX-2 (16.61 ± 0.26 %).

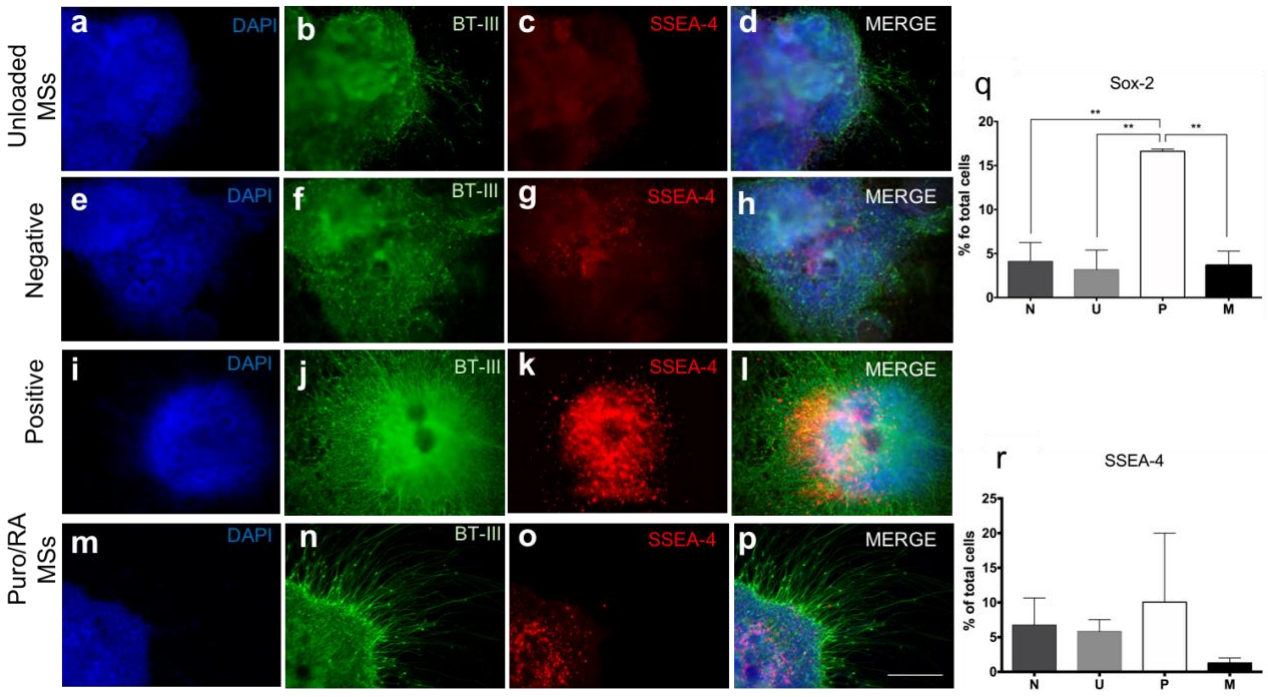

Figure 2.4 Analysis of neural cell cultures and engineered neural tissues after 15 days of differentiation *in vitro.*

All groups (n=3) were stained for β-tubulin III (βT-III neuronal marker, green), SSEA-4 (pluripotency marker, red), and DAPI (nuclear stain, blue). a-d) Cell aggregates combined with unloaded microspheres (U), e-h) negative control (N - untreated), i-l) positive control (P - soluble puro/RA), and m-p) engineered neural tissues containing puro/RA loaded-microspheres. q-r) Quantification of cell marker expression with flow cytometry after 15 days of differentiation in vitro. Each condition was represented by a letter; Positive (P), Negative (N), aggregates combined with unloaded microspheres (U), and aggregates combined with puro/RA loaded microspheres (M). All groups were stained for Sox-2 (pluripotent cells and undifferentiated cells in the neural epithelium) and SSEA-4. n=3 for all conditions. The data being reported as the average with the error bars representing the standard deviation. One-way ANOVA and Tukey post-hoc analysis was performed for statistical analysis using a confidence level of 95% ($p<0.05$) and 99.9% ($p<0.001$). *for $p< 0.05$, ** for $p< 0.001$. Scale bar represents (300 μm).

2.3.4. Analysis of protein expression in Day 28 cultures

Cell aggregates were stained for βT-III, NeuN (a mature neuronal nucleus marker), and counterstained with DAPI on day 28 **(Figure 6.2- Appendix B)**. All conditions showed significant amounts of neurite growth as visualized by βT-III expression (**Figure 6.2-b, f, j, n- Appendix B**). P showed dense and organized neurites while M showed thinner, organized neurites. By comparison, neurites formed in N and U appeared disorganized. NeuN expression was positive for all conditions (**Figure 6.2-** c, g, k, o). In addition, cell aggregates were stained for Olig2 and HB9 (mature MN marker) on day 28 **(Figure 2.5)**. Qualitative Olig2 expression was negative for N and U, slightly positive for M with high expression for P cultures. Slight HB9 expression was observed for the M and P groups. Quantitative marker expression was performed for SSEA-4, βT-III and Olig2 as well (**Figure 2.5-q-r**). SSEA-4 expression was negligible for all groups. Expression of βT-III was observed for all groups. The quantitative expression of Olig2 for M was 8.19 ± 7.99 % with no statistical differences observed.

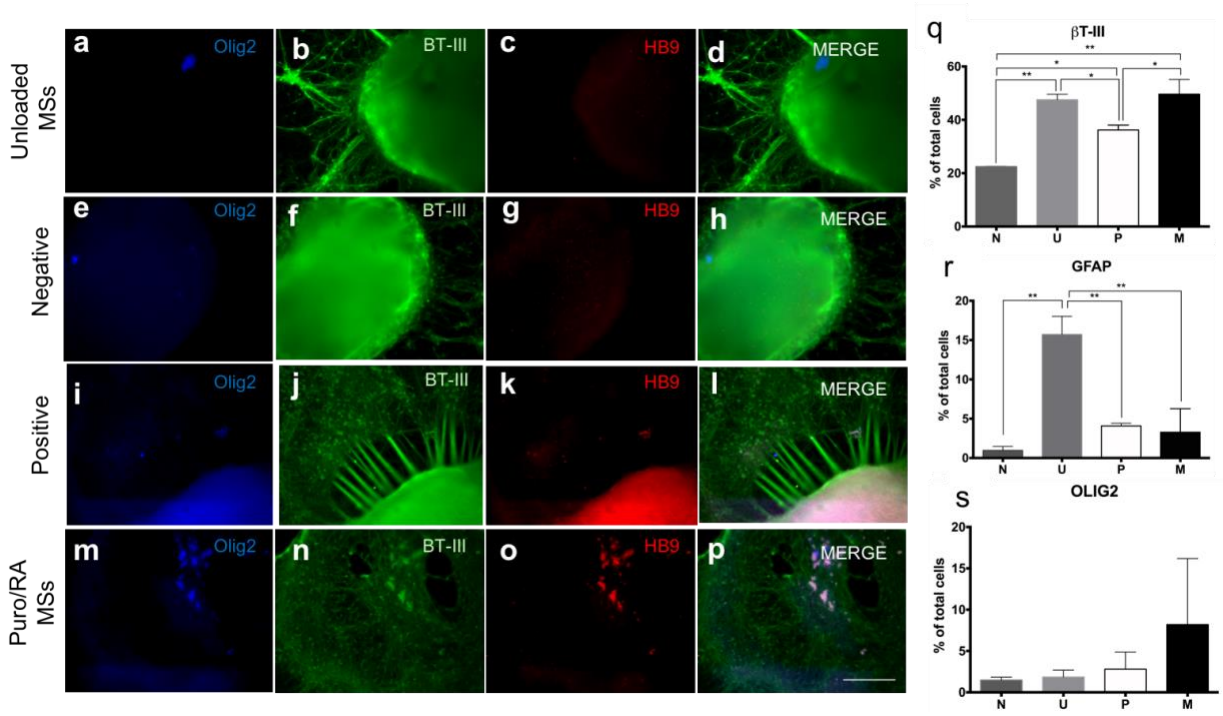

Figure 2.5 Analysis of neural cell cultures and engineered neural tissues after 28 days of differentiation *in vitro.*

All groups (n=3) were stained for Olig2 (oligodendrocyte transcription factor 2, blue), β-tubulin III (βT-III neuronal marker, green), HB9 (Motor neuron marker, red). a-d) Cell aggregates combined with unloaded microspheres (U), e-h) negative control (N - untreated, i-l) positive control (P - soluble puro/RA), and m-p) engineered neural tissues containing puro/RA loaded-microspheres (M). q-s) Quantification of cell marker expression with flow cytometry after 28 days of differentiation in vitro. All groups were stained for βT-III, GFAP (astrocyte) and Olig2 (oligodendrocyte transcription factor 2). n=3 for all conditions. The data being reported as the average with the error bars representing the standard deviation. One-way ANOVA and Tukey post-hoc analysis was performed for statistical analysis using a confidence level of 95% ($p<0.05$) and 99.9% ($p<0.001$). * for $p<0.05$, ** for $p< 0.001$. Scale bar represents (300 μm).

2.3.5. Analysis of protein expression in Day 35 cultures

Expression of Olig2, βT-III, and Syn1 (presynaptic marker) was analyzed using ICC **(Figure 2.6).** The expression of Olig2 was slightly positive for P and negative for the other groups. Syn1 staining was negative for all conditions. βT-III expression was observed in conjunction with neurite outgrowth for all conditions. U exhibited the least neurite growth extension and no organization. P and M show extensive and organized neurites **(Figure 2.6-b, f, j, n).** Quantitative expression of Olig2, HB9 and ISL-1 (mature MN marker) on day 35 was analyzed using flow cytometry. Increased expression of Olig2 (8.83 ± 3.84%) was observed for P in comparison with day 28. M showed similar levels of Olig2 expression on days 28 and 35. The P group showed enhanced levels of HB9 on day 35 in comparison to other groups. The N group showed a higher expression of ISL-1 (6.4 ± 2.86) by day 35 **(Figure 2.6-s**) in comparison to other groups.

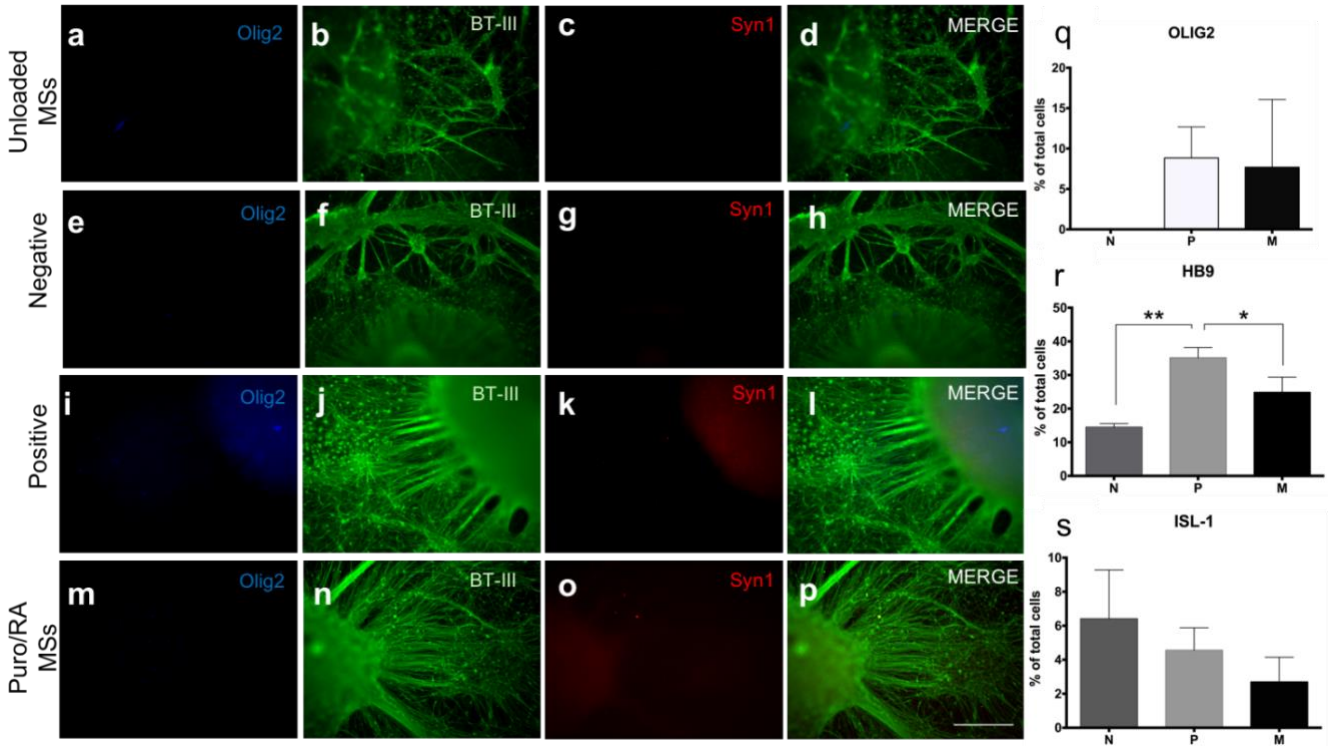

Figure 2.6 Analysis of neural cell cultures and engineered neural tissues after 35 days of differentiation *in vitro.*

All groups (n=3) were stained for βT-III (green), Syn1 (synapsin, red), and Olig2 (blue). a-d) Cell aggregates combined with unloaded microspheres (U), e-h) negative control (N - untreated), i-l) positive control (P - soluble puro/RA), and m-p) engineered neural tissues containing puro/RA loaded-microspheres (M). q-s). Quantification of cell marker expression with flow cytometry after 35 days of differentiation in vitro. All groups were stained for Olig2, HB-9 (motor neuron) and ISL-1 (motor neuron). n=3 for all conditions. The data being reported as the average with the error bars representing the standard deviation. One-way ANOVA and Tukey post-hoc analysis was performed for statistical analysis using a confidence level of 95% ($p<0.05$) and 99% ($p<0.01$). * for $p<0.05$, ** for $p< 0.01$. Scale bar represents (300 μm).

2.3.6. Analysis of protein expression in Day 60 cultures

The expression of mature neural markers, O4 (oligodendrocyte marker), and ChaT (MN neurotransmitter marker), were quantified on day 60 **(Figure 2.7)**. ChAT expression was similar for P (12.63 ± 8.74) and M (12.35 ± 4.17). O4 and Sy38 expression were negligible for all groups.

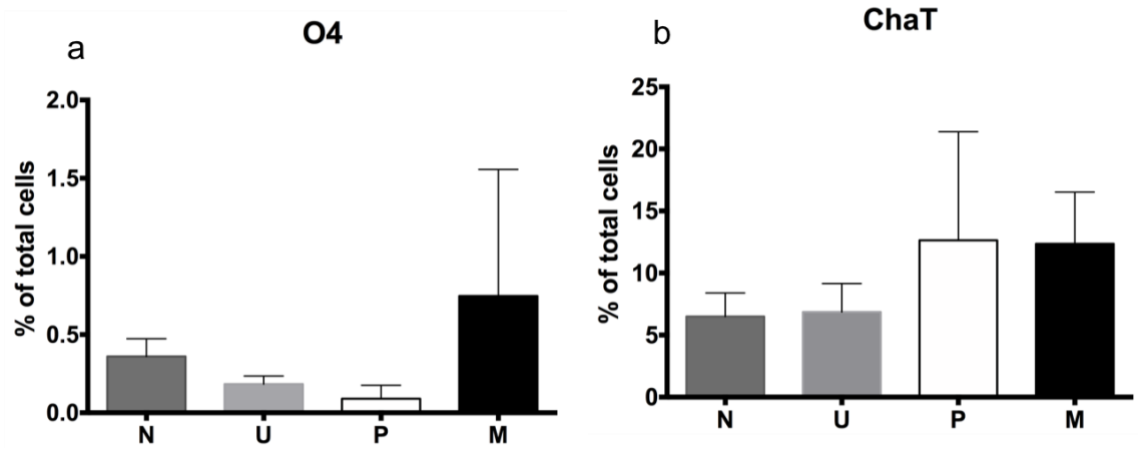

Figure 2.7 Quantification of cell marker expression with flow cytometry after 60 days of differentiation *in vitro.*
All groups were stained for a) O4 (oligodendrocyte marker O4), and b) ChAT (Choline Acetyltransferase). Data is reported as the mean with the error bars representing the standard deviation. n=3 for all conditions. One-way ANOVA and Tukey post-hoc analysis was performed for statistical analysis using a confidence level of 95% ($p<0.05$) and 99.9% ($p<0.001$), * for $p< 0.05$, ** for $p< 0.001$.

2.4. Discussion

In this study, we successfully encapsulated the small molecule puro in microspheres capable of generating its sustained release over 46 days for the first time. These microspheres were then incorporated into a novel microsphere-based protocol for the efficient derivation of MNs from hiPSC aggregates. Compared to previous methods, this protocol avoids selection steps and allows for the sustained release of puro, lowering the amount of drug required. The EE of puro into the microspheres (84%) was higher than previously reported of other encapsulated drugs like RA (60.0%) [171] and guggulsterone (42.4%), [58] and similar to Clonazepam (72.6-95.1%) [178] and tamoxifen. [179] The average microsphere diameter size was (3.4 ± 1.17 µm), similar in size to unloaded and RA-loaded microspheres with diameters of (2.24 ± 1.04 µm) and (3.59 ± 2.48 µm) respectively. [58,171] The amount and size of microspheres serve as important parameters for the sustained delivery of morphogens when combined with cell aggregates. In particular, Carpenedo *et al*. reported that smaller microspheres in a range of (2-5 µm) allow for a better incorporation within the cell aggregates, [54] while Gomez *et al*., reported that an excessive numbers of microspheres disrupts cell-to-cell interactions required for cell survival, proliferation and differentiation. [171] The total amount of microspheres per cell aggregate used in this study was optimized previously based on aggregate formation, survival and differentiation **(Figure 6.1-Appendix B)** [58,171] The microspheres used (puro, RA, and unloaded) all fell within the ideal size range for incorporation into cell aggregates.

The release study for puro was performed over 46 days to analyze the effect of the drug and microspheres on hiPSCs when exposed for > 35 days, which is the time period reported by Zhang *et al.* for differentiating immature MNs. [180] An initial burst release of puro was observed during the first 24 hours. This initial effect often occurs when delivering small molecules from

polymeric materials, and it can be attributed to the increased surface-to-volume ratio of the small particles. [128] 68 % of the encapsulated puro was released by day 28, which was higher than the levels of RA released at the same time point (28%). By day 44, (~87%) of puro was released. 91 ± 1.7 % was released by the end of day 46 (**Figure 2.1-d**) which corresponds to 2.2 µg of puro released every day from 10 mg of microspheres. 0.3 mg of puro-loaded microspheres were added to the cell aggregates. Therefore, ~0.0748 µg of puro was released on average per day into the aggregates.

The overall release profile was linear as regression analysis gave an R_2 value of 0.95, which was similar to the observed release profile of encapsulated Taxol® in poly (L-lactic acid) (PLLA) microspheres by Liggins *et al.* [181] This response is also consistent with other studies where linear or near-linear release profiles for smaller microspheres 30-50 µm, [128,181,182] while larger microspheres of 50-100 µm generate a sigmoidal release profile as reported by Kim *et al.* [128]

For the P group, an average amount of puro of (0.38 µg) total was used per day of media change for the first 46 days of the study. Media changes were performed every day from day 0-7, followed by media changes every third day. Our differentiation method microspheres to deliver puro requires significantly smaller quantitates of puro than traditional differentiation protocols. Moreover, microsphere incorporation proves another advantage by leading to efficient differentiation similar to the protocol reported by Hu *et al.* [51] This group reported the expression of HB9+ (10-23%) from the differentiation of iPSCs after selection of neuroepithelial (NE) cells and treatment with soluble RA and SHH for two weeks. [51] In contrast, by allowing the cell aggregates to form in combination with the drug-loaded microspheres, the inside layers of these aggregates are directly exposed to the morphogens that are continuously released. Our approach

yields tissues with significant expression of HB9 after 35 days. This protocol provides an efficient method of differentiation by generating similar levels of MN marker expression with less manipulation and smaller quantities of drug. On the other hand, our P group, where only the outside layer of the cell aggregates is in direct contact with the drug, resulted in concentration gradients and less efficient differentiation as indicated by low HB9 expression.

Quantitative analysis of neurite length and branching was performed for days 15, 28 and 35. The number of branches and neurite length were larger for P and M groups on day 28. Results for neurite growth on day 35 were as expected where extensive, organized neurites extended from the cell aggregate for both P and M treatments. The length of neurites per aggregate area was larger for the P group than the M group, while neurite branching was similar for both groups. N and U groups showed lower levels of neurite length and branching. These results suggest that the constant presence of both morphogens promotes neurite branching and extension.

The positive control group P stained 10.05 ± 9.95% for SSEA-4 on day 15. Negligible levels of the pluripotency marker SSEA-4 were observed for all groups by day 28 as opposed to day 15, suggesting that the exposure and sustained release of these morphogens from day 1 contributes to induced differentiation. Elimination of undifferentiated cells is crucial for the translation of laboratory protocols into clinic. The low expression of SSEA-4 indicates the mature differentiation of the cell aggregates into neural tissues. The quantitative analysis of SOX-2 (another pluripotency marker) at this stage showed (3.62 ± 1.65 %) of total cells in the aggregates treated with M, (3.17 ± 2.21 %) of cell aggregates with U, (4.09 ± 2.16 %) for N, and (16.56 ± 0.34 %) in the P. The high expression for P could be attributed to a neuronal precursor state,

whereas similar lower levels of expression in the other groups can be attributed to a more pluripotent state on day 15. [183,184]

Unlike the results reported by Zhang *et al.,* we did not observe expression of the neural progenitor markers PAX6 and Nestin, possibly due to a difference in protocols. We used drug releasing microspheres instead of the addition of soluble morphogens to the culture media. Furthermore, neural rosettes were not selected in this study as such a selection process could not be implemented *in vivo*. Additionally, our study exposed hiPSCs to sustained release of RA and puro starting from day 1, while Zhang *et al.* added these molecules at day 10 and 15 respectively. It is hypothesized that these markers were expressed earlier during this protocol of differentiation. βT-III expression was expressed for all groups by day 28, M, P and U showed the higher levels of expression in comparison with N. In addition, the expression of the glial fibrillary acidic protein (GFAP) which is a marker expressed in astrocytes was analyzed at this time point. The levels of expression were (3.28 ± 2.98) for M, (5.16 ± 0.33) for P, (1.13 ± 0.53) for N, and (15.71 ± 2.31) for U. Other studies have shown that astrocytes can regulate the development and functional maturation of hiPSCs derived neurons. [185] However, in this study the glial population for P (5.16 ± 0.33) and M (3.28 ± 2.98) was found to be low in comparison with U (15.71 ± 2.31) that had the highest level of expression for GFAP **(Figure 2.5-r).** The lower expression of GFAP for P and M can be attributed to the constant presence of puro and RA in the media that promoted MN differentiation.

The expression of Olig2, a transcription factor expressed in MN progenitors, was also analyzed on day 28. The latter occurs when expression of the MN phenotype markers HB9 and ISL-1 upregulate and Olig2 expression levels downregulate. [65,186,187] The quantitative expression

with flow cytometry showed (8.19 ± 7.99 %) of total cells were expressing Olig2 in cell aggregates combined with puro and RA loaded microspheres. Olig2 expression is lower in comparison to the marker expression stated by Zhang *et al.*, potentially due to the differences in protocols and lack of purification steps in our method. Furthermore, the qualitative ICC expression of Olig2 appeared to be negative for all groups except for an increased expression for P and slightly for aggregates with M. By day 35, the quantitative expression of Olig2 was upregulated for P and was similar on day 28 for M and was followed by the expression of HB9 and Isl1. Zhang *et al.*, have reported 10-23% B9 positive expression from differentiated IPSCs by day 35 after the addition of RA and SHH at specific time points and several selection steps. [51] In this study, we report 24.8 ± 4.5 % of cells staining positive for HB9 for the M group. The qualitative analysis of Syn1, a protein expressed in the synaptic vesicles required for neurotransmitter release, was negative for all groups. These results are not surprising, as maturation of MN for another 3-4 weeks is required for neurotransmitter release and signal transduction. [180,188,189]

After 8 weeks of culture *in vitro*, quantification of the cell marker expression of the oligodendrocyte phenotype (O4), the myelinating support cells of the nervous system, was negligible for all groups. On the contrary, the expression of ChaT, an enzyme that catalyzes the production of the neurotransmitter acetylcholine which is found in cholinergic neurons such as MNs, was expressed twice as much in M (12.35 ± 4.17 %) and P (12.63 ± 8.74 %) in comparison with other groups. Synaptophysin (Sy38), the most abundant integral membrane protein of small synaptic vesicles and an important regulator of synaptic plasticity, [188] was not expressed at this time point. These results suggest that the drug-loaded microsphere treatment has similar capabilities as the positive group to produce mature MNs derived from hiPSCs after 8 weeks of culture *in vitro*, however, further maturation might be required for the expression of Sy38. In the

future, the expression of ChaT and Sy38 as well as the electrical activity of mature MNs differentiated with puro and RA loaded microspheres can be analyzed in both monoculture and as a co-culture in a substrate of myoblast cells as suggested by Zhang *et al.* to demonstrate their ability to form functional neuromuscular junctions.

The end goal of this work is to produce an engineered tissue that could be delivered as a cell therapy for treatment of SCI by combining patient derived-hiPSCs with drug loaded microspheres. In the absence of *in vitro* purification techniques, efficient derivation of the desired cell phenotype is an important limitation to *in vivo* hiPSC therapies. [190,191] For this reason, any techniques that could not be implemented *in vivo,* such as the selection of neural rosettes, were not performed in this study. We addressed this limitation by using a novel inside-out approach in which morphogens are released within the aggregates allows for efficient MN differentiation from neural aggregates. A second major limitation yet to be addressed is the immunogenicity of hiPSCs, which must be deeply understood prior to implementation of hiPSC-derived therapies. For example, Zhao *et al.*, has demonstrated differential immune responses to hiPSC-derived smooth muscle cells versus retinal pigmental epithelial cells, suggesting that immunogenicity of other hiPSC-derived phenotypes may vary between cell lines. [192]

Another potential use for these drug-loaded microspheres is the differentiation in both 2D culture and in 3D printed tissues, which would avoid the laborious work of frequently adding the soluble morphogens in the media. Our novel puro loaded microspheres could be incorporated in bioinks used during 3D printing of tissue. 3D bioprinting has the potential to make TE automated and replicable while minimizing human intervention. These 3D printed neural tissues can be used as drug screening tools and to create physiologically relevant disease models.

2.5. Conclusion

We have developed and characterized the first biomaterial-based system for controlled release of the small molecule puro. We then successfully incorporated a mixture of puro and RA loaded microspheres into hiPSC aggregates that differentiated efficiently into mature motor neurons. This work confirms the value of drug-releasing microspheres as a tool for engineering neural tissue and illustrates its potential for *in vivo* applications. Such microspheres can also be used as an alternative to constantly adding soluble puro during media changes when performing neural differentiation of PSCs *in vitro*. Future work includes evaluating these engineered tissues *in vivo* as way of promoting regeneration in a pre-clinical model of SCI.

2.6. Experimental Section

2.6.1. Fabrication of small molecule releasing microspheres

Microspheres were fabricated using a single emulsion oil-in-water (o/w) protocol followed by the evaporation of the organic solvent dichloromethane (DCM) (Fisher Scientific) as previously described. [171]A poly(vinyl alcohol) (PVA) solution (2%) (Mw ~13,000-2,3000, Sigma-Aldrich) was made as previously described. [58] Briefly, PVA was dissolved in de-ionized water at 50 ºC constantly stirring with a magnetic stir bar. PCL (321 mg) (Mn ~45,000, Sigma-Aldrich) was dissolved in (3 mL) DCM in a (25 mL) Erlenmeyer flask on a Corning PC-420D magnetic mixer for 15 minutes at 900rpm. An adapted stopper covered with PTFE tape (TaegalSeal) was placed on top of the flask to avoid evaporation. Puro stock solution was prepared by diluting the drug in 100% ethanol to make a stock concentration (190.2 μM) (Cayman Chemical). Before adding the drug, the stock solution was warmed up to room temperature, the drug was added (0.3mg) to the oil phase to make the final concentration (0.93 μg/mg) of microspheres (w/w, puro/PCL). After the addition of the drug, 2% PVA (3 mL) was added to the oil phase, the solution was then emulsified on a vortex mixer for 30 seconds at maximum speed. Once emulsified, the solution was delivered into the water phase at 35ºC and stirred at 500rpm for 4 hours. The solution was centrifuged at 3000 rpm (Eppendorf 5810R) and washed with de-ionized water to collect the microspheres. The pellet was and frozen at -20 ºC and then lyophilized. RA-loaded and unloaded microspheres were prepared as previously described. [58,171]

2.6.2. Microsphere characterization using scanning electron microscopy

Microsphere characterization of size and shape was performed using the Hitachi S-4800 FE scanning electron microscope (SEM) as done previously. [58,171]The microspheres (0.1 mg) were placed into a microtube with 100% ethanol (50 μL) and mixed vigorously with the vortex mixer.

The solution was placed on the SEM stub mount (2 μL). The sample was coated using a gold-palladium using the Anatech Hummer VI sputter coater. Images were obtained with an accelerated voltage of (1.0 kV) and a working distance of (8 mm). The microspheres' size was determined using ImageJ software - version 1.48. A minimum of 600 microspheres were analyzed for each batch of microsphere characterization. The density plot of microsphere data was produced using R studio software.

2.6.3. Determination of encapsulation efficiency and characterization of controlled release of purmorphamine

A 46-day release study was performed to determine the release kinetics of puro. Each sample of microspheres (10 mg) and (1 mL) PBS was placed on microtubes (1.5 mL, Axygen). Samples for each day of collection (n=3) were placed on a VWR® mini shaker at 330 rpm at 37 °C and were collected every 4 days. After collection samples were washed with de-ionized water and freeze dried for further analysis. The drug was extracted from the microspheres and then quantified with high-performance liquid chromatography (HPLC) to estimate puro concentration in the microspheres. 10 mg of microspheres were placed in microtubes (1.5 mL) by triplicate. To melt the microspheres, 250 μL of acetonitrile (ACN) was added and mixed with the vortex mixer at 3000 rpm for 30 seconds (Caledon Laboratory Chemicals). The samples were then placed on the vortex mixer (Eppendorf ® MixMate®) at 2500 rpm for 5 minutes. 250 μL ACN was added to the sample followed by the same mixing procedure to obtain a final volume of 500 μL. The samples were then placed at -80 ºC for 5 minutes, followed by centrifugation (Eppendorf 5424) at (1500 rpm) for 5 minutes. The samples were filtered using 0.2 μm PTFE syringe filters (Thermo Fisher Scientific) before adding the supernatant to amber vials (Agilent). HPLC was performed using an Agilent 1200 equipped with quaternary pump and diode-array detector (DAD) to quantify the amount of puro present in samples. A standard of puro with eleven dilutions of a stock solution

diluted in ACN was used to determine the concentrations of the samples. The column used was an Eclipse Plus C18 (Agilent) with 5 μm particle size, 4.6 mm internal diameter (ID) and was 150 mm long with similar phase and ID guard column. Samples were analyzed at 300 nm after determination of the spectrum of puro with mass spectroscopy. Mass spectral information was acquired using an Ultimate 3000 HPLC system connected to an Orbitrap (Thermo Fisher Scientific). The system was used in direct infusion mode with no separation. Solvents used for this analysis were HPLC grade ACN mixed with water dispensed from a Milli-Q integral purification system (Millipore, ON, Canada). Both contained 0.1 % (V/V) Trifluoroacetic acid (TFA) (Fisher Scientific). Runs were done isocratic at a 70 %: 30 % ratio respectively with and injection volume of (20 μL), flow rate of (1 mL/min) at 21ºC. ChemStation software was used for data analysis with auto-integration adjusted manually when needed. EE was determined as previously described [58] by comparing the amount of puro encapsulated ($P_{encapsulted}$) to the amount of drug initially added ($P_{theoretical}$) .

2.6.4. hiPSC culture and formation of engineered tissues

Experiments using hiPSCs were conducted with the approval of the University of Victoria's Human Ethics Committee under protocol number: 12–187. hiPSCs (iPS(Foreskin)-1, Lot 1-DL-01, WiCell) were cultured in 6-well plates coated with Vitronectin XF™ in the presence of E8™ medium (STEMCELL Technologies) until 80% confluency was reached as previously described. [193]Eleven confluent wells were used for the formation of uniform cell aggregates in AggreWell™ 800 plate (STEMCELL Technologies) as previously described. [58] Four conditions were tested; unloaded microspheres, 2:1 Puro/RA microspheres, negative control group, and positive control group 2:1 Puro/RA soluble drugs added from day 1. For the microsphere groups, a total of (0.5 mg) of microspheres was suspended in STEMdiff™ NIM (STEMCELL

Technologies) and were incorporated into the aggregates to make a total volume of (2 mL) per AggreWell™ 800 well. Negative group cultures contained no microspheres, nor soluble drug. Positive group cultures contained final puro concentration of (1 μm) and (0.5 μm) RA. Media changes were performed by replacing (1.5 mL) of STEMdiff NIM with 1% Penicillin Streptomycin (PenStrep) (Sigma-Aldrich) every day until day 7. On day 7, cell aggregates were transferred to each well of a poly-L-ornithine (PLO)/laminin coated 24-well plate (Sigma-Aldrich). The number of cell aggregates in each well ranged from 2 to 5. Cell aggregates were cultured in (1mL) STEMdiff™ NIM and media changes were performed every third day by replacing (500 μl) with fresh media. By day 16, puro and RA concentrations for the positive group were decreased to (0.5 μm) and (0.25 μm) respectively. BrainPhys™ Neuronal Medium (STEMCELL Technologies) gradually replaced STEMdiff™ NIM and by day 25 each well contained 100% BrainPhys™ Neuronal Medium. In order to promote MN differentiation BrainPhys™ was supplemented with N2(1%), B27(1%), cyclic-AMP (c-AMP) (1μM), Ascorbic acid (AA) (200ng/ml) (Sigma-Aldrich), BDNF(10ng/ml), GDNF(10ng/ml), IGF-1(10ng/ml) (Peprotech), and PenStrep(1%). [51]

2.6.5. Analysis of cell cultures using flow cytometry

Cell marker expression was quantified with flow cytometry on days 15, 28, 35 and 60. Aggregates were enzymatically dissociated with (0.125 %) trypsin-EDTA (Fisher Scientific) for 2 minutes at 37 ºC followed by the addition of TNS (ScienCell). The resulting cells were washed three times by adding PBS (Invitrogen) and centrifuging at (600 g) for 5 minutes. The cells were then fixed and stained per the manufacturer's instructions (R&D systems). Expression of SSEA-4 (pluripotency marker) (FAB1435, R&D) and SOX-2 (pluripotent cells and undifferentiated cells in the neural epithelium) (IC2018P, R&D), was evaluated on day 15. Expression of βT-III

(IC1195C, R&D), GFAP (astrocyte marker) (NBP2-33184PCP, Novusbio), and Olig2 (MN progenitor marker) (IC2230P, R&D), was evaluated on day 28. Flow cytometry was performed to evaluate expression of Olig2, HB9 (mature MN) (bs-11320R, Bioss antibodies) and ISL-1 (mature MN) (562547, BD Pharmingen™) on day 35. Expression of O4 (FAB1326P, R&D), ChAT (ab2803, Abcam) and Sy38 (ab8049, Abcam) was evaluated on day 60. Isotype controls for flow cytometry consisted of Mouse IgG_1 Fluorescein-conjugated Antibody (IC002F), Mouse IgG2A PerCP-conjugated Isotype Control (IC003C), Normal Mouse IgM PE-conjugated Control (IC015P) (R&D Systems) and Isotype Control (ab91366, Abcam).

2.6.6. Analysis of cell cultures using immunocytochemistry

Cell cultures and engineered tissues were stained for various markers according to the ICC protocol previously published. [58,130,193,194] (**Table S1)**[d] shows the antibodies, catalogue number, vendor and dilution used for ICC analysis on days 15, 28 and 35. Cell aggregates were stained for βT-III (1:500), SSEA-4 (1:250), PAX6 (1:500, neural precursor marker) and Nestin (1:500, NSC marker) on day 15. On day 28 the cell aggregates were stained for βT-III (1:500), NeuN (1:1000), HB9 (1:1000), Olig2 (5ug/ml). ICC was performed using βT-III (1:500), Syn1 (1:200), Olig2 (5ug/ml), and HB9 (1:100) on day 35. All the primary antibodies were diluted in 5% normal goat serum (NGS) blocking solution (Sigma-Aldrich) and incubated overnight. Cells were then washed three times with PBS and incubated with the secondary antibodies for 4 hours at room temperature. Finally, the cells were washed three more times and counterstained with DAPI (nuclear stain) with a 3-minute incubation at room temperature. Cell cultures were imaged with a Leica DMI3000 B microscope using a XCite Series 120Q fluorescent light source and QImaging RETIGA 2000R

[d] Table S1 is available as supplemental information from the original publication: De la Vega L, Karmirian K, Willerth SM. **Engineering Neural Tissue from Human Pluripotent Stem Cells Using Novel Small Molecule Releasing Microspheres.** Advanced Biosystems 2018.

camera with 100X magnification. Captured images were done using QCapture Software 2.9.12. Composite images were created using the image-processing program ImageJ with the Magic Montage tool. [58]

2.6.7. Analysis of the morphological properties of engineered tissues:

Neurite growth and branching metrics were performed using the IncuCyte® ZOOM (Essen BioScience) automatic live-cell imaging system as previously reported. [58,171] The cells were imaged by an IncuCyte ZOOM®, and these images were processed using a software module called NeuroTrack™ that uses an algorithm to mask and analyze neurite length and branching. It has been validated for a variety of neuronal types with a sensitivity equivalent to that of an immunofluorescence-based, high content imaging assay. The NeuroTrack™ software module was used to process the images, previously stained with βT-III, on days 15, 28 and 35. For day 15 cultures, neurite aggregate analysis was performed using the Basic Analyzer processing definition. Briefly, a processing definition was created for the analysis by selecting a collection of images taken at the same magnification (10X). The settings for adjusting the proper segmentation for the cell body cluster area were first customized for each of the images selected from the image collection. Appropriate parameters were adjusted to differentiate cells from the background of the phase image. These settings were used to mask the entire neural aggregate body (center of sphere where neurites extend outward from). By masking this region as cell body cluster area, the algorithm calculates the neurite extension start point from the neural aggregate body. Neurite mask parameters were defined by adjusting the neurite sensitivity and preventing background noise and debris for every image of the image collection. For day 28 and 35, the processing definition was created by adjusting thresholds to mask the cell body cluster area and selecting the green fluorescence channel to visualize neurite labelling (βT-III). Once all the images were

previewed, the processing definition was saved, and the metrics of average neurite length and branch points were recorded. A collection of 36 images per well was taken and the creation of the montage was done with Image J.

2.6.8. Statistics

All data is reported as the mean ± standard deviation of the mean. Puro EE and release study results (n=3), microsphere size (n=600), flow cytometry and ICC (n=3), neurite extension and branching (n=6) with 1-5 cell aggregates per well. Cell aggregates from N were used to normalize the data against U, P, and M groups for the quantitative analysis of neurite extension and branching. Statistical significance was assessed using one-way ANOVA followed by Tukey's post-hoc analysis with confidence levels of 95 % ($p<0.05$) and 99.9 % confidence ($p<0.001$). Statistical analysis for puro EE and release study results was performed using Microsoft® Excel. The density plot of microsphere data was produced using R studio software. Flow cytometry data was obtained using the Guava® Incyte software and the statistical analysis was performed using GraphPad prism 6 statistics software. Statistical analysis for neurite growth and branching was also performed using GraphPad prism 6 statistics software.

Chapter 3 3D Bioprinting Human Induced Pluripotent Stem Cell-Derived Neural Tissues Using a Novel Lab-on-a-Printer e

Laura de la Vega [1], Diego Rosas Gomez [2], Emily Abelseth[3], Laila Abelseth[3], Victor Alisson da Silva[4], Emily Abelseth[3], and Stephanie M. Willerth [1,3,5,]*

[1] Department of Mechanical Engineering, University of Victoria
[2] School of Bioengineering and Chemical Processes, Monterrey Institute of Technology and Higher Education, Mexico City, Mexico.
[3] Biomedical Engineering Program, University of Victoria
[4] Center for Mathematics, Computing and Cognition, Federal University of ABC, São Bernardo do Campo, Brazil.
[5] Division of Medical Sciences, University of Victoria

Key words:

3D bioprinting; neural tissue; motor neurons; pluripotent stem cells; biomaterials; spinal cord injury; lab on a printer; fibrin

Author contribution:

De la Vega L designed, set-up, performed, and supervised experimental procedures and data analysis. Wrote, reviewed, and edited manuscript. Abelseth E. and Abelseth L. developed methodology and assisted on experimental set-up. Rosas Gomez D. and Allison da Silva D. assisted on experimental set-up, data analysis, and writing of the initial manuscript. Willerth SM. provided input into experimental design, provided feedback and supervision on the experimental analysis, as well as editing on the manuscript.

[e] The following chapter is from: De la Vega L, Rosas Gomez D, Abelseth E, Abelseth L, Alisson da Silva V, Willerth SM. **3D bioprinting human induced pluripotent stem cell-derived neural tissues using a novel Lab-on-a-Printer technology**. *Applied Science* 2018 In press.

3.1. Abstract

Most neurological diseases and disorders lack true cures, including spinal cord injury (SCI). Accordingly, current treatments only alleviate the symptoms of these neurological diseases and disorders. Engineered neural tissues derived from human induced pluripotent stem cells (hiPSCs) can serve as powerful tools to identify drug targets for treating such diseases and disorders. In this work, we demonstrate how hiPSC-derived neural progenitor cells (NPCs) can be bioprinted into defined structures using Aspect Biosystems' novel RX1 bioprinter in combination with our unique fibrin-based bioink in rapid fashion as it takes under 5 min to print four tissues. This printing process preserves high levels of cell viability (>81%) and their differentiation capacity in comparison to less sophisticated bioprinting methods. These bioprinted neural tissues expressed the neuronal marker, βT-III (45 ± 20.9%), after 15 days of culture and markers associated with spinal cord (SC) motor neurons (MNs), such as Olig2 (68.8 ± 6.9%), and HB9 (99.6 ± 0.4%) as indicated by flow cytometry. The bioprinted neural tissues expressed the mature MN marker, ChaT, after 30 days of culture as indicated by immunocytochemistry. In conclusion, we have presented a novel method for high throughput production of mature hiPSC-derived neural tissues with defined structures that resemble those found in the SC.

3.2. Introduction

Spinal cord injury (SCI), a neurological disorder that disrupts communication within the central nervous system (CNS), can lead to impaired function [195]. The World Health Organization (WHO) reports 250,000–500,000 new cases annually, with the majority (90%) being caused by traumatic lesions to the spinal cord (SC) [196]. The economic burden of SCI in Canadian patients ranges from $1.5 million to $3 million per patient, depending on the type of injury. These lesions can result from car crashes, violence-related wounds, and recreational activities [197]. The type of injury determines the effects on essential bodily functions performed by the motor, sensory, and autonomic systems, which can lead to movement impairment and deficiencies in the somatosensory system [197,198]. Furthermore, SCI increases the risk of developing diseases, such as multiple sclerosis [199].

Currently, no cure exists for SCI, so treatment methods focus on rehabilitation, reduction of pain and swelling, and pharmacological interventions. Cox et al. reported research on possible pharmacological treatments for different aspects of SCI in 2015. These treatments include Oxycyte, which provides oxygen to the injury site, reducing apoptosis [200]. Furthermore, the inhibition of the nuclear transcription factor, NF-Kβ, may reduce inflammation, and the antibiotic, Minocycline, has shown promising results in decreasing apoptosis in animal models [200]. The steroid, methylprednisolone, was used to treat acute SCI, but the side effects outweighed the benefits and its use has been discontinued [195]. One reason for the lack of effective treatments stems from the fact that the current tools for assessing promising drug targets for treating neurological disorders, like SCI, do not accurately predict toxicity and efficacy. Thus, the field of TE has been developing new techniques and methodologies that mimic the pathophysiology and functionality of the tissue found in the spinal cord.

TE uses different combinations of cells, biomaterials, and biochemical factors to produce 3D tissues that resemble human physiology [201]. 3D models offer a significant advantage over 2D models. The 3D environments enable cells to develop into their correct morphology, resulting in more physiologically relevant function [202]. They also offer a microenvironment for encouraging cell-cell and cell-scaffold interactions, similar to how cells would develop normally in vivo [202]. Thus, tissue engineering allows us to study the cell function more precisely in vitro to determine how they would behave under the influence of certain drugs or varying physicochemical conditions.

Recent tissue engineering efforts have focused on the use of 3D bioprinting as a novel way to engineer tissues. 3D bioprinting produces 3D structures, often called constructs, using biocompatible materials known as bioinks where encapsulated cells can grow and proliferate [202]. Alternatives to 3D printing include freeze drying, gas foaming, mold casting, electrospinning, and heat compression to create a 3D structure [203]. Nevertheless, most of these methods cannot correctly mimic the necessary micro-architecture for stem cells to differentiate efficiently into neural phenotypes, as some of the aforementioned methods use toxic solvents that affect cell viability and function [203]. In order for the constructs to correctly mimic the SC tissue and serve as a pre-clinical model of SCI for drug screening applications, specific biological, chemical, and physical conditions must be met [202]. Bioprinting conditions enable the construction of favorable biochemical and mechanical environments, as well as the tunable construction of microstructures, generating an acceptable model to study SCI [203]. Nevertheless, it is important that during the printing protocol, cells remain undamaged. It has been reported that low cell viability can occur due to shear stress acting upon the cells during the printing process [202]. Parameters, such as pressure

and temperature, may inflict changes on a cell's phenotype and thus, they should be carefully managed and their effects assessed [204].

Stem cells, such as human induced pluripotent stem cells (hiPSCs), can play a huge role in understanding SCI due to their ability to self-renew and to differentiate into any cell type in our body [205,206]. Scientists can design *in vitro* lab experiments that can directly translate into clinical studies by creating patient-specific tissues [49]. Differentiation protocols for hiPSCs need to ensure the development of a homogeneous neural cell population, as it has been reported that hiPSCs develop into neurons with less efficiency and more variability than embryonic stem cells (ESCs) [205,207]. Moreover, the use of hiPSC-derived neural progenitor cells (NPCs) limits differentiation to neuron-specific cell fates. Mothe et al. reported neuroregeneration and neuroprotection after NPCs transplant in rats with SCI [205].

Another important component to take into consideration for the generation of neural tissue is the bioink to be used for printing. For this study, a novel fibrin-based bioink was used to bioprint NPCs. The use of a fibrin-based bioink promotes neuronal differentiation and survival as it is biocompatible, human derived, contains cell adhesion signaling molecules, and allows the flow of nutrients [208]. In addition, this material will enable neural differentiation as it can mimic the biochemical and mechanical environment of the SC [202]. Being a naturally-derived material, fibrin has a decreased mechanical stability and a slow polymerization process [202,208]. The polymerization of fibrin starts with the addition of the enzyme, thrombin [209]. Alginate, which polymerizes quickly, can be mixed with fibrin as a second component and make the bioink suitable for bioprinting [202]. To address the challenge of the lack of mechanical stability of fibrin scaffolds, small molecules, such as genipin, can enhance the structural properties of the scaffold and promote neural outgrowth

[209]. The cationic polysaccharide, chitosan, is the third component of the novel bioink used to provide mechanical strength to the scaffolds by ionically interacting with alginate and covalently crosslinking with genipin [17].

Inkjet, extrusion, laser-assisted, and stereolithography are the main strategies for bioprinting tissues [139,210]. However, one of the major challenges faced when using these technologies is the amount of shear stress the cells receive as they are extruded, which leads to low cell viability and lack of long term-functionality of the tissues [140]. The Lab-on-a-Printer™ (LOP) technology integrates microfluidic channels with printing technology that allows material processing prior to printing and programmable parameters to obtain specific compositions in the printed materials [211]. In this study, the RX1™ Bioprinter from Aspect Biosystems™ was used to bioprint NPCs. This bioprinter offers the possibility of printing 3D scaffolds with cell-laden bioinks where programmable patterns can be created [212]. Speed and fiber composition are regulated while printing on a layer-by-layer basis. The RX1™ uses a LOP™ microfluidic printhead that prints complex and heterogeneous structures with different cell types and materials in a reproducible manner [212]. These characteristics lead to the bioprinting of a precise design with specific micro and macro architectures while the bioink components are evenly distributed in the 3D structure. In the case of SC, it is necessary to mimic precisely the anatomical and physiological characteristics in order to develop a correct model of the disease to perform drug screening. Tuning the aforementioned characteristics will enable the differentiation of NPCs into MNs, one of the main type of neurons affected during SCI and whose functionality needs to be re-established [213].

The objective of this study was to bioprint hiPSC-derived neural tissues that matured into MNs in combination with a novel fibrin-based bioink using the RX1™ bioprinter in rapid manner.

Here, we analyze the composition of 30-day cultures of bioprinted hiPSC-derived NPCs exposed to the small molecules, CHIR99021 (CHIR), SB431542 (SB), LDN-193189 (LDN), purmorphamine (Puro), and retinoic acid (RA), to promote MN differentiation. Previous studies have demonstrated that the small molecules, SB431542 and DMH1, induce dual-SMAD inhibition, a requirement for neural pattering in stem cells [66,214]. The molecule, LDN-193189, is also a BMP inhibitor and can be used instead of DMH1 [214]. Moreover, the small molecule, CHIR99021, activates the Wnt pathway, enhancing neural patterning of pluripotent stem cells [66]. In addition, the combination of RA and puro promote pluripotent stem cell differentiation into MNs [66,215,216]. Cylindrical constructs were printed using the RX1™ bioprinter with seven layers and a 1 cm diameter in a process that took under 5 min to generate four constructs. Cell viability, immunocytochemistry (ICC), and flow cytometry studies were performed to analyze the bioprinted constructs and their differentiation into MNs.

3.3. Materials and Methods

3.3.1. Culture and Expansion of NPCs

hiPSC-derived NPCs were obtained as previously described from the hiPSC line, 1-DL-01, from WiCell [193,209]. Experiments using hiPSC-derived NPCs were conducted with the approval of the University of Victoria's Human Ethics Committee under protocol number: 12-187. Briefly, NPCs were cultured in STEMdiff™ Neural Progenitor Medium (NPM) (05834, Stemcell Technologies, Vancouver, BC, Canada) containing 1 X STEMdiff™ Neural Progenitor Supplement A (05836, Stemcell Technologies, Vancouver, BC, Canada), 1 X STEMdiff™ Neural Progenitor Supplement B (05837, Stemcell Technologies Vancouver, BC, Canada), and 1% Penicillin-Streptomycin (Penstrep) (P4333, Sigma, St. Louis, MO, USA) in 6-well cell culture plates coated with laminin (L2020, Sigma, St. Louis, MO, USA) and poly-L-ornithine (PLO) (P4957, Sigma, St. Louis, MO, USA). The cultured NPCs were maintained at 37 °C with 5% CO_2 and media change was performed on a daily basis. Once the cultures reached 80% confluence the cells were cryopreserved in liquid nitrogen.

3.3.2. Bioprinting Process

NPCs were thawed and resuspended in the bioink solution composed of 20 mg/mL of fibrinogen (341578, Sigma, St. Louis, MO, USA), 0.5% *w*/*v* of alginate (120,000–190,000 g/mol, M/G ratio 1.56) (180947, Sigma, St. Louis, MO, USA), and 0.3 mg/mL of Genipin dissolved in de-ionized water (G4796, Sigma, St. Louis, MO, USA) in tris-buffered saline). The conical tube containing the bioink and NPCs was coupled to the Material 1 channel of the LOP™ printhead (Aspect Biosystems, Vancouver, BC, Canada). The crosslinking solution contained 20 mg/mL of calcium chloride (449709, Sigma, St. Louis, MO, USA), 0.075% *w*/*v* of chitosan (C3646, Sigma, St. Louis, MO, USA), and 1.7 U/mL of thrombin (T7009-1KU, Sigma, St. Louis, MO, USA).

Cylindrical constructs of 1 cm diameter were bioprinted using the RX1 bioprinter (Aspect Biosystems, Vancouver, BC, Canada) with 7 layers of ~176 μm diameter. The cross-linking process takes a few seconds as it is initiated inside the printhead at the intersection point between the bioink and crosslinker channels shown in (**Figure 1.7)**. Specified pressures are applied to each channel, controlling the flow rate to allow enough time for the crosslinking reaction. Fibers coming out of the printhead are crosslinked before they are deposited. The printing speed was 20 mm/s and channel pressures consisted of 20 mbar for the bioink, 40 mbar for the crosslinker, and 100 mbar for buffer solution. Four structures were bioprinted simultaneously in a layer-by-layer fashion in under 5 min. **Figure 1.7** shows a schematic representation of the LOP™ printhead.

Figure 3.1 shows the bioprinted cylindrical construct. All the procedures were performed under sterile conditions. After bioprinting, the constructs were gently transferred to culture plates coated with laminin and PLO. 1.5 mL of NPM was added to each well and these cultures were incubated at 37 °C with 5% CO_2. Measurements of fiber diameters were performed using the software, Image J, after imaging with a Leica DMI3000B (Leica Biosystems, Wetzlar, Germany) microscope and QImaging RETIGA 2000R camera (QImaging, Surrey, BC, Canada) at 100× magnification. Imaging and diameter measurement of the bioprinted construct was performed using Cytation 5™ and the software, Gen5 version 3.05 (BioTek instruments, Winooski, VT, USA).

3.3.3. Culture of Bioprinted Constructs

The printed constructs were treated with a cocktail of small molecules suspended in NPM containing 1% Penicillin-Streptomycin to promote differentiation of the bioprinted NPCs into MNs. Media changes were performed every third day by replacing 750 μL with fresh media from day 1 to day 15. Table 3.1 shows the five different treatments analyzed with the combinations of

small molecules added, each treatment is represented by a letter. Treatments consisted of: (i) Negative (N+); 2 μM of SB, 2 μM of LDN and 1 μM of CHIR; (ii) Puro positive (P+); 0.5 μM of Puro, 2 μM of SB, 2 μM of LDN and 1 μM of CHIR; (iii) RA positive (R+); 0.1 μM of RA, 2 μM of SB, 2 μM of LDN and 1 μM of CHIR; (iv) Puro and RA positive (PR+); 0.5 μM of Puro, 0.1 μM of RA, 2 μM of SB, 2 μM of LDN and 1 μM of CHIR; (v) Puro and RA negative (PR-); 0.5 μM of Puro and 0.1 μM of RA [f]. Starting on day 15, concentrations of Puro and RA were 0.1 μM and 0.5 μM, respectively. By day 15, the media was gradually replaced as previously reported by BrainPhys Neuronal Medium (BP) (05790, Stemcell, Vancouver, CA) supplemented with growth factors; 10 ng/mL of GDNF 10 ng/m (450-10, Peprotech, Rocky Hill, NJ, USA), 10 ng/mL of IGF-1 (AF-100-11, Peprotech, Rocky Hill, NJ, USA), 1 μM of C-AMP (A6885, Sigma, St. Louis, MO, USA), 1% of N2 (17502048 Thermo Fisher,Waltham, MA, USA), 1% of B27 (17504001, Thermo Fisher,Waltham, MA, USA), 200 ng/mL of Ascorbic Acid (Sigma, St. Louis, MO, USA), 10 ng/mL of BDNF (450-02, Peprotech, Rocky Hill, NJ, USA), and 1% penstrep [27]. The bioprinted constructs were maintained at 37 °C with 5% CO2.

f Correction made from the original publication from: De la Vega L, Rosas Gomez D, Abelseth E, Abelseth L, Alisson da Silva V, Willerth SM. **3D bioprinting human induced pluripotent stem cell-derived neural tissues using a novel Lab-on-a-Printer technology**. Applied Science 2018 In press.

Name	Letter code	Treatment
Negative	N+	CHIR, SB, LDN
Puro	P+	Puro + CHIR, SB, LDN
RA	R+	RA+ CHIR, SB, LDN
Puro and RA	PR-	Puro and RA
Puro and RA	PR+	Puro and RA + CHIR, SB, LDN

Table 3.1 Name, letter code, and treatment for each group.

3.3.4. Cell Viability

On day 7, the constructs (n = 3) were degraded by removing culture media followed by incubation with a solution of 25 mM of Sodium Citrate (Sigma, St. Louis, MO, USA). The constructs were then placed on a shaker at 25 rpm at 37 °C. Once most of the bioink was degraded, 0.125% of trypsin-EDTA (Fisher Scientific, Pittsburgh, PA, USA) was added for 5 min followed by the addition of fetal bovine serum (FBS) (10438018, Thermo Fisher, Waltham, MA, USA). Each treatment was placed on a 15 mL conical tube and centrifuged at 300 g[g] for 5 min. Preparation of the cell suspension was performed as previously reported following the Guava ViaCount® protocol for cell viability determinations [209]. The supernatant was removed, and the pellet was resuspended in 1 mL of phosphate buffered solution (PBS) (10010023, Thermo Fisher Waltham, MA, USA). 20 µL of the cell suspension was mixed with 380 µL of Guava ViaCount reagent® (4000-0040, Millipore, Burlington, MA, USA). 100 µL were placed on each of the 96-well plate

[g] Correction made from the original publication from: De la Vega L, Rosas Gomez D, Abelseth E, Abelseth L, Alisson da Silva V, Willerth SM**. 3D bioprinting human induced pluripotent stem cell-derived neural tissues using a novel Lab-on-a-Printer technology**. Applied Science 2018 In press.

and cell viability was determined using the Guava EasyCyte HT (Millipore, Burlington, MA, USA) flow cytometer. Statistical analysis was done using one-way ANOVA followed by Tukey's post-hoc analysis using GraphPad prism 6 statistics software. Confidence levels were 95% ($p < 0.05$).

3.3.5. Flow Cytometry

Cell marker expression of the early neuronal markers, βeta tubulin-III (βT-III) ((IC1195C R&D), oligodendrocyte transcription factor 2 (Olig2) (IC2230P R&D systems, Minneapolis, MN, USA), and the protein homeobox 9 (HB9) (bs-11320R, Bioss antibodies), was quantified on day 15. The bioprinted constructs were degraded as previously mentioned using a solution of 25 mM of sodium citrate, 0.125% of trypsin-EDTA, and FBS. The resulted cell suspension was processed as previously reported [58,216]. Briefly, the cell suspension was washed three times with PBS by centrifuging at 300 g for 5 min. The cell suspension was then fixed and stained per the manufacturer's instructions (R&D systems, Minneapolis, MN, USA). Isotype controls consisted of mouse IgG2A PerCP-conjugated Isotype control (IC003C R&D systems, Minneapolis, MN, USA) and normal mouse IgM PE-conjugated Control (IC015P R&D systems, Minneapolis, MN, USA). The analysis was performed using the Guava EasyCyte HT flow cytometer (Millipore, Burlington, MA, USA). Statistical analysis was done using one-way ANOVA followed by Tukey's post-hoc analysis using GraphPad prism 6 statistics software. Confidence levels were 95% ($p < 0.05$) and 99.9% ($p < 0.001$).

3.4. Immunocytochemistry

Immunohistochemical analysis of protein expression was performed on day 30 for βT-III, choline acetyl transferase (ChaT), and glial fibrillary acidic protein (GFAP). The constructs were collected and fixed for 1 h in 4% paraformaldehyde (PFA) (AC416785000, Acros Organics, Geel,

Belgium) in PBS solution. Three washes were performed by adding fresh PBS and agitating at 25 rpm at 4 °C. The cells were permeabilized by adding 0.1% of Triton-X (HT501128, Sigma, St. Louis, MO, USA) in PBS for 45 min under agitation at 25 rpm at 4 °C. Blocking was done using 5% Normal Goat Serum (NGS) (NS02L, Sigma, St. Louis, MO, USA) in PBS for 2 h under the same conditions. Primary antibodies were incubated overnight under the same conditions at the concentrations of 1:500 for mouse anti-TUJ1 (60052, Stemcell, Vancouver, BC, Canada), 1:1000 rabbit anti-GFAP (Ab7260, abcam, Eugene, OR, USA) [h], and 1:50 goat anti-ChAT (ab144p abcam). Following three washes with PBS, the constructs were incubated for 4 h under agitation at 25 rpms and room temperature with the secondary antibodies at the concentrations of 1:500 for AlexaFluor [i] Donkey anti-goat (405) (Ab175664 abcam, Eugene, OR, USA), 1:500 AlexaFluor 568 Donkey Anti-Mouse (Ab175700 abcam, Eugene, OR, USA), and 1:500 AlexaFluor 488 Donkey Anti-Rabbit (Ab150073, abcam, Eugene, OR, USA).

[h i] Correction made from the original publication from: De la Vega L, Rosas Gomez D, Abelseth E, Abelseth L, Alisson da Silva V, Willerth SM. **3D bioprinting human induced pluripotent stem cell-derived neural tissues using a novel Lab-on-a-Printer technology**. Applied Science 2018 In press.

3.5. Results

3.5.1. Bioprinted NPCS in Cylindrical Constructs

The bioprinted constructs were printed in a layer-by-layer fashion. The structures consisted of 1 cm diameter- cylinders with seven layers of fibers with an average diameter of 176 ± 16 μm and the total construct height was ~1.2 mm **(Figure 3.1).** The NPCs were homogeneously placed throughout the fibers within the constructs as shown in **Figure 3.2** during days 0 to 10. The bioink provided mechanical and biochemical support for the cells and slowly degraded over time. By day 30, most of the bioink had degraded while the remaining cellular structures remained attached to the tissue culture well.

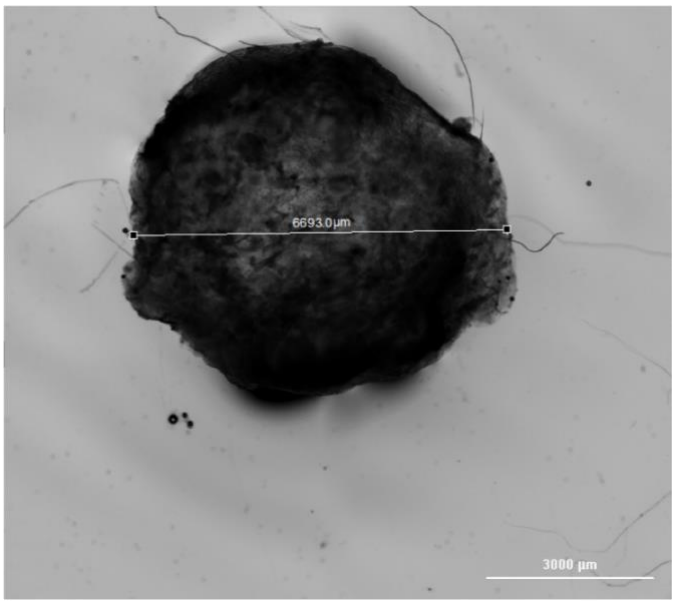

Figure 3.1. Bioprinted cylindrical construct.
Bioprinted cylindrical construct consisting of hiPSC-derived NPCs and our novel fibrin-based bioink. Scale bar represents 3000 μm.

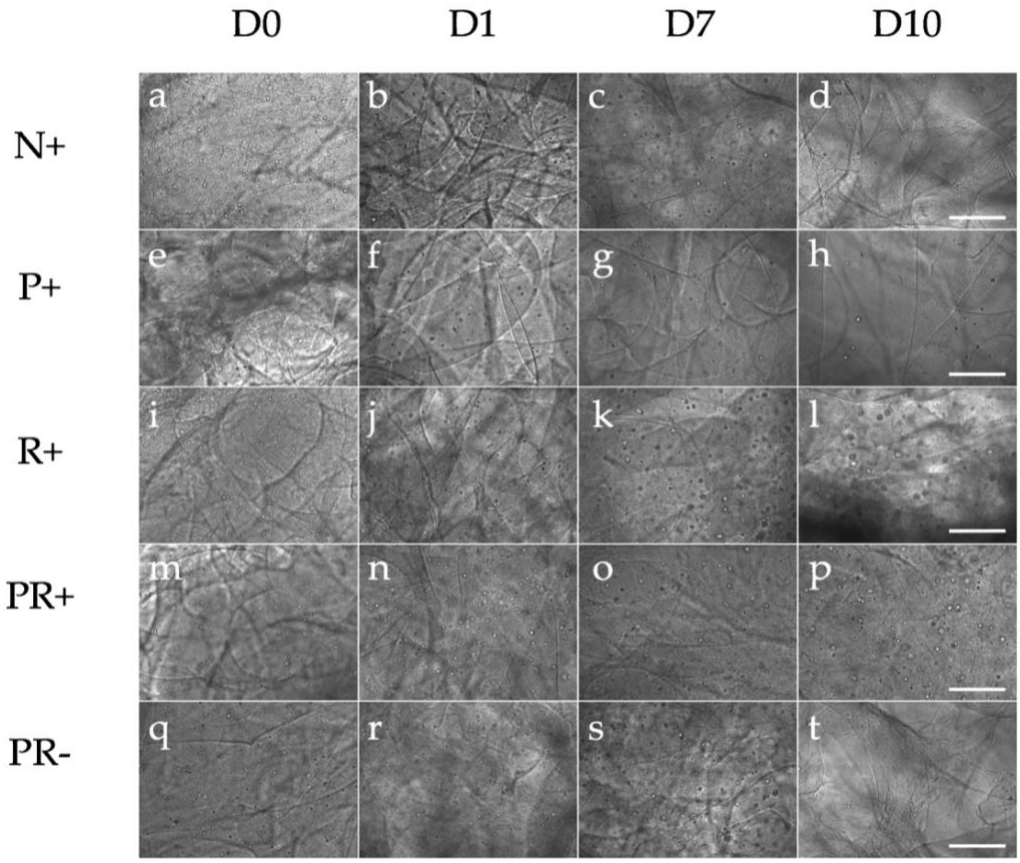

Figure 3.2 Phase contrast images of bioprinted constructs on days 0, 1, 7, and 10. (**a**–**d**). Negative group (N with small molecules); (**e**–**h**) Puro (P+ with small molecules); (**i**–**l**) RA (RA+ with small molecules), (**m**–**p**) Puro and RA (PR+ with small molecules); (**q**–**t**) Puro and RA (PR- no small molecules). Scale bar represents 300 μm.

3.5.2. Cell Viability

Quantitative analysis for cell viability was performed at day 7 using ViaCount assay from Millipore (n = 3 for all groups) **(Figure 3.3).** On day 7, cell viability for N+ was (89.2 ± 8.9%), P+ (93.3 ± 5.1%), R+ (90.9 ± 6.3%), PR+ (87.3 ± 0.8%), and PR- (81.2 ± 1.8%). No statistically significant differences were observed.

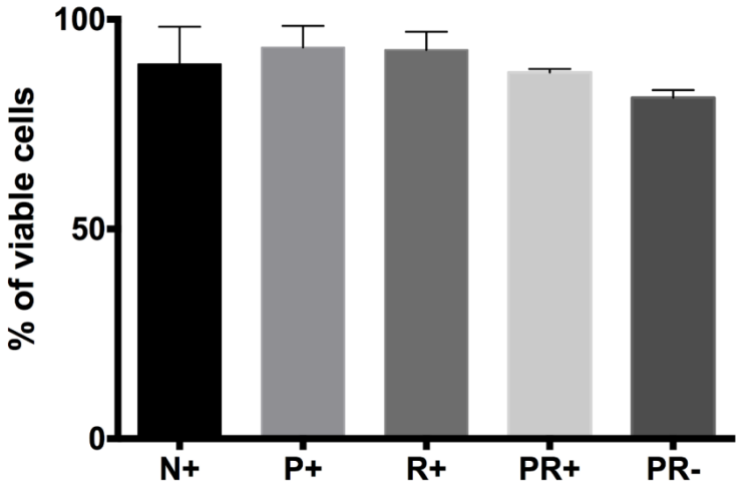

Figure 3.3 Cell viability of the Neural progenitor cells (NPCs) for all groups on day 7 after being bioprinted
n = 3 for all groups. Data is reported as the mean with the error bars representing the standard deviation. One-way ANOVA and Tukey post-hoc analysis was performed for statistical analysis using a confidence level of 95% ($p < 0.05$). No statistically significant differences were observed.

3.5.3. Protein Expression of 3D Bioprinted Neural Tissues

3.5.4. Flow Cytometry

On day 15, flow cytometry was performed to quantify cell marker expression of βT-III, Olig2, and HB9 (mature MN) **(Figure 3.4)**. Expression of βT-III was the highest for P+ (45 ± 20.9%), followed by PR+ (33.1 ± 13.4%), N+ (21.3 ± 21.3%) and PR- (4.3 ± 1.6%). No statistically significant differences were observed for βT-III expression. Olig2 expression was the highest for N+ (68.8 ± 6.9%), followed by PR- (61.1 ± 9.9%) and R+(46 ± 4.8%). The lowest level of expression was observed in PR+ (3.16 ± 1.10%). Statistically significant differences were observed between N+ and PR+, R+ and PR+, and PR+ and PR-. HB9 expression was highly expressed for all groups at this time point. R+ showed the highest level of expression (99.6 ± 0.4%), whereas PR+ and PR- had lower and similar levels of HB9 expression, (76.7 ± 10.8%) and (75.5 ± 10.3%),

respectively. N+ showed the lowest level of expression for HB9 (61.1 ± 5%). Statistically significant differences were observed for N+ and R+.

3.5.5. Immunocytochemistry

ICC was performed at day 30 for all groups for βT-III, ChaT, and GFAP **(Figure 3.5)**. βT-III expression was positive for all groups. ChaT expression was primarily expressed in PR+, however, N and PR-also showed expression of ChaT. GFAP expression was positive for N, R+, and PR-.

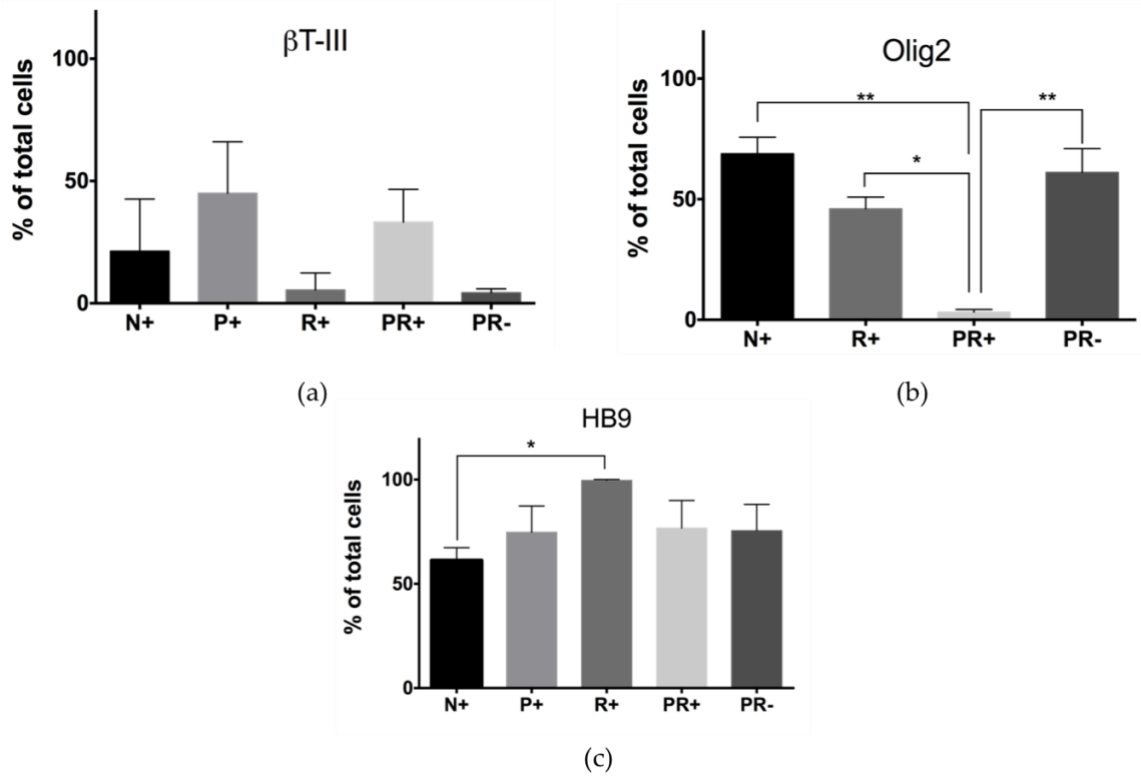

Figure 3.4 Flow cytometry of 3D bioprinted NPCs after 15 days of culture *in vitro*.
n = 3 for all groups. One-way ANOVA and Tukey post-hoc analysis was performed for statistical analysis using a confidence level of 95% ($p < 0.05$) and 99.9% ($p < 0.001$). * represents $p < 0.05$ and ** 99.9% $p < 0.001$.

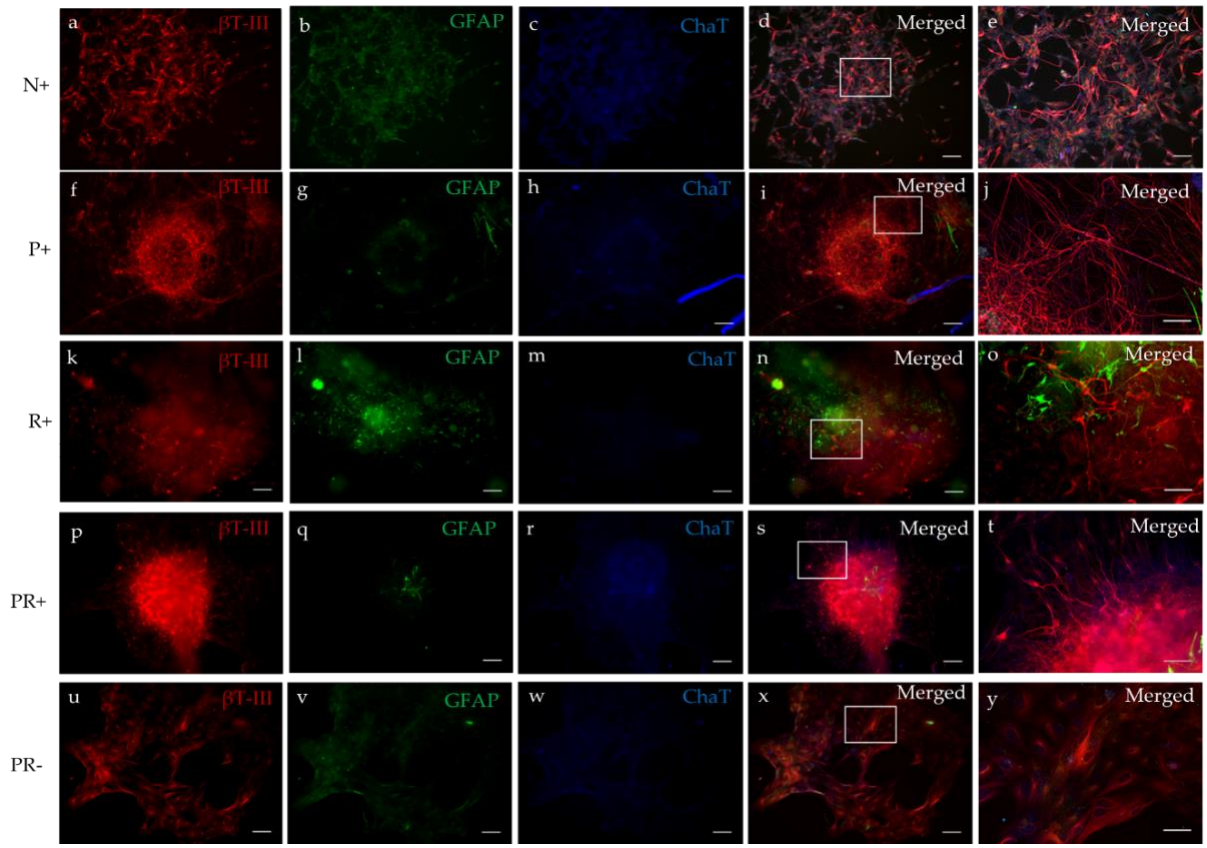

Figure 3.5 Immunocytochemistry after 30 days of culture *in vitro*.(a) βT-III; (b) Olig2; (c) HB9.
(a–e) N+; (f–j) P+; (k–o) R+; (p–t) PR+; (u–y) PR-. Scale bar for (a–d,f–i,k–n,p–s,u–x) represents 100 µm. Scale bar for (e,j,o,t,y) represent 50 µm.

3.6. Discussion

Previous studies have extensively explored the use of a 3D environment to create neural tissue by using natural or synthetic polymers. Such strategies are focused on the creation of hydrogel constructs, nerve guidance channels, or electrospinning [157,209,217,218]. However, those approaches require a large amount of labor and raw materials while their reproducibility remains challenging. Bioprinting technologies offer great advantages over conventional TE methods as they require less labor and materials and can be automated, producing high-throughput and reproducible processes [139,210]. In addition, patterned-specific structures with micro-architectures at the micrometer size resolution can be created to mimic the native tissues [139,210]. Recent studies have used 3D bioprinting technologies where multichannel scaffolds were 3D printed and NPCs within a bioink were extruded in a layer-by-layer fashion [219]. A different study performed by Gu et al. created functional mini tissues by bioprinting human neural stem cells (hNSCs) using a 3D-bioplotted system where the bionk is extruded, followed by incubation in crosslinking solution [127].

In this study, we successfully bioprinted NPCs using the microfluidic LOP™ and differentiated these cells into ChaT expressing MNs after 30 days. With this LOP™ technology, all the components of the bioink are mixed prior to the printing process and crosslinked at the 200 μm "Y" junction prior to ejection from the single nozzle. This special feature, where the bioink is surrounded by two crosslinking channels at the Y junction, initiates the crosslinking process from both sides and creates a sheath surrounding the bioink that protects the cells from shear-stress while being extruded. In addition, the 700 μm extrusion nozzle contained in this LOP™ is made out of PDMS and is therefore flexible and less stiff in comparison with other expression needles used in other studies [105,127,219]. Using a pneumatic pressure driven flow, our fibers are extruded at

20[j] mbar for the bioink, and an increased pressure of 40 mbar for the crosslinker, leading to the creation of printed fiber diameters of (176 ± 16 μm), with all the bioink components homogenously distributed. These diameters are similar to those reported previously when bioprinting NPCs using a point dispensing printing method [219].

On day 7, cell viability was above 81% for all groups, where P+ and R+ showed the highest levels of cell viability at 93% and 91%, respectively. These percentages are higher than those reported by Joung et al., where cell viability is reported to be >75% after four days of printing iPSC-derived spinal neural progenitor cells (sNPCs) and oligodendrocyte progenitor cells (OPCs) in a 50% Matrigel bioink [219]. Flow cytometry analysis was performed to assess the differentiation of the bioprinted NPCs cultured with combinations of small molecules that have shown to promote MN differentiation after 15 days of culture[66,215]. At this time point, P+ and PR+ showed the highest levels of the neuronal marker, βT-III, expression, with no statistically significant differences between groups. Expression of the oligodendrocyte transcription factor 2 (Olig2) was also quantified at this time point, and the overall expression for most groups was higher in comparison, with βT-III. N+ and PR+ showing the highest levels of expression (>60%), suggesting that either combination of small molecules (CHIR, SB, and LDN for N+) or (puro and RA for PR-) have a similar impact on the differentiation of NPCs into Olig2+ cells. These levels of βT-III and Olig2 expression are significantly higher than that reported by Gu et al., where hiPSC-derived NPCs were bioprinted and differentiated, with a maximum gene expression of βT-III of ~ 2% and 15% for Olig2 after three weeks of differentiation [127].

[j] Correction made from the original publication from: De la Vega L, Rosas Gomez D, Abelseth E, Abelseth L, Alisson da Silva V, Willerth SM. **3D bioprinting human induced pluripotent stem cell-derived neural tissues using a novel Lab-on-a-Printer technology**. Applied Science 2018 In press.

The expression of the mature MN marker, HB9, at this time point was highly expressed for all groups at >61%. The highest level of HB9 expression was observed in the R+ group, however, the only statistically significant differences were observed between N+ and R+. Interestingly, P+, PR+, and PR- showed very similar levels of expression, suggesting that the presence of puro, alone or in combination with RA, is crucial for differentiating HB9+ neurons from NPCs using our novel bioink. However, given that PR+ and PR- have similar levels of HB9 expression with a yield of ~ 76%, either treatment could be used for future analysis. However, R+ with the combination or RA and CHIR, SB, LDN is the most efficient, showing 99% yield of HB9+ MNs after 15 days.

Our 3D bioprinted tissues were cultured for up to 30 days in vitro for further maturation, and characterization of MNs compared with previous studies where ICC staining was performed after seven days of culture [219]. Nonetheless, Gu et al. cultured their bioprinted constructs for up to 40 days, showing the expression of mature neural markers, such as microtubule associated protein 2 (MAP2), gamma-aminobutyric acid GABA), and Synaptophysin [105]. ICC was performed for βT-III, the astrocyte marker (GFAP), and choline acetyl transferase (ChaT) to assess neuronal and glial cell differentiation. All of the groups showed βT-III expression; interestingly, P+ and PR+ self-aggregated into a spheroid structure as previously observed [105]. At this time point, all the scaffolds had been degraded, demonstrating that our bioink supported the cellular secretion of the required extra cellular matrix (ECM) components to maintain a 3D structure. GFAP expression was positive for N, R+, PR+, and PR-. ChaT expression was positive for N+, PR-, and PR+. Interestingly, PR+ showed the most cell aggregation and expression of βT-III and ChaT, and the lowest expression for GFAP, suggesting that the combination of these small molecules provides a better environment for MN differentiation and maturation.

Further maturation and characterization of the tissues will be necessary in order to fully characterize their maturity and electrophysiological characteristics. These bioprinted neural tissues can be used as a complementary pre-clinical model to assess drug safety and toxicity in the early development of clinical trials. hiPSCs can be derived from the patient and matured into neural progenitor cells in order to perform such an analysis with patient specific cells. In the future, drug releasing microspheres can be deposited along with the cell-suspension within the bioink, where each fiber contains the required drug-releasing microspheres to promote differentiation into different cell types. More than one type of cell can be differentiated within these bioprinted tissues in order to mimic a more defined micro-architecture of the SC tissue along with a blood spinal cord barrier (BSCB).

3.7. Conclusions

Here, we use a novel bioprinting method for generating hiPSC-derived neural tissues similar to the tissue found in the SC as indicated by their survival and expression of the MN markers, Olig2, HB9, and ChaT. Such bioprinted neural tissues can potentially serve as a tool for screening potential drugs for treating SCI, as well as give insight into developing potential cell therapies for treating SCI.

Chapter 4 3D Bioprinting Human Pluripotent Stem Cells and Drug Releasing Microspheres to Produce Responsive Neural Tissue[k]

Laura de la Vega [1], Ruchi Sharma[1], Laila Abelseth [2], Juan Triviño-Paredes [3], Milena Restan [2], Stephanie M. Willerth [1,2,3 *]

[1] Department of Mechanical Engineering, University of Victoria. Victoria, BC, Canada.
[2] Biomedical Engineering Program, University of Victoria. Victoria, BC, Canada.
[3] Division of Medical Sciences, University of Victoria. Victoria, BC, Canada.

*Manuscript to be submitted at Biomaterials.

Key words:

3D bioprinting, microspheres, neural tissue, bioink, Lab-on-a-printer, motor neurons, spinal cord injury, drug screening tool.

Author contribution:

De la Vega L. designed, set-up and performed most of the experimental procedures, analysis and preparation of manuscript. Abelseth L. assisted on tissue culture, bioprinting, and editing of the manuscript. Triviño-Paredes J. performed confocal microscopy imaging and assisted on writing confocal microscopy methodology. Restan M. and Sharma R. assisted on preparation of the bioink and bioprinting. Willerth S.M. provided feedback on the experimental analysis and editing of the manuscript.

k De la Vega L, Abelseth L, Tiviño-Paredes J, Sharma R, Restan M, Willerth S.M. **3D bioprinting functional neural tissues derived from human induced pluripotent stem cell.** To be submitted at Biomaterials, 2019.

4.1. Abstract

In this study, we show for the first time that responsive neural tissues can be engineered by combining bioprinting technologies with small molecule-releasing microspheres and pluripotent stem cells. To generate responsive neural tissues, we used our novel fibrin-based bioink to bioprint human induced pluripotent stem cell (hiPSC)- derived neural progenitor cells (NPCs), in combination with purmorphamine (puro) and retinoic acid (RA) releasing microspheres. Such tissues were bioprinted in a layer-by-layer using the Lab-On-a-Printer (LOP™) associated with the RX1 bioprinter. With this bioprinting approach, we were able to create reproducible cylindrical structures with a total 7 layers composed of aligned fibers that provided a defined microarchitecture to the constructs. Our bioprinted tissues showed high levels of cell viability after printing (~80%). The expression of cellular markers was analyzed using immunocytochemistry and flow cytometry on days 15, 30, and 45. By day 45, the bioprinted tissues showed the presence of neurons (MAP2 and CHAT+), astrocytes (GFAP), and oligodendrocytes (O4). The membrane potential was analyzed using a voltage sensitive dye on days 30 and 45. The bioprinted tissues showed an increase in membrane potential when exposed to acetylcholine (Ach) and a decrease in membrane potential after exposure to gamma-Aminobutyric acid (GABA). Furthermore, the addition of drug-loaded microspheres to the bioprinted tissues, showed to be an efficient way to promote neutral tissue differentiation and maturation *in situ* using a significantly smaller amount of morphogens in comparison to adding the morphogens to the culture media. This method could potentially lead to a more cost-effective solution for creating drug screening tools.

4.2. Introduction

3D bioprinting is an additive manufacturing technique used in tissue engineering (TE) that combines cells and bioinks to generate structures layer-by-layer based on the specifications of a computer aid design (CAD) file [220]. 3D bioprinting has a great potential for developing new strategies to generate viable and functional tissues *in vitro* [210]. Different types of tissues such as bone, vascular, neural, and skin have been bioprinted using novel bioinks and printing techniques [102,147,221-224]. These bioprinted tissues can be used in the process of pre-clinical studies as drug screening platforms to identify target compounds in order reduce the cost and time of clinical trials [50].

Currently, two main strategies can create bioprinted tissues. The first involves the 3D printing of the scaffold, followed by the seeding of the cells on top. This process has several disadvantages as it requires more time to process, more manual work, the cells cannot always get throughout the scaffold and it is difficult to differentiate into multiple cell types [219,225]. The second strategy combines the cells in the bioink where the fibers are printed with the cell-laden bioink [71,106]. A significant challenge when bioprinting neural tissue is achieving adequate mechanical properties as these tissues are one of the softest with a compressive modulus of 2000Pa [25]. However, the brain and SC have a range of stiffness depending on the region (white or gray matter) and a variety of measurements and methods have been reported [139,226,227]. Furthermore, studies have shown that NPC proliferation and differentiation varies depending on the stiffness of the substrate where scaffolds with an elastic modulus <10kPa favored NPC proliferation [73]. This study conducted by Leipzig *et al.*, mechanical testing was performed using a stress-relaxation test in uniaxial compression and reported that NPCs differentiated into oligodendrocytes and astrocytes in substrates of >7kPa and 1-3.5kPa, respectively while neural differentiation was observed in

substrates <1kPa [73]. Consequently, the bioink must produce a structure with similar properties to those of neural tissues while being viscous enough to be bioprinted [71,228]. Other factors to consider when bioprinting are crosslinking time, print speed, temperature, and shear stress as they can significantly affect the cell viability and survival of neural tissues [71,220].

Extrusion based bioprinting, one of the main types of bioprinting, uses a pneumatic pressure driven flow to extrude the bioink [224]. One of the advantages of using extrusion based bioprinting, is that continuous fibers are deposited from the nozzle. However, limitations of this method include the exposure of the cells to shear stress while being extruded through as the nozzles are often narrow and made of metal or plastic [141-143,224]. Length of the nozzle has been shown to have an impact in cellular viability post-printing as a result of the exposure time to shear forces while being extruded thought the nozzle [142,224]. Faulkner-Jones *et al.* showed that when bioprinting human embryonic stem cells (hESCs), a nozzle of 8.9 mm led to more than 84% cell viability, whereas a nozzle of 24.4 mm led to more than 71% cell viability[142]. This group also showed that increased pressures led to lower cell viability.

The novel microfluidic device called Lab-On-a-Printer™ (LOP), has shown promising results for the generation of neural tissues [102,103,229]. In combination with an extrusion based bioprinter (RX1), the LOP™ technology is a versatile tool where programmable patterns can be extruded with continuous fibers and defined micro-architectures [102]. The LOP™ microfluidic device is made of polydimethylsiloxane (PDMS) consisting of many microchannels where different bioinks and a crosslinker can be loaded and dynamically bioprinted. This device contains a soft nozzle of 28 mm that uses the crosslinker solution to create a protective sheath surrounding the cell-laden bioink while being extruded. This contributes to increased cell survival and long

term functionality of the tissues [103]. This feature also allows for the initiation of polymerization while in the nozzle before being extruded which effectively creates more stable structures [103].

Combinations of natural and synthetic biomaterials have been used in order to create bioinks -materials that mimic the ECM for 3D bioprinting [210]. Natural biomaterials often contain desirable physiological and biological properties such as binding sites for mammalian cells to attach [71,230]. Synthetic biomaterials are also widely studied as their properties can be tuned according and produce more consistent results, however they lack bioactivity. [230]. Exampled of synthetic biomaterials include polylactic acid (PLA), poly(lactic-co-glycolic acid) (PLGA), polyethylene glycol (PEG), polycaprolactone (PCL) and Poly(2-hydroxyethyl methacrylate) (pHEMA) [25,230-232].

Some groups have bioprinted scaffolds using synthetic materials such as silicone in order to create a multichannel structure for the neural tissues [219]. While these structures possess microchannels that can guide axonal elongation, the biomaterial used is not bioactive and the method used in this study consists of a two-step process with a 5-hour curing time post-printing [219]. Polyurethane (PU) is another example of a synthetic polymer used for bioprinting NSCs where the cells were embedded in two PU thermoresponsive hydrogels and printed at physiological temperatures without the use of a crosslinker [148,224].

Other bioinks have been developed for the bioprinting neural tissues using a combination of natural biomaterials [105,149,223,233,234]. For instance, a combination of 5% alginate, 5% chitosan and 1.5% agarose was used to bioprint hNSCs. The bioprinted constructs showed mechanical properties similar to brain tissue and expression neuronal and glial markers were observed [233]. Alginate is a common biomaterial used in bioprinting as it provides suitable viscosity for

bioprinting and structural support [103,233]. However, large concentrations of alginate have shown to inhibit neurite extension, and therefore high concentrations of alginate should be avoided when bioprinting neural tissues [235]. A novel bioink for engineering neural tissues also used in this study, was developed by Abelseth *et al*. consisting of a combination of natural biomaterials [103]. Fibrin, alginate, and chitosan were combined in order to create a printable bioink while providing a suitable environment for hiPSC-derived neural cells to survive and differentiate. High levels of cell viability were observed post printing and the bioink supported neural differentiation from human induced pluripotent stem cells (hiPSCs) for up to 4 weeks after which neural cell marker expression and neurite extension were observed [102,103].

In addition to the bioink, 3D bioprinting also requires other components that must be strategically chosen in order to create the desired type of tissue such as types of cells and biochemical factors used to promote differentiation, maturation, and survival of the tissues *in vitro* [71,106,228]. Due to the limited availability and passaging limitations of primary neural cells, stem cells are often a better approach for the development of neural tissues [71]. Pluripotent stem cells (PSCs) can be derived from the inner mas of a human embryo- (ESCs), or reprogrammed from somatic cells- hiPSCs [12,26,48,49]. PSCs have self-renewal capabilities, and pluripotency, which means that they can become any type of cell in our body [48]. Differentiation of hiPSCs into neural tissue has been widely studied and used in the field of TE [51,65,66,236]. Specifically, hiPSC differentiation into motor neurons, which are the cells present in the SC that in charge of voluntary movement has been achieved with a highly pure cell population in a reproducible way [66]. hiPSCs-derived cells have also been bioprinted for the generation of neural tissues using a variety of bioinks and biochemical factors that support their differentiation [102,103,219]. Such biochemical factors are of great relevance in order to promote the growth and maturation of the differentiated cells.

The use of drug delivery systems (DDS) is another component commonly used in the field of TE. DDS are formulations or devices designed to efficiently convey a therapeutic into the body or engineered tissue at a controlled rate and over a period of time [237]. Drug-loaded microspheres are a type of DDS that are commonly made of polymeric materials such as PCL, that have been used to deliver water insoluble drugs, proteins, and small molecules [132-134]. In particular, retinoic acid (RA)- and purmorphamine (puro)- loaded microspheres have been shown to contribute to efficient differentiation of hiPSCs into neuronal subtypes [102,129]. Some of the major advantages of using drug-loaded microspheres on engineered tissues are the localized, slowed, and controlled delivery of such morphogens over time [128]. Furthermore, the incorporation of drug-loaded microspheres into the engineered tissues can be used as a cost-effective way to deliver such morphogens in comparison with the constant media changes where the morphogens, which need to be soluble, are added to the media in larger amounts [37].

The purpose of this study was to build on our previous work where we show the efficient differentiation of hiPSCs into neuronal subtypes and bioprinting of hiPSC-derived neural progenitor cells (NPCs) using a fibrin based bioink [37,58,129]. In this study, we show the successful and homogeneous distribution of the bioprinted puro and RA-loaded microspheres in combination with NPCs and fluorescent microspheres within the fibers of cylindrical constructs using the microfluidic device LOP™. Furthermore, we bioprinted hiPSCs-derived NPCs in combination with drug releasing microspheres to promote motor neuron differentiation for 45 days. Spinal motor neurons (SMN) were also bioprinted in order to compare cell viability, cell marker expression and membrane potential.

All groups showed ~80% viability on days 0 and 1 post printing. Cell marker expression was analyzed using Immunocytochemistry (ICC) and flow cytometry analysis. Flow cytometry analysis after 15 days showed that the bioprinted constructs containing drug-loaded microspheres had 37% expression of beta tubulin III (βT-III), 31% expression of the oligodendrocyte marker 2 (OLIG2), 82% expression of the homeobox protein 9 (HB9), and 91% expression of NESTIN. By day 30, the bioprinted constructs showed the expression of the glial fibrillary acidic protein (GFAP) (astrocytes), βT-III, gamma-Aminobutyric acid (GABA), myelin, and choline acetyl transferase CHAT as observed by our ICC analysis.

After 45 days, flow cytometry analysis revealed the expression of the neuronal marker - microtubule associated protein (MAP2), astrocytes (GFAP), and oligodendrocytes (O4). Expression of CHAT was observed at 20% for the drug-loaded microsphere group, followed by 15% and 13% of GFAP and O4 expression, respectively. Electrical properties of the bioprinted constructs were also characterized using a voltage sensitive dye. All of the bioprinted tissues showed an increase in membrane potential upon exposure to acetylcholine (Ach) and decreased membrane potentials after exposure with GABA.

4.3. Materials and Methods

4.3.1. Culture and expansion of hiPSC-derived NPCs

Cell culture and expansion of hiPSC-derived NPCs was performed as previously described using the 1-DL-01 (male) cell line from WiCell under the approval of the University of Victoria's Human Ethics Committee protocol number: 12-187 [238]. hiPSC-derived NPCs were cultured and passaged in cell culture plates coated with poly-L-ornithine (PLO- (P4957, Sigma) and laminin (L2020, Sigma) [102]. Culture media consisted of STEMdiff™ Neural Progenitor Medium (NPM) (05834, Stemcell Technologies) containing 1 X STEMdiff™ Neural Progenitor Supplement A (05836, Stemcell Technologies), 1 X STEMdiff™ Neural Progenitor Supplement B (05837, Stemcell Technologies). Media changes were performed every day until reaching 80% confluency at 37 °C with 5% CO2. Cryopreservation of hiPSC-derived NPCs was performed at a cell density of 1x10^6 cells/ml in STEMdiff™ Neural Progenitor freezing medium (05838, Stemcell Technologies).

4.3.2. Preparation of the neuro-bioink

The neuro-bioink was prepared was previously described [103,229,238]. Briefly, fibrinogen (341578, EMD Millipore) was prepared at a concentration of ~50 mg/ml in tris-buffered saline solution (TBS) and sterilized using 0.2 μm syringe filters. The final concentration for fibrinogen was adjusted to 20 mg/ml in the neuro-bioink. Sodium alginate (180947, 120,000-190,000 g/mol, M/G ratio 1.56 Sigma-Aldrich) was prepared at 2% w/v by reconstituting in distilled water and sterilized using 0.2 μm syringe filter. The final concentration of alginate in the neuro-bioink was 0.5% w/v. Genipin (G4796, Sigma-Aldrich) was reconstituted at a concentration of 25 mg/ml in

DMSO. The final concentration of genipin in the neuro-bioink was 0.3 mg/ml. The crosslinking solution consisted of calcium chloride ($CaCl_2$) (C1016, Sigma-Aldrich), thrombin (T7009, Sigma-Aldrich), and chitosan (C3646, Sigma-Aldrich). $CaCl_2$ was prepared at a concentration of 20 mg/ml in TBS. Thrombin was reconstituted at a concentration of 1000 units (U)/ml in sterile TBS. The final concentration of thrombin was 1.7 U/ml in the crosslinker. Chitosan was prepared at a concentration of 25 mg/ml using 1% acetic acid. The pH was adjusted by using β-Glycerolphosphate (β-GP) (G9422, Sigma-Aldrich). The final concentration of chitosan in the crosslinker was 0.075% w/v. The crosslinking solution was sterilized by filtering using 0.2 μm syringe filters. For visualization purposes while printing, a solution of phenol red TBS (PR-TBS) at 0.5 mg/ml was prepared and sterilized using 0.2 μm syringe filter before being added to the bioink.

4.3.3. Bioprinting NPCs using the neuro-bioink using the RX1 bioprinter

hiPSC-derived NPCs were thawed by placing in a water bath for 3 min and then resuspended in warm DMEM and centrifuged at 300 rfc for 5 min. The supernatant was removed, and the hiPSC-derived NPCs were resuspended at a concentration of 1x10^6 cells/ml in fibrinogen, alginate, genipin, 1% penicillin-streptomycin- amphotericin B (PSA) (A5955, Sigma-Aldrich), and PR-TBS. For the M+ and U+ groups, drug-loaded and unloaded (no drug) microspheres were resuspended in the bioink at a concentration of 0.25 mg/ml of bioink. M+ consisted of puro and RA loaded microspheres at a ratio of 2:1 respectively. Drug-loaded and unloaded microspheres were made of PCL and fabricated as previously described using a single emulsion oil-in-water (o/w) [37,129]. The puro-loaded microspheres had a puro loading of 0.92 μg/mg PCL with an encapsulation efficiency (EE) of 84% and an average diameter of 3.4 ± 1.17 μm [37]. The RA loaded microspheres had a RA loading of 30μg/mg PCL with an EE 58.4 ± 3.3% and an average size of

3.41 ± 1.6 μm [129]. During the bioprinting process, the crosslinker was kept on ice to facilitate printing as chitosan begins to gel at higher temperatures [17,116]. The bioprinted design a consisted of a cylinder, 13 mm in diameter and 2.7 mm in height. The bioprinting software used was Aspect Studio v1.2.59.0 and the infill pattern was rectilinear with 40% fiber density, a layer height of 0.4 mm and layer diameter of 0.2 mm. Pressure parameters consisted of 50 mbar for the neuro-bioink with or without microspheres, 60 mbar for the crosslinker, 100 mbar for the buffer and printing speed was 25 mm/s. All procedures were performed under sterile conditions. Four structures were bioprinted at a time in ~5 min. After printing the structures were gently placed in previously coated PLO/laminin plates and cultured with the appropriate NP media.

4.3.4. Bioprinting of drug-loaded microspheres and fluorescent microspheres

Puro and RA-loaded microspheres were fabricated as previously described [37,129]. Red FluoSpheres™ (F8842, Thermo Fisher), and green FluoSpheres™ (F21010, Thermo Fisher) were also used for bioprinting to show the microsphere distribution within the construct. Several combinations of microspheres were bioprinted to replicate their printability and distribution. A total of 0.25 mg/ml of microspheres were bioprinted for every combination. The final ratio was 2:1 for the groups containing red and green fluorescent microspheres. Red microspheres were combined with puro microspheres in a 1:1 ratio and RA microspheres were combined with green microspheres on a 1:1 ratio. For bioprinting the puro-red:RA-green microspheres the final ratio was 2:1. For the groups containing NPCs the cell density was $1x10_6$ cells/ml bioink. The bioprinted constructs containing combinations of drug and/or fluorescent microspheres were imaged using an Olympus IX-81 inverted microscope using the Metamorph imaging software 7.6.1 from MAG Biosystems.

4.3.5. Characterization of the controlled release of purmorphamine-loaded microspheres from the bioprinted constructs

A 7-day release study was performed to determine the release kinetics of puro from drug loaded microspheres bioprinted using the fibrin-based bioink, the LOP™ technology and RX1 bioprinter. The drug was extracted from the remaining microspheres on each sample and quantified using high-performance liquid chromatography (HPLC) to estimate puro concentration. The bioprinted structure, pattern, and printing parameters used were as previously mentioned this study. Collection days were 0, 1, 4, and 7 and media change was performed for each of these days. All samples (n=4) contained 4 cylindrical structures (0.25 ml of bioink each) with a total of 1 ml of bioink per replicate, 0.166 mg of total puro microspheres and 0.83 mg of RA microspheres cultured in 4 ml of PBS. The constructs were placed in petri dishes and incubated at 37 °C. At each time point, the samples were placed in 15 ml conical tubes and frozen at -20 °C for further processing. For scaffold degradation, each sample was thawed at room temperature and then placed in C-tubes and processes as further described under section 4.3.9 using the MACS Miltenyi Biotech Neural Tissue Dissociation kit. After enzymatic dissociation of the scaffolds, the samples were vortexed vigorously until broken apart followed by centrifugation at maximum speed and washing with dH2O twice. Supernatant was removed and the samples were freeze-fried overnight. Puro extraction from the recovered microspheres was performed by adding 300 µl of acetonitrile (ACN) and mixed by vigorously pipetting and placing in the vortex mixer (Eppendorf ® MixMate®) at 3000 rpm for 10 minutes. The samples were then placed at -80 °C for 5 minutes, followed by centrifugation at 15000 rpms for 5 minutes. The remaining supernatant was collected and filtered through 0.2 µm PTFE syringe filters using a 1ml syringe (Norm-Ject tuberculin) and placed in HPLC amber vials (Agilent). Quantification of puro using HPCL was performed as previously described [216].

4.3.6. Analysis of the physical properties of the bioprinted constructs

Bioprinted constructs containing no microspheres or 0.25 mg/ml of unloaded microspheres were weighted immediately after bioprinting (wet weight) using a Mettler Toledo balance. The bioprinted constructs with no microspheres and unloaded microspheres were imaged using the Cytation 5™, and the software Gen5 version 3.05 (BioTek instruments) to determine their diameters. Statistical analysis was performed using unpaired t-test with equal SD using the software Prism 6 statistics (Graphpad). Confidence level was 95% ($p<0.05$).

4.3.7. Culture of the bioprinted hiPSC-derived neural constructs

From days 0-5 the all of the bioprinted constructs were cultured in NPM supplemented with a cocktail of small molecules consisting of SB431542 (SB), CHIR99021 (CHIR), and LDN193189 (LDN) as indicated by the (+) in the abbreviated notation. SB is a activin nodal, bone morphogenic protein (BMP), and transforming growth factor beta (TGFβ) inhibitor and LDN- a BMP inhibitor [239,240]. CHIR has shown to promote neural induction as it acts as a WNT pathway agonist [66]. Concentrations of these molecules from days 0-5 consisted of 1μM of CHIR 99021 (CHIR 72052, Stemcell Technologies), 2 μM of LDN 193189 (LDN- SML0559, Sigma), 2 μM of SB 431542 (SB- 72234, Stemcell Technologies), and 1% PSA. For PR+, puro (SML0868, Sigma) was also added at a concentration of 0.5 μM and RA (R2625, Sigma) at a concentration of 0.1 μM from days 0-5. From day 6, CHIR, LDN, and SB were removed for all groups and the constructs were cultured with NPM [66]. For PR+, puro was added at a concentration of 0.1 μM and RA at a concentration of 0.5 μM until day 45. By day 15, the cell culture media was gradually replaced with Brainphys Neuronal Medium (BP) (05790, Stemcell) supplemented with 0.1 μM of Compound E (CpdE) (73952, Stemcell Technologies), 10 ng/mL of GDNF (450-10, Peprotech),

10 ng/mL of IGF-1 (AF-100-11, Peprotech), 1μM of C-AMP (A6885, Sigma), 1% of N2 (17502048 Thermo Fisher), 1% of B27 (17504001, Thermo Fisher), 200 ng/mL of L-ascorbic acid (AA) (A5960, Sigma), 10 ng/mL of BDNF (450-02, Peprotech), and 1% PSA [102,238]. Media changes were performed every third day by replacing half of the total volume with fresh media. The bioprinted constructs were maintained at 37 °C with 5% CO_2 [102].

4.3.8. Bioprinting and culture of motor neurons

Each cryovial of hiPSC-derived SMNs from BrainXell (BX-0100) containing 5x10^6 cells was removed from the liquid nitrogen and thawed in a water bath at 37°C. The MNs were slowly resuspended in Neurobasal™ Medium (NBM) (21103-049, Life Technologies) at a rate of ~1 drop/sec and centrifuged at 300 rfc for 5 min. After pellet formation, the supernatant was removed and the SMNs were gently resuspended in the neuro-bioink for bioprinting. Printing conditions and design were the same used for NPCs. Culture conditions were performed as recommended by BrainXell[241]. On day 0, the bioprinted SMN constructs were cultured in seeding medium containing 0.5X of DMEM/F12 (11330-032, Life Technologies), 0.5X of NBM, 1X B27 (17504-044, Life Technologies), 1X N2, 0.5mM GlutaMAX (35050-061, Life Technologies), and 1X of Neuron seeding supplement (provided by BrainXell). On day 1, all the media was removed and the cells were cultured with containing 0.5X of DMEM/F12, 0.5X of NBM, 1X B27, 1X N2, 0.5mM GlutaMAX, and 1X of Neuron seeding supplement, 10 ng/ml BDNF (PHC7074 -Thermo Fisher), 10 ng/ml GDNF (PHC7045, Thermo Fisher), 1 ng/ml TFG- β1 (PHG9214, Thermo Fisher), and 15 ug/ml of Geltrex (A15696-01, Gibco). On day 4, all the media was removed and the bioprinted constructs were cultured with 0.5X of DMEM/F12, 0.5X of NBM, 1X B27, 1X N2, 0.5mM GlutaMAX, and 1X of Neuron day 4 supplement (provided by BrainXell), 10 ng/ml BDNF, 10 ng/ml GDNF, and 1 ng/ml TFG- β1.

4.3.9. Assessment of cell viability

Cell viability for bioprinted NPCs and SMNs was performed by first degrading the scaffolds using the MACS Miltenyi Biotech Neural Tissue Dissociation kit [242]. Triplicate samples (n=3) for each group were prepared for cell viability by removing cell media and transferring constructs to a C-Tube. Mix 1 was prepared by adding 1.432 ml of Buffer Z and 37.5 µl of enzyme P. The culture wells were washed with the 1470 µl of mix 1 and then placed in the C-tube with the constructs. After addition of mix 1, the c-tubes were inverted twice gently in order to ensure that the constructs were located in the rotator area and placed in the gentleMACS™ dissociator (130-093-235, Miltenyi Biotech) and the m_brain_01 program was run twice. The samples were then incubated at 37°C for 20 min, followed by the addition of 22.5 µl of mix 2. Preparation of mix 2 was performed by adding 15 µl of Buffer Y and 7.5 µl of enzyme A. The C-tubes were inverted twice gently and placed in the gentleMACS™ dissociator and the m_brain_02 program was run twice. The samples were incubated once more at 37°C for 20 min. The m_brain_03 was run twice and 2ml of FBS were added to each C-tube. The samples were then strained into 15 ml conical tubes using a 37 µM reversible strainer (27215, Stemcell Technologies). Lastly, the C-tubes were washed with 2ml of PBS and the remaining solution was strained. The samples were then washed three times by centrifuging at 300 rfc for 5 min and adding 1 ml of PBS. Statistical analysis was performed using one-way ANOVA, followed by Tukey's post-hoc analysis using 95% ($p<0.05$) confidence intervals for each day for the groups containing bioprinted NPCs. Statistical analysis was also performed for the bioprinted SMNs on days 0 and 1 using unpaired t-test with equal SD using a 95% ($p<0.05$) confidence interval. Statistical analysis was performed using the software Graphpad prism 6 statistics.

4.3.10. Flow cytometry analysis of bioprinted neural constructs

Degradation of the scaffolds was performed as previously described using the MACS Miltenyi Biotech Neural Tissue Dissociation kit. After the samples were washed three times in PBS, the resulted cell suspension was processed as previously described following the manufacturer's instructions (R&D systems) [37,102]. Cell marker expression was quantified on the hiPSC-derived NPCs prior to bioprinting for the sex determining region Y-box2 (SOX-2) (CS202594, Millipore), stage specific embryonic antigen-1 (SSEA-1) (FAB2155c, R&D), and NESTIN (IC1259P R&D). On day 15, quantification was performed for the expression of beta tubulin-III (βT-III) (IC1195C, R&D systems), Homeobox protein 9 (HB9) (bs-11320R, Bioss antibodies), Oligodendrocyte transcription factor 2 (OLIG2) (IC2230P, R&D), and NESTIN. On day 30, quantification was performed for the expression of βT-III, HB9, Islet-1(Isl-1) (562547, BD Pharmigen), and Choline Acetyl Transferase (ChAT) (ab22400, abcam). On day 45, cell marker expression was quantified for the Microtubule-associated protein 2 (MAP2) (FCMAB318, Millipore), Glial fibrillary acidic protein (GFAP) (NBP2-33184PCP, Novusbio), oligodendrocyte marker (O4) (FAB1326P, R&D systems), and CHAT (ab22400, abcam). Isotype controls were Phycoerythrin (PE) (IC015P, R&D systems), and Peridinin Chlorophyll Protein Complex (PerCP) (IC003C, R&D systems). The samples were analyzed on the Guava easyCyte HT flow cytometer using the InCyte software 2.6.

4.3.11. Immunocytochemistry

Immunocytochemistry (ICC) was performed as previously described by removing cell media and washing the constructs with PBS, followed by fixation with 10% formalin at 4°C, under agitation at 10 rpm for 2 hours [102]. Permeabilization was performed by adding 0.1% of triton-X (HT501128, Sigma) diluted in PBS and incubating for 45 min under the same conditions. Blocking

was accomplished by adding 5% NGS (NS02L, Sigma) diluted in PBS and incubating at 4°C under the same conditions. Primary antibodies were incubated overnight under the same conditions at the following concentrations: HB9 (1:1000, ABN174, Millipore), OLIG2 (5µg/ml, AF2418, R&D systems), CHAT (5µg/ml, AF3447, R&D systems), βT-III (1:500, ab18207, abcam), GFAP (1:1000, ab10062, abcam), MAP2 (1:200, ab32454, abcam), Myelin (1:500, MAB328, Millipore), GABA (1:500, ABN131, Millipore). Following incubation with the primary antibodies, samples were washed twice with PBS under agitation at 4°C for 25 min for the first wash and 40 min for the second wash. Secondary antibodies were incubated for 2 hours under the same conditions. Donkey anti-mouse 568 (1:500, ab175700, abcam), donkey anti-goat 405 (1:500, ab175664, abcam), and donkey anti-mouse 488 (1:500, ab150073, abcam), goat anti-rabbit 568 (1:500, ab175471, abcam), donkey anti-goat 488 (1:1000, 705-545-147, Jackson immuno). Following incubation, the samples were washed twice with PBS under agitation at 4°C for 25 and 40 min, respectively. After washing, the samples were stained with 4′,6-diamidino-2-phenylindole (DAPI) at 0.105 µg/ml (D1306, Molecular probes) under agitation at 100 rpm for 7 min, followed by 2 washes with PBS under agitation at 4°C for 25 min. Fluorescence imaging was performed using the Olympus IX-81 inverted microscope using the Metamorph imaging software 7.6.1 from MAG Biosystems.

4.3.12. Confocal imaging

Immunofluorescence imaging of the bioprinted tissues was performed using the Olympus BX61WI confocal microscope and the FluoView-1000 software (Olympus, Toronto, ON). A small sample of the bioprinted tissue was excised using dumont tweezers and McPherson-Vannas micro dissecting spring scissors (Roboz Surgical Instrument, Gaithersburg, MD) under a SMZ-168 stereomicroscope (Motic, Richmond, BC). Samples were placed in precleaned superfrost glass

slide (Fisher Sceintific, Pittsburhh, PA) and coverslipped using Vectashield (Vector Laboratories, Burlingame, CA). Images were acquired with Olympus UPlanSApo objectives at 10X, 10X + 4 digital zoom and/or 20X + 2 digital zoom using a 4, 2 or 1 µm z-step respectively and a 1024x1024-pixel frame size. Samples were imaged using the 405, 488, 568 filters. FIJI (ImageJ; National Institutes of Health) was used to create maximum intensity projections from image stacks.

4.3.13. Characterization of membrane potential

Characterization of the membrane potential of the bioprinted hiPSC-derived NPCs was performed on days 35 and 45 using the voltage sensitive dye FLIPR Membrane Potential Assay kit- blue component diluted in buffer component B (R0842, Molecular Devices) [243]. Characterization of the bioprinted SMN's membrane potential was performed on days 0, 1 and 7. The FLIPR blue dye was added to the bioprinted constructs on a ratio of 1:1 of dye to cell culture media. The plates were then covered from light exposure and incubated at 37 °C with 5% CO2 for 45 min. After incubation, the cell culture plate cover was removed and a Microseal® B adhesive sealer (MSB-1001, Biorad) was placed on top of the plate under sterile conditions. Fluorescence scans of the constructs at rest were run using the microplate reader as previously described by Robinson et al. with excitation at 530 nm, emission at 565 nm, 25 flashes and a 5x5 reads per well [243]. Background readings were obtained by adding 1:1 dye to cell media in wells containing constructs with bioink only to normalize for N+ and PR+, and constructs containing 0.25 mg/ml of unloaded PCL microspheres to normalize for M+ and U+ and processed under the same conditions. After reading the fluorescence at rest, the bioprinted neural tissues were then excited by adding 100 µM of acetylcholine (ACh) (A2661, Sigma) and incubated under the same conditions for 25 min. Fluorescence readings of the bioprinted tissues at excitation were then performed as previously described. After excitation of the bioprinted constructs at day 45 with

ACh, the tissues were then exposed gamma-Aminobutyric acid (GABA) (A2129, Sigma) at a concentration of 10 μM and incubated for 25 min under the same conditions [244]. Fluorescence readings were performed as previously described. Change in fluorescence was normalized following the equation (1) where F_0 is the average background reading. Normalized fluorescence readings were then converted to membrane potential ΔE following equation (2) as described by Robinson et al [243] where R is the gas constant, F is Faraday's constant, T is the average temperature of the readings, and z' is the apparent charge of the external dye concentration.

$$\frac{F-F_0}{F_0} \quad (1)$$

$$\Delta E = \frac{R*T}{z'*F} * \ln\left(\frac{1}{\frac{\Delta F}{F_0}+1}\right) \quad (2)$$

4.4. Results

4.4.1. Characterization of the bioprinted constructs

Bioprinted constructs containing no microspheres or unloaded microspheres were measured and weighted after bioprinting in order to assess whether the mass of the constructs containing microspheres differed from the constructs without microspheres. The constructs without microspheres showed a diameter of 9.1 mm with a height of 3.9 mm, whereas the construct containing microspheres showed 11.3 mm of diameter and height of 2.7 mm **(Figure 4.1-a,b).** The average wet mass of the constructs without microspheres was 156.06 ± 38.93 mg, while the average mass of the constructs containing unloaded microspheres was 154 ± 47.28 mg. No statistical differences were observed **(Figure 4.1-c).**

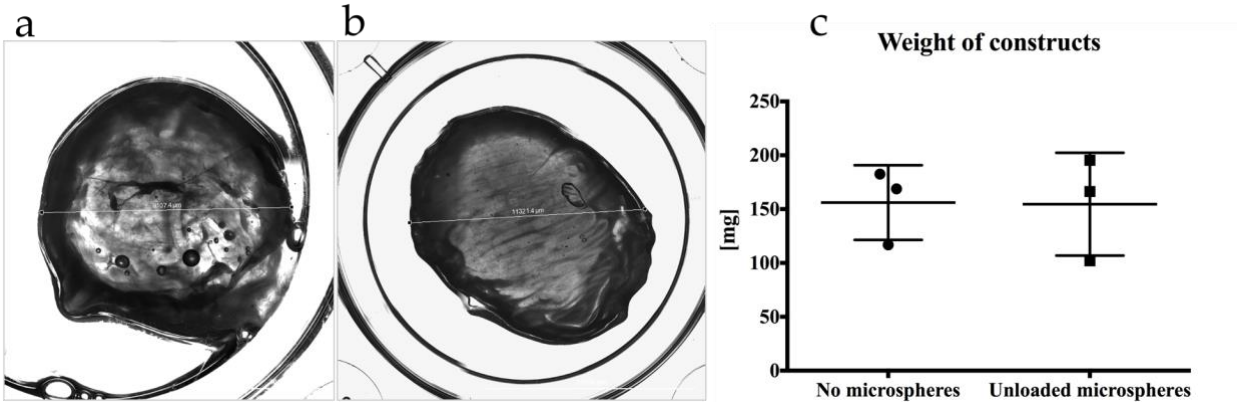

Figure 4.1 Characterization of the bioprinted constructs

a) Bioprinted cylinder structure containing constructs with no microspheres, b) bioprinted structure containing unloaded microspheres showing diameter measurements, and c) wet weight of constructs (n=3) with and without microspheres. Scale bar is 1 mm.

4.4.2. Qualitative assessment of the distribution of the bioprinted microspheres within the constructs

The following groups containing fluorescent and/or drug-loaded microspheres were bioprinted: Red and green, puro and red, RA and green, puro-red :RA-green microspheres, red and green fluorescent microspheres with NPCs, puro-red: RA-green with NPCS. These groups were printed containing drug-loaded and fluorescent microspheres in order to visualize the distributions of the microspheres within the fibers of the construct **(Figure 4.2-4.4**). The group containing puro-red microspheres showed no differences in comparison with the green-RA microsphere group in terms of distribution. The latter applies to all of the other groups as the microspheres are homogeneously distributed within the constructs and the different ratios used in the puro-red/RA-green (2:1) can be visually recognized. The groups containing NPCs in addition to drug-loaded and/or fluorescent microspheres also showed even distribution of the NPCS as observed by the stain with DAPI and fluorescence imaging. **Figure 4.3-4.4** shows the homogeneous distribution of NPCs, stained with DAPI, when bioprinted with drug-loaded (puro and RA) and fluorescent microspheres. The diameter of the bioprinted construct was 12.8 mm and a height of 2.7 mm **(Figure 4.2)**. Furthermore, **Figure 4.5** shows phase contrast images of the bioprinted groups (N+, PR+, M+, U+) containing NPCS on days 2, 12 and 30 where the distribution of the NPCs and microspheres can be identified. The groups M+ and U+ consisted of drug-loaded (puro and RA), and unloaded microspheres, respectively.

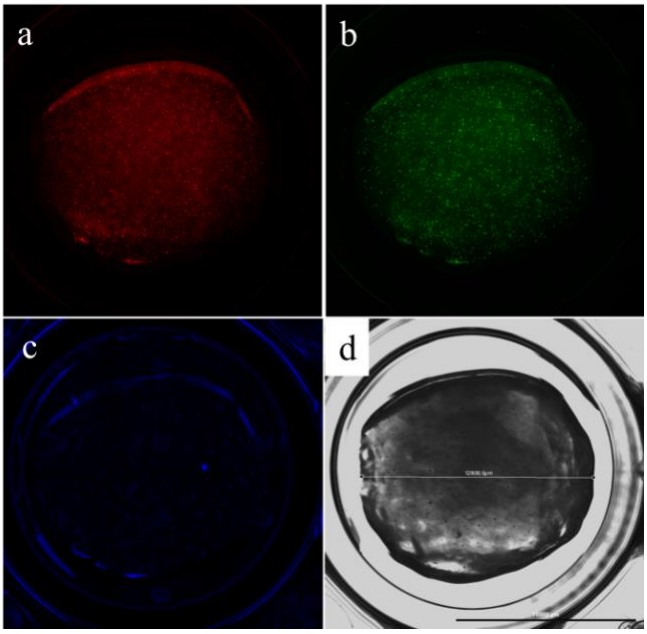

Figure 4.2 NPCs, drug and fluorescent microspheres distribution within the bioprinted construct.
a) red fluorescent microspheres, b) green fluorescent microspheres, c) DAPI stain of bioprinted NPCs, d) phase contrast image showing bioprinted NPCs with drug-loaded and fluorescent microspheres. Scale bar is 1 mm.

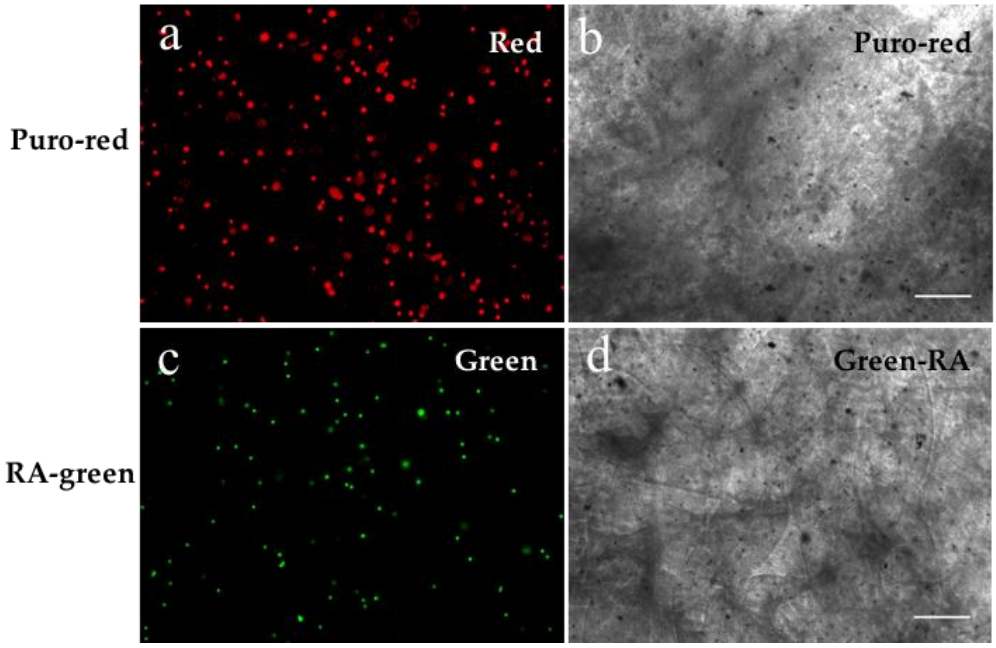

Figure 4.3 Distribution of bioprinted drug-loaded and fluorescent microspheres.
a-b) Bioprinted constructs with puro and red fluorescent microspheres, c-d) bioprinted constructs with RA and green fluorescent microspheres. Figures taken at 4X, scale bar is 300 μm.

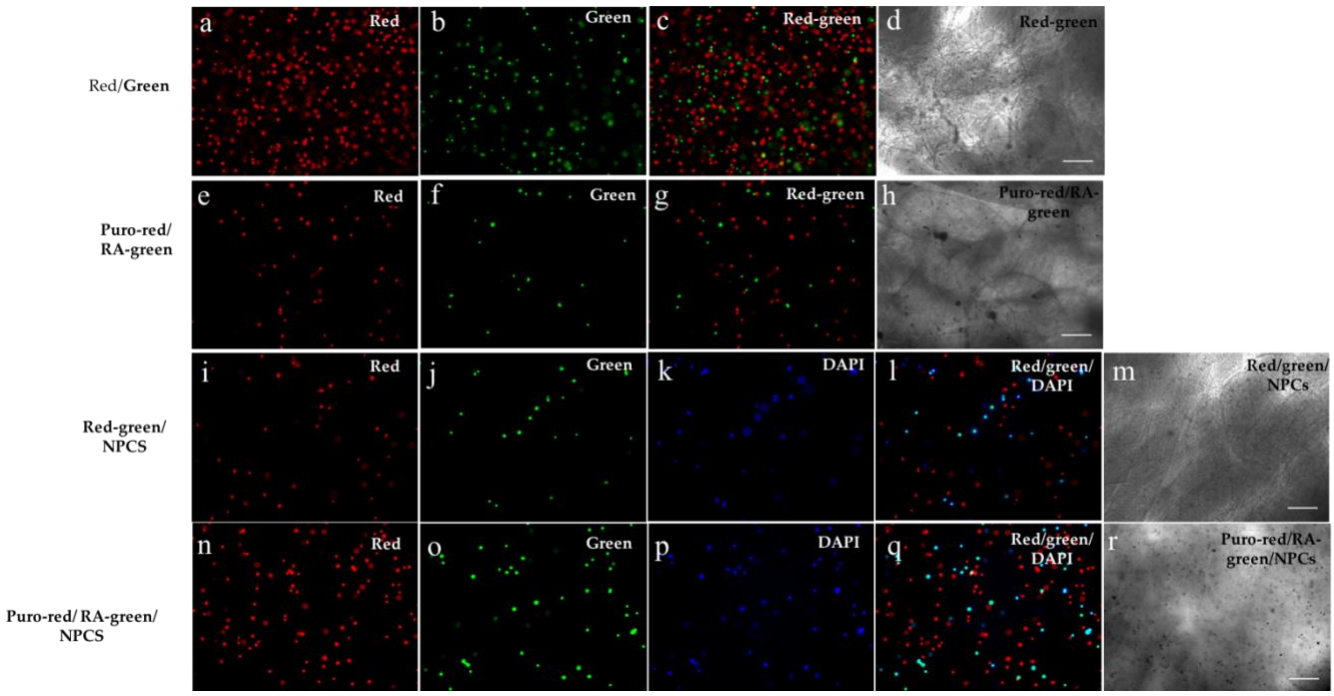

Figure 4.4 Bioprinted drug-loaded, fluorescent microspheres, and NPCs.
a-d) Red and green fluorescent microspheres, e-h) puro-red: RA-green microspheres, i-m) NPCs bioprinted with red, green microspheres, n-r) NPCs bioprinted with puro-red: RA-green microspheres. Figures taken at 4X, scale bar is 300 μm.

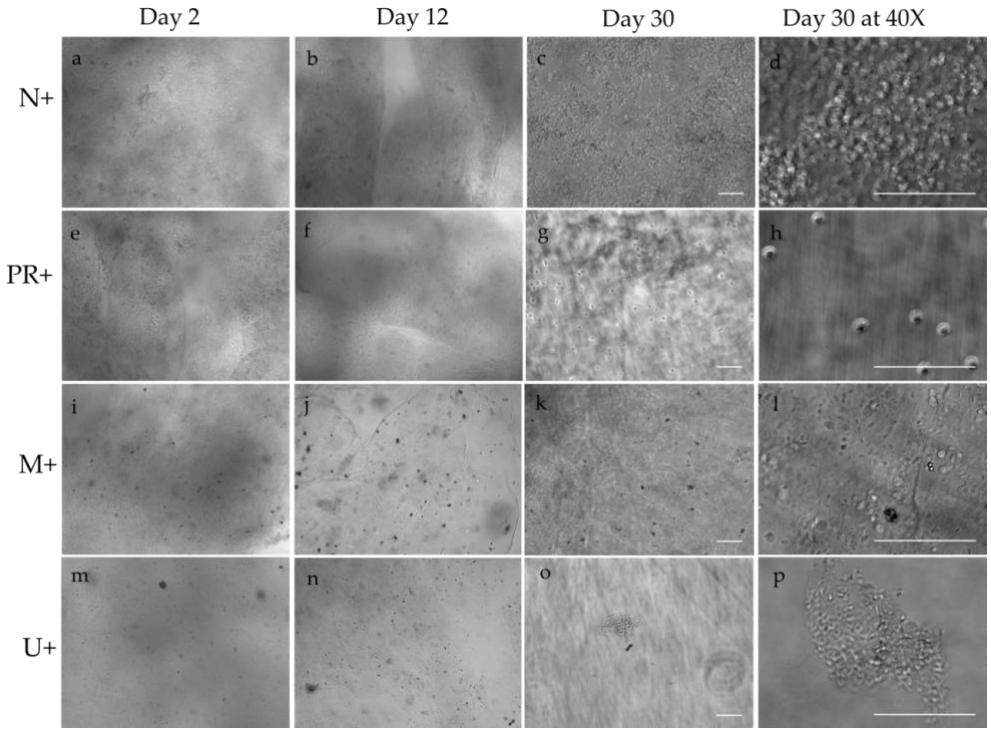

Figure 4.5 Phase contrast imaging of the bioprinted NPCs at days 2, 12, and 30.

a-d) N+, e-h) PR+, i-l) M+, m-p) U+. a-c, e-g, i-k, m-o were taken at 10X, d, h, l, p were taken at 40X. Scale bar is 100 μm for all.

4.4.3. Release kinetics of puro-loaded microspheres

HPLC analysis determined that the encapsulation efficiency (EE) of puro into the microspheres was 89.74 ± 0.12 % with a loading of 0.84 μg/mg (w/w, puro/PLC). After 1 day of culture an initial burst of 25% of the drug released was observed, followed by another increase of up to 45% release on day 4. By day 7, the release was slowed and continuous with a similar trend as observed in previous release studies [216]. The average puro release per day without the initial burst on day 1 was 3.37×10^{-3} μg **(Figure 4.6)**.

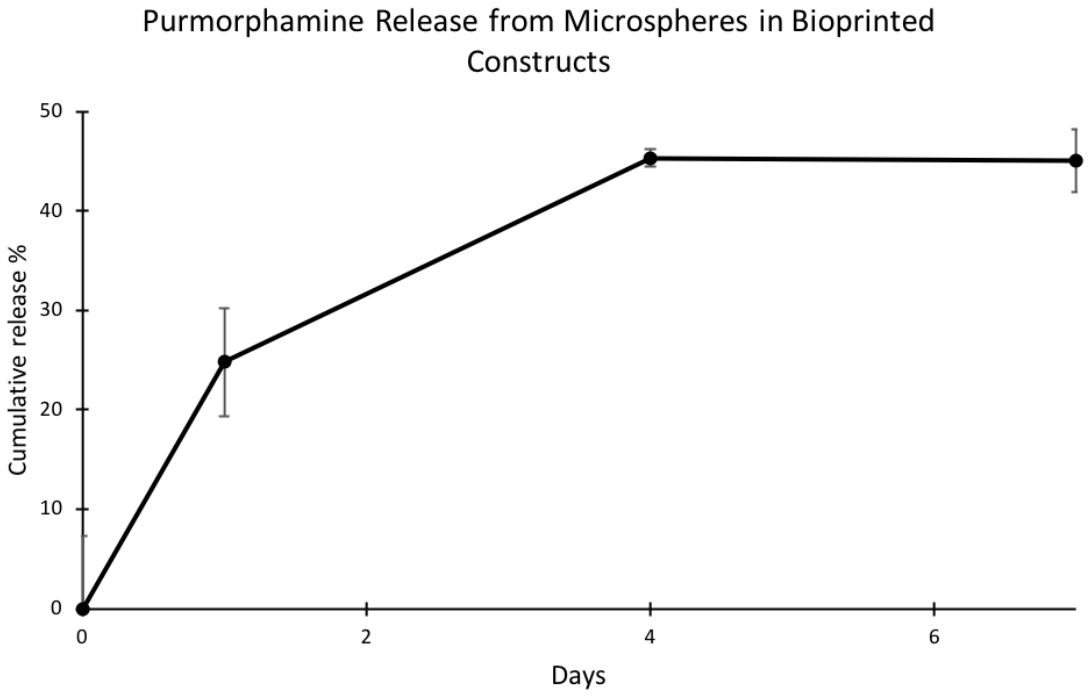

Figure 4.6 Release kinetics of puro over 7 days.
Quantification of puro for 7 days (n=3)- (45%) of the drug was released by day 7. The data reported is the average with error bars representing the standard deviation.

4.4.4. Cell viability of the bioprinted tissues

Cell viability of the bioprinted NPCs was quantified on days 0 and 1 for N+, PR+, M+, and U+. On day 0, the groups without microspheres showed higher viability where N+ was 88.2 ± 0.6 % and PR+ was 87.3 ± 1.2 %. M+ was 77.8± 1.5% while U+ was 75.3 ± 2.9%. Statistical differences were observed for N+ and M+, N+ and U+, PR+ and M+, PR+ and U+. On day 1, cell viability was higher for both groups containing drug-loaded and unloaded microspheres. The highest levels of cell viability were observed in M+ with 98.2 ± 0.5 % and U+ with 83.9 ± 0.5 %. N+ was 79.4 ± 3% which was lower in comparison with day 0 while PR+ showed also lower with 80.4 ± 3%. Statistical differences were observed for N+ and M+, PR+ and M+, M+ and U+. Viability of the bioprinted SMNs was also quantified on days 0 and 1 where 97.4 ± 0.3% of cell viability was observed in day 0 and 84.8 ± 3.4 % on day 1. Statistical differences were observed for cell viability of the SMNs for days 0 and 1 **(Figure 4.7)**.

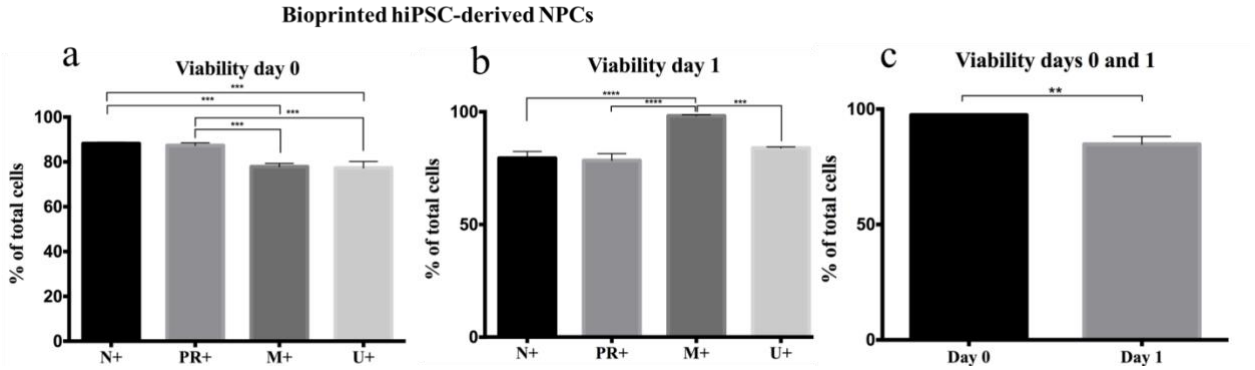

Figure 4.7 Cell viability of the bioprinted NPCs and SMNs on days 0 and 1.
(n=3 for all) N+ (negative control), PR+ (puro and RA added as soluble drugs in the media), M+ (puro and RA-loaded microspheres), U+ (unloaded microspheres), + sign indicates the presence of the small molecules CHIR, SB, and LDN from days 0-5. One-way ANOVA and Tukey post-hoc analysis was performed for statistical analysis between groups per day using a confidence level of 95% ($p < 0.05$). For the SMNS, unpaired T test with equal SD was performed using a confidence level of 95% ($p < 0.05$). * represents $p < 0.05$, ** $p< 0.01$, *** $p< 0.001$.

4.4.5. Cell marker expression of NPCs prior to bioprint

Cell marker expression was quantified on the hiPSC-derived NPCs prior to bioprint. The levels of expression observed were 32.3 ± 1.3 % for the sex determining region box-2 (SOX2) which is a pluripotency and neural stem cell marker, and 95.99 ± 2.1, the neuroectodermal stem cell marker NESTIN. Expression of stage-specific embryonic antigen-1 (SSEA-1) expression was negligible, therefore not shown in **Figure 4.7**. Statistical differences were observed for SOX2 and NESTIN **(Figure 4.8)**.

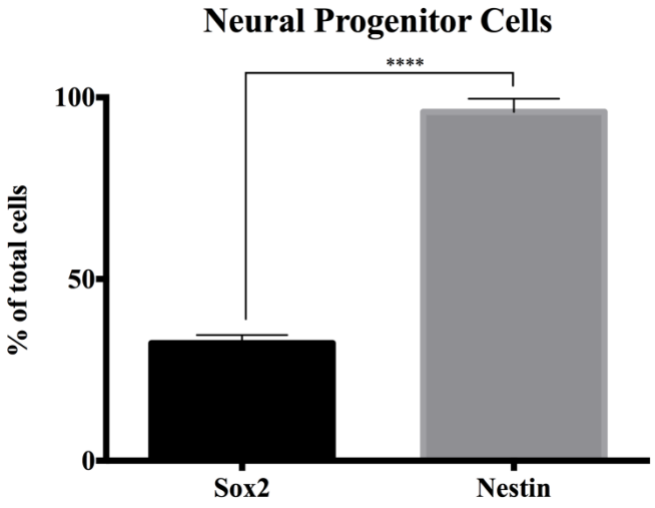

Figure 4.8 Cell marker expression of the NPCs prior to bioprinting.
(n=3 for all) unpaired T test with equal SD was performed using a confidence level of 95% ($p < 0.05$), **** $p < 0.0001$.

4.4.6. Cell marker expression of the bioprinted NPCs on day 15

ICC analysis was performed for the bioprinted NPCs on day 15 for beta tubulin III (βT-III) which is a microtubule protein present exclusively in neurons, the oligodendrocyte marker 2 (OLIG2) which determines MN and oligodendrocyte fate, and the mature motor neuron marker (HB9) **(Figure 4.9)**. Expression of βT-III was observed in all groups **(Figure 4.9-a, f, k, p**). HB9

expression was mainly observed in PR+, M+, and U+, similar to the expression of OLIG2 **(Figure 4.9-b, g, l)**. Quantification of cell marker expression was also analyzed for the bioprinted NPCs using flow cytometry analysis on days 15 **(Figure 4.10)**. Expression of βT-III on day 15 was 28.2 ± 5.5% for N+, 38.5 ± 4.4% for PR+, 37.5 ± 5.5% for M+, and 13.8 ± 0.8 % for U+. Statistical differences were observed for N+ and U+, PR+ and U+, M+ and U+ **(Figure 4.10-a)**. Expression of NESTIN on day 15 remained expressed for all groups with M+ showing the highest level of expression of 91.7 ± 0.5%, followed by N+ with 76.4 ± 10.2%, P+ was 61.4 ± 7.7%, and U+ was 50.4 ± 5.4%. Statistical differences were observed for N+ and U+, PR+ and M+, M+ and U+ **(Figure 4.10-b)**. Expression of HB9 was >50% of expression for all the groups, M+ 82.6 ± 6.4%, PR+ 80.2 ± 0.7%, N+ was 76.8 ± 11.1%, and U+ was 56.5 ± 3.6%. Statistical differences were observed for N+ and U+, PR+ and U+, M+ and U+ **(Figure 4.10-c)**. OLIG2 expression on day 15 was 31 ± 7.1% for M+, followed by 23.17 ± 1.8% for U+, 20.2 ± 3% for PR+, and 15.1 ± 1.9% for N+. Statistical differences were observed for N+ and M+, PR+ and M+ **(Figure 4.10-d)**.

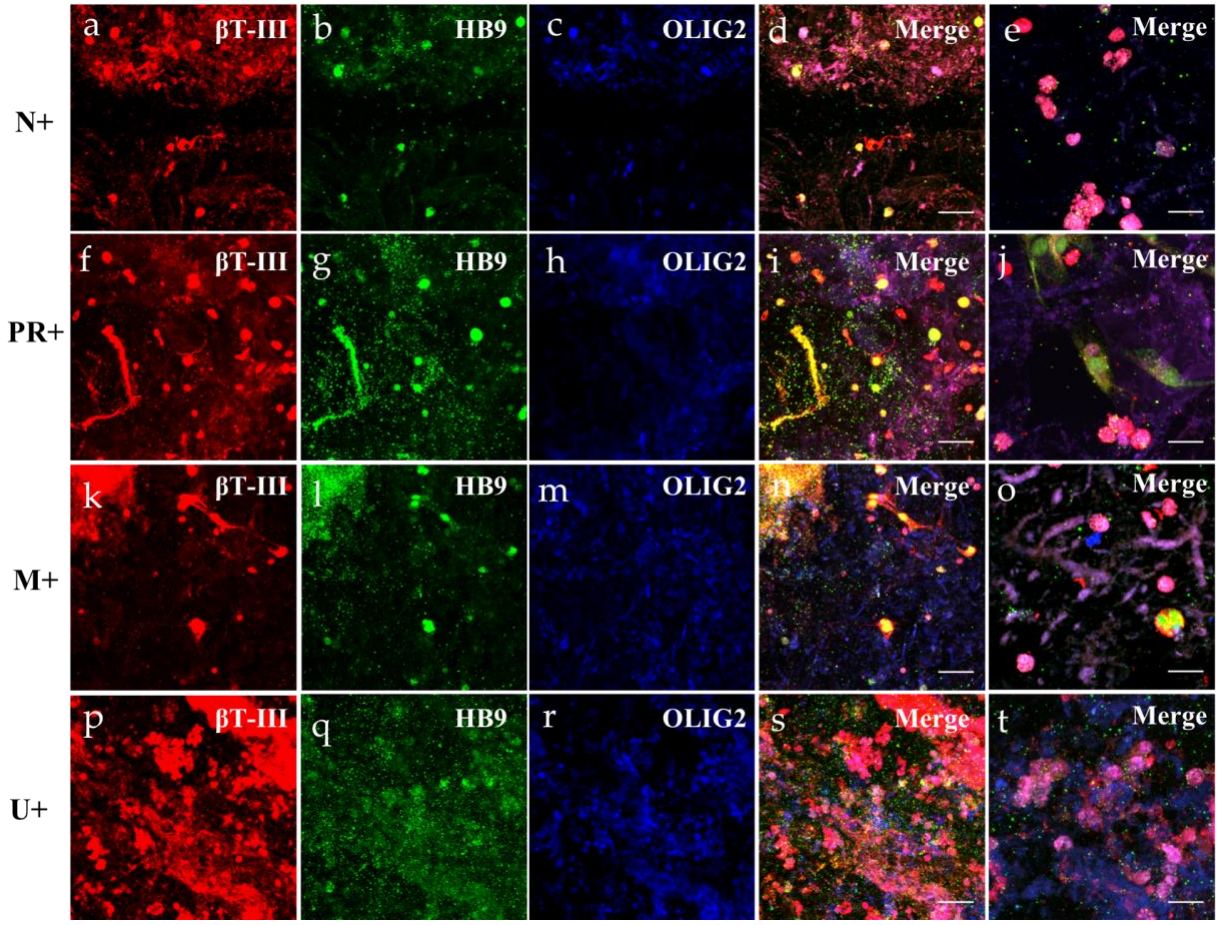

Figure 4.9 Immunocytochemical analysis of the bioprinted NPCs after 15 days.
Expression of beta tubulin III (βT-III- red), homeobox protein 9 (HB9-green), and oligodendrocyte marker 2 (OLIG2-blue) is observed. a-e) N+, f-j) PR+, k-o) M+, p-t) U+. a-d, f-i, k-n, p-s are at 10x, with scale bar of 300 μm. e, j, o, t, are at 4x digital zoom, scale bar is 50 μm.

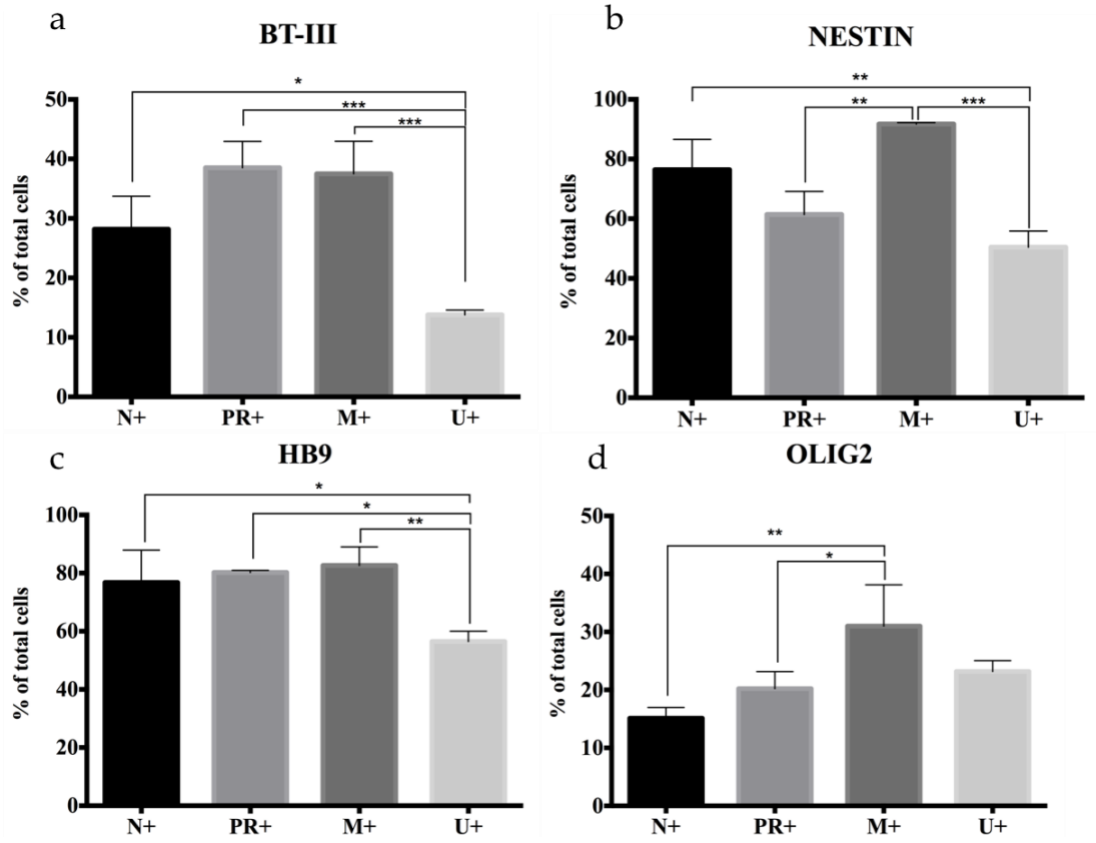

Figure 4.10 Quantification of cell marker expression of the NPCs after 15 days of bioprinted.

Markers quantified were a) βT-III, b) NESTIN, c) HB9, d) OLIG2. (n=3 for all) One-way ANOVA and Tukey post-hoc analysis was performed for statistical analysis using a confidence level of 95% ($p < 0.05$). * represents $p < 0.05$, *** $p < 0.001$.

4.4.7. Cell marker expression of the bioprinted NPCs on day 30

ICC analysis was performed for the bioprinted NPCs on day 30 for βT-III, the glial fibrillary acidic protein (GFAP) which is an intermediate filament protein expressed in astrocytes, and CHAT, enzyme in charge of synthesizing the production of the neurotransmitter acetylcholine **(Figure 4.11)**. GFAP expression was observed for all groups **(Figure 4.11-a, f, k, p)**. βT-III was expressed in all groups, M+ showing the highest levels of expression **(Figure 4.11-l)**. CHAT expression was observed for PR+ and M+ **(Figure 4.11-h, m)**. Furthermore, expression of the lipid-rich membrane of myelin was observed on day 30 for N+, M+, and U+ (data not available

for PR+). The inhibitory neuron marker GABA observed mainly for N+ and M+ **(Figure 4.12)**. Quantification of cell marker expression on day 30 was analyzed for βT-III, HB9, the transcription factor Islet-1 (ISL-1) that is required for survival and specification of MNs, and CHAT **(Figure 4.13)**. N+ showed the highest expression of βT-III with 70.1 ± 24.7%, followed by PR+ with 31.04 ± 5.6%, M+ with 25.6 ± 11.2%, and U+ with 13.9 ± 10.1%. Statistical differences were observed for N+ and PR+, N+ and M+, N+ and U+ **(Figure 4.13-a)**. HB9 expression was also quantified at this time point where PR+ showed the highest level of expression at 52.1 ± 6.5%, followed by M+ with 23.6 ± 2.6%, U+ with 14.7 ± 0.7%, and N+ with 5.7 ± 1.3 %. Statistical differences were observed for N+ and PR+, N+ and M+, PR+ and M+, PR+ and U+ **(Figure 4.13-b)**. ISL-1 expression was 10.4 ± 3.1% for PR+, 6.1 ± 0.8% for M+, 2.5 ± 0.2 % for U+, and 1.6 ± 0.3% for M+. Statistical differences were observed for N+ and PR+, N+ and M+, PR+ and M+, PR+ and U+ **(Figure 4.13-c)**. CHAT expression was 15.9 ± 4.6 % for M+, 14.5 ± 2.3% for PR+, 14.3 ± 2.7% for N+, and 10.8 ± 0.4% for U+. No statistical differences were observed **(Figure 4.13-d)**.

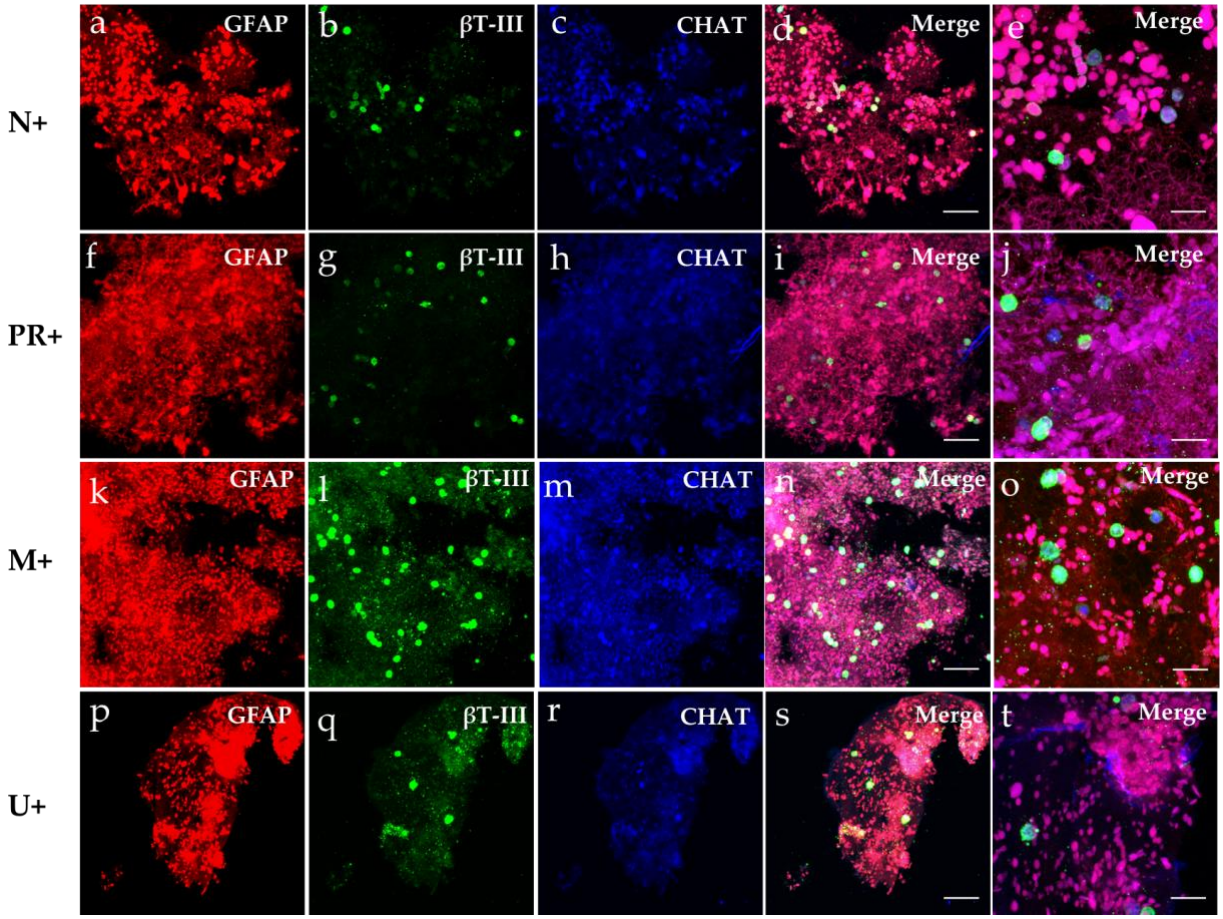

Figure 4.11 Immunocytochemical analysis of the bioprinted constructs after 30 days of bioprinted NPCs.
Expression of GFAP-red, βT-III- green, and CHAT-blue is observed. a-e) N+, f-j) PR+, k-o) M+, p-t) U+. a-d, f-i, k-n, p-s are at 10x, with scale bar of 300 μm. e, j, o, t, are at 4x digital zoom, scale bar is 50 μm.

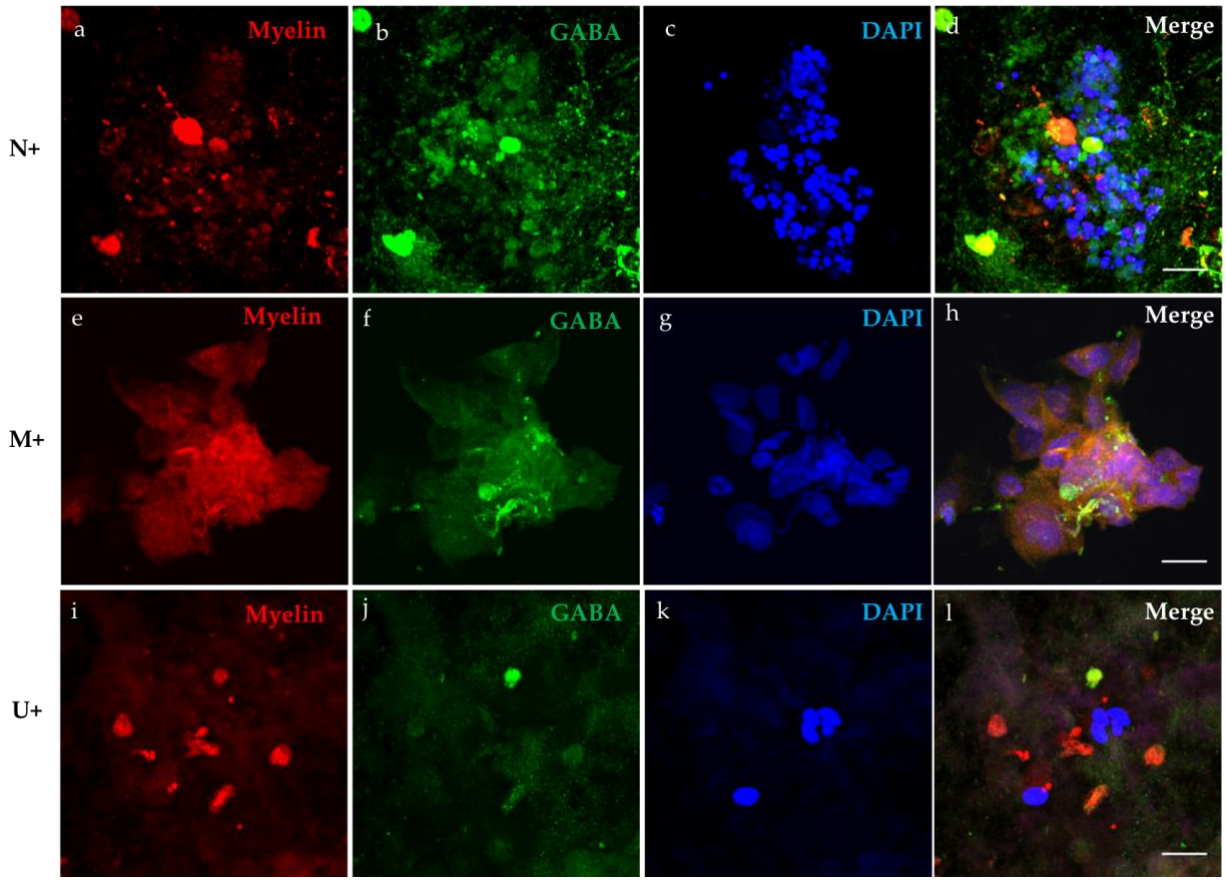

Figure 4.12 Immunocytochemical analysis of the bioprinted constructs after 30 days of bioprinted NPCs.
Expression of Myelin-red, GABA- green, and DAPI-blue is observed. a-d) N+, e-h) M+, i-l) U+. Figure taken at 20x + 5x digital zoom, scale bar indicates 20 μm.

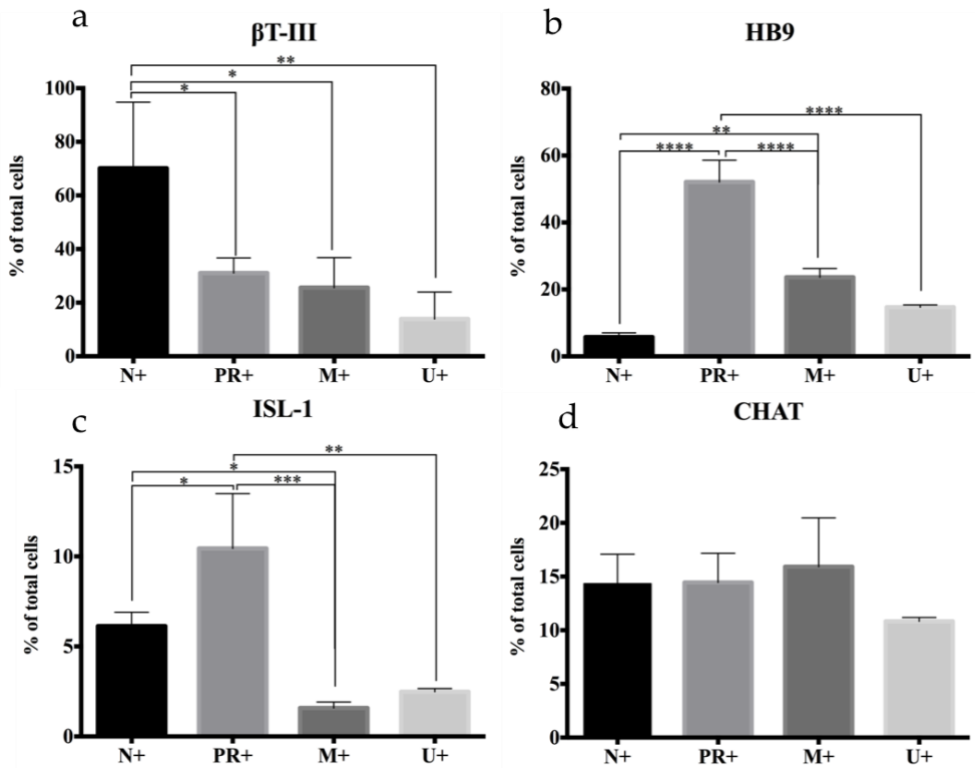

Figure 4.13 Quantification of cell marker expression of the NPCS after 30 days of bioprinted.
Markers quantified were a) βT-III, b) HB9, c) ILS-1, d) CHAT. (n=3 for all) One-way ANOVA and Tukey post-hoc analysis was performed for statistical analysis using a confidence level of 95% ($p < 0.05$). * represents $p < 0.05$, ** $p< 0.01$, *** $p< 0.001$.

4.4.8. Cell marker expression of the bioprinted NPCs on day 45.

Quantification of cell marker expression was analyzed on day 45 for MAP2, CHAT, GFAP, and the oligodendrocyte factor 4 (O4). Expression of MAP2 was the highest for M+ with 13.3 ± 0.8%, followed by 11.5 ± 1.2% for N+, 7.8 ± 0.5% for PR+, and 2.9 ± 0.3% for U+. Statistical differences were observed for N+ and PR+, N+ and U+, PR+ and M+, PR+ and U+, M+ and U+ **(Figure 4.14-a)**. Expression of CHAT was the highest for N+ with 25.0 ± 3.8%, followed by M+ with 19.1 ± 1.7%, U+ with 6.9 ± 1.4%, and PR with 4.3 ± 0.2%. Statistical differences were observed for N+ and PR+, N+ and M+, N+ and U+, PR+ and M+, M+ and U+ **(Figure 4.14-b)**.

GFAP expression was 11.1 ± 1.3% for M+, 10.9 ± 1.7% for N+, 8.9 ± 0.3% for PR+, and 4.9 ± 1.7% for U+. Statistical differences were observed for N+ and U+, PR+ and U+, M+ and U+ **(Figure 4.14-c)**. Expression of O4 was 15.2 ± 0.8% for N+, 12.9 ± 0.6% for M+, 8.4 ± 0.6% for PR+, and 6.4 ± 0.2% for U+. Statistical differences were observed for N+ and PR+, N+ and M+, N+ and U+, PR+ and M+, PR+ and U+, M+ and U+ **(Figure 4.14-d)**.

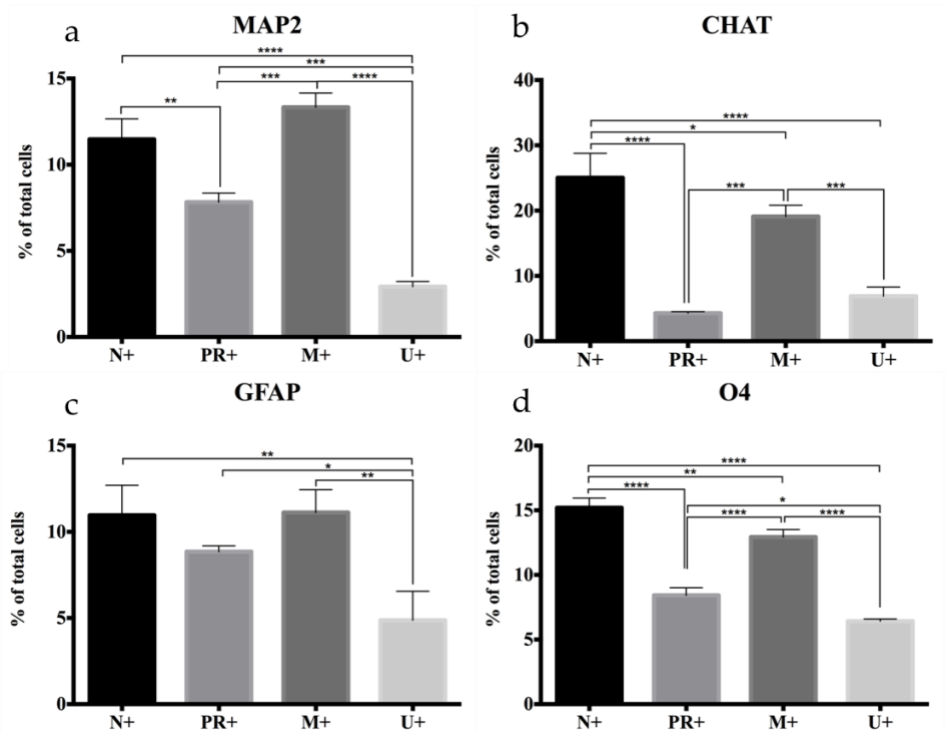

Figure 4.14 Quantification of cell marker expression of the NPCs after 45 days of bioprinted.
Markers quantified were a) the microtubule associated protein 2 (MAP2), b) CHAT, c) GFAP, and d) oligodendrocyte factor 4 (O4). (n=3 for all) One-way ANOVA and Tukey post-hoc analysis was performed for statistical analysis using a confidence level of 95% ($p < 0.05$). * represents $p < 0.05$, ** $p< 0.01$, *** $p< 0.001$, **** $p< 0.0001$.

4.4.9. Quantification of membrane potential for the bioprinted NPCs on days 30 and 45

Cell membrane potential was quantified on days 30 and 35 for the bioprinted NPCs, and on days 0, 1, and 7 for the bioprinted SMNs **(Figure 4.15)**. The bioprinted tissues were incubated

with the FLIPR blue dye for 45 min, followed by quantification of the membrane potential at rest. The tissues were the incubated with Ach for 25 minutes followed by readings for excitation. Lastly all NPC bioprinted groups on day 45 were inhibited with GABA for 25 minutes after exposure to Ach, followed by readings for inhibition. All cell culture treatments were responsive to the excitation treatments as observed by an increase in the membrane potential. On day 30, statistical differences were observed for all groups at rest versus excitation. On day 45, all groups showed statistical differences after excitation and after inhibition except for M+ which would be explained by the large standard deviations. For the bioprinted SMNs, statistical differences were observed after excitation on day 0.

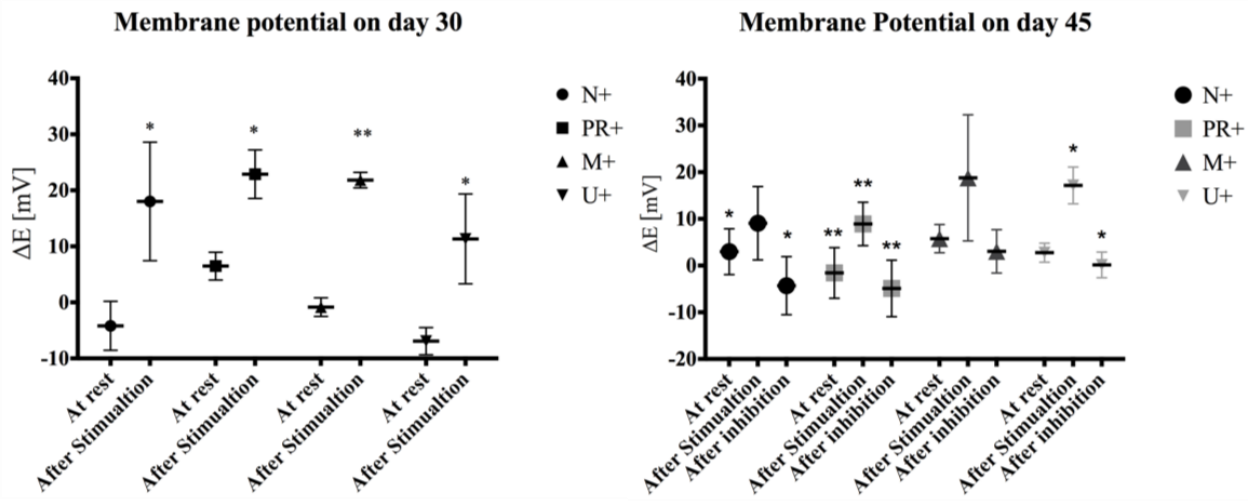

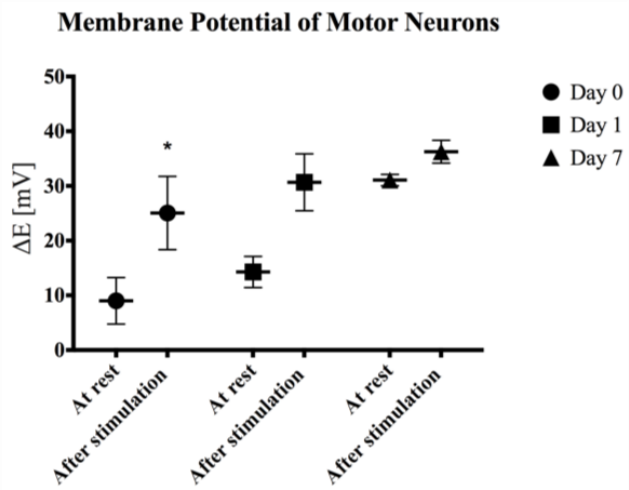

Figure 4.15 Membrane potential of the bioprinted NPCs at days 30 and 45 and SMNs at day 0, 1, and 7.
The membrane potential was quantified at rest, followed by excitation with acetylcholine (Ach), for all. After excitation, the bioprinted tissues were inhibited with GABA on day 45. (n=3 for all) Repeated measures ANOVA was performed for each group at each time point using a confidence level of 95% ($p < 0.05$). * represents $p < 0.05$, ** $p< 0.01$.

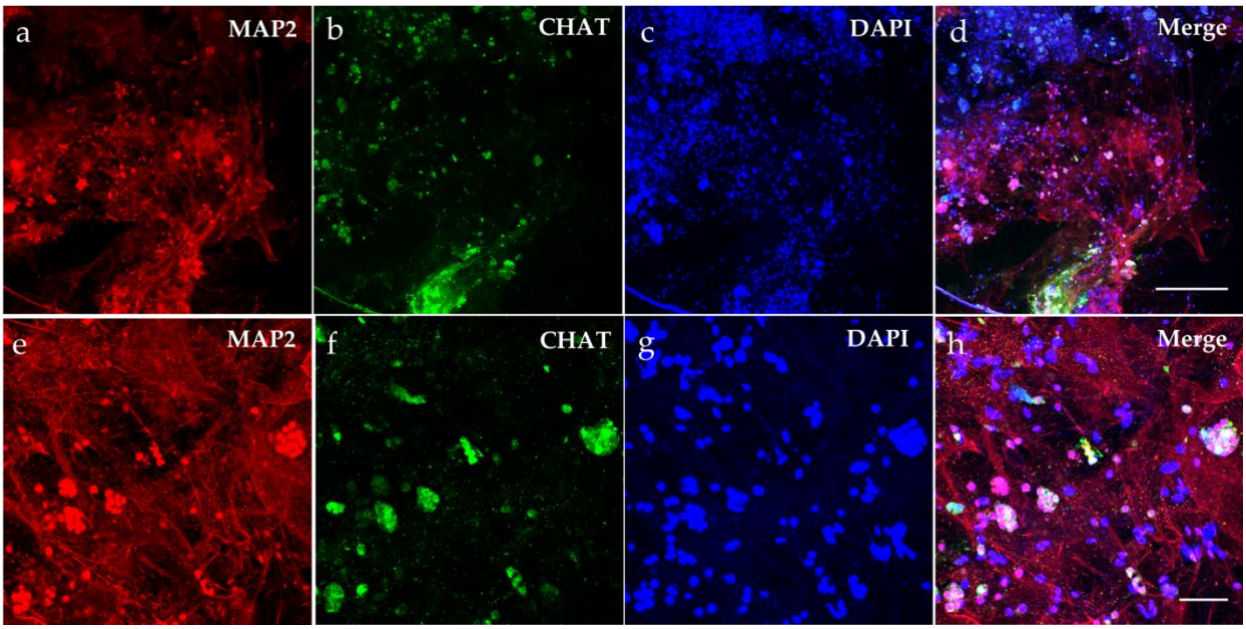

Figure 4.16 Immunocytochemical analysis of bioprinted SMNs after 7 days of bioprinted.
Cell marker expression is observed for MAP2-red, CHAT-green, and DAPI-blue. a-d are at 10X with scale bar of 300 μm, e-h are at 20x with scale bar of 50 μm.

4.5. Discussion

In this study, we bioprinted drug-loaded microspheres, fluorescent microspheres and hiPSC-derived NPCs using our neuro-bioink in combination with the LOP™ and RX1 bioprinting technologies. The cell-laden bioink contained hiPSC-derived NPCs that were successfully differentiated into neural tissues after 45 days using the slow release of puro and RA loaded microspheres. These neural tissues also showed cell maturation and responsiveness through characterization of their cell marker expression and membrane potentials upon excitation and inhibition. We are the first group to bioprinting small molecule releasing microspheres for the differentiation of neural tissues to our knowledge. Other groups have bioprinted encapsulated protein or growth factors in a diverse range of polymers such as PLGA, gelatin and alginate, for bone and vascularized TE 245-247. Bioprinting stem cell derived tissues along with small molecule releasing microspheres opens up a field TE where the bioprinted tissues can be differentiated *in situ* and provide an efficient delivery of a variety of morphogens.

The diameter and height for the bioprinted constructs were evaluated, and our results show that the bioprinted constructs containing no microspheres had a diameter and height of 9.1 mm and 3.9 mm, respectively. Dimensions for the constructs containing unloaded microspheres were 11.3 mm and 2.7 mm of diameter and height, respectively. These dimensions are similar to the specified in the original CAD design which was 13 mm of diameter and height of 2.7 mm. The difference in dimensions could be attributed to the presence of microspheres within the constructs contributing to larger diameter of the construct. While no statistical differences were observed in the wet weight of the constructs, here we observe that the constructs containing unloaded microspheres have a larger diameter and shorter height. Future measurements of the dry weight of the constructs could provide a different cue on the weight provided by the microspheres within the

constructs and their effect in the total height. However, differences in dimensions could also be attributed to some deformation when transferring the constructs from the bioprinting stage to the cell culture plate. To prevent deformation, the tissues could be directly printed and cultured inside of cell culture inserts.

Homogenous distribution of the drug-loaded microspheres within the fibers is crucial for differentiating the hiPSC-derived NPCs. Therefore, we bioprinted the neuro-bioink with fluorescent microspheres with the purpose of analyzing their distribution within the construct. Our qualitative results showed that all the group combinations of bioprinted with fluorescent and/or drug-loaded microspheres, with or without NPCs, showed a homogenous distribution when bioprinted with our neuro-bioink. Similarly, concentration gradients and localized drug delivery of different drug-loaded microspheres within the same construct can be achieved in order to promote differentiation into different types of cells.

Cellular viability after bioprinting is one of the main challenges when bioprinting tissues as the cells tend to be exposed to high shear forces while being extruded through the nozzle on extrusion bioprinting systems [224]. While some groups have reported that longer nozzles of 24.4 mm lead to an increased exposure of shear stress for the cells with a cell viability of 71%, here we demonstrate that the LOP™ soft nozzle of 28 mm leads to a cell viability >75% after being bioprinted on day 0 and >79% on day 1 [142]. Our previous study also showed an increase in cell viability of >81% after 7 days of bioprinted using our neuro-bioink and the LOP™ [102]. Interestingly, our drug-loaded microsphere group (M+) showed the highest percentage of cell viability 98.2 ± 0.5 % in comparison with the other groups where the lowest viability was observed for N+ with 79.4 ± 3%. These results suggest that either the controlled release of the small

molecules or the physical properties of the construct could be promoting cellular differentiation for the constructs containing drug-loaded or unloaded microspheres. However, given that there are statistical differences for M+ and U+ on viability day 1, these results suggests that controlled drug release leads to cellular proliferation, and therefore, an increase in the number of viable cells after being bioprinted.

As previously reported, the continuous release of puro and RA from drug-loaded microspheres, can efficiently differentiate hiPSCs into neural cell types by lowering the amount of drug required compared to using soluble drugs added into the media and also reducing the need for media changes to add more drug, consequently reducing human intervention and room for error [37]. In this study, a total amount of 0.25 mg of microspheres was added per ml of bioink with a ratio of 2:1 puro to RA microspheres. Previous studies have demonstrated that 0.5 mg of puro and RA-loaded microspheres on a 2:1 ratio provided enough small molecules for the differentiation of ~2.5x10^6 hiPSCs-derived neural aggregates (NAs) [216]. Given that in this study 1x10^6 cells/ml were used, a total of 0.25 mg of microspheres was used in order to evaluate the printability and effect on differentiation of the NPCs. Based on the 7-day release study, on day 1 an initial burst of 25% (0.21 ug of puro) was released and by day 7 a total of 45% of the initial drug encapsulated was released. The average puro release per day from day 2-7 was $3.37x10^{-3}$ ug, at this rate the microspheres released puro for a total number 31 days including the initial burst on day 1. Given this release profile, a total of 0.13 ug of puro/ml of bioink was used to differentiate the bioprinted NPCs into mature neural tissues. Furthermore, the release curve observed in this release study shows a similar trend to previously reported, however in this study the puro release was faster potentially due to an increased exposure to aqueous environment and accelerated degradation rate of the microspheres [216]. For PR+, where the soluble puro was constantly added to the media, an

average of 0.06 μg of puro was added on each media change and a total of 3.7 μg of puro/ml bioink was used for the 45 days of culture *in vitro*. The release of RA from the microspheres was calculated based on our previous release studies. For the RA-loaded microspheres, an average of 4.5x10^-2 μg of RA was released per day and a total of 2.08 μg of RA was released from the microspheres per ml of bioink for the 45 days duration of this study. The average soluble RA added on each media change was 0.07 μg, with a total amount of 1.2 μg being used for the whole study.

Here, we show again that the constant and slow release of these two morphogens can promote the efficient production of mature neuronal subtypes form hiPSCs as observed in our previous study [37]. Notwithstanding, the constant exposure of the NPCs to the drugs within the bioprinted construct, provides an efficient and less labor- intensive way to differentiate and mature the tissues. This can be observed by the high expression of the mature MN marker HB9 for PR+ and M+ (~80%) by day 15, similar to other protocols where hiPSC derived MNs were cultured in 2D and our previous study where different bioprinted NPCs groups were treated with soluble puro and RA [66,102]. Interestingly, the expression of the OLIG2 MN progenitor at this time point was >20% for both PR+ and M+, we hypothesized that the expression of this marker at this time point could lead to the further differentiation into oligodendrocytes. Furthermore, by day 15 expression of the intermediate filament marker NESTIN in NPCs was observed in M+ at >80%. The elevated expression of this marker could be attributed to the bioink degradation rate and ECM remodeling as observed by Madl *et al.*, [248]. Since the maturation media was added until day 12, it is possible that the initial population of NPCs proliferated. Further studies analyzing total number of cells and scaffold degradation could be performed to confirm this hypothesis. Notwithstanding, mature neurons co-expressing NESIN and CHAT have been found in the adult brain in the basal forebrain region which is the main region for cholinergic output in the brain [249]. The high expression of

NESTIN on day 15 could also be attributed to the nature of the cholinergic neurons present in the bioprinted tissues.

By day 30 and 45, cell marker expression was characterized for the presence and level of maturation of different types of cells in the CNS. On day 30, all the groups showed the presence of astrocytes as observed by the expression of GFAP, as well as the expression of βT-III. Our ICC analysis revealed that the neurons expressing βT-III seem to be surrounded by the astrocytes. Expression of CHAT was mainly observed for M+ and slightly for PR+. This expression was also observed in our previous study where NPCs were bioprinted with the same neuro-bioink and treated with the cocktail of small molecules CHIR, LDN, and SB. However, in this current study, the NPCs, were only exposed to this cocktail from days 0-5, as opposed to days 0-15 as previously reported [102]. This suggests that an early exposure to BMP inhibitor and WNT pathway agonist are only needed for a few days after bioprinting and is enough for the NPCs to commit to a neural lineage. Flow cytometry analysis revealed the expression of both HB9 and ILS-1 which indicates the presence of mature motor neurons, as well as the expression of CHAT. Moreover, ICC analysis revealed the presence of myelin and the inhibitory neurotransmitter GABA in the bioprinted tissues after 30 days of culture, suggesting the presence of multiple neuronal subtypes and myelinating oligodendrocytes in the matured tissues.

By day 45, the presence of all the relevant CNS cell types present in the CNS was observed with the expression of MAP2 for neurons, CHAT- cholinergic neurons, GFAP, and O4 oligodendrocytes. Overall, M+ showed >13% expression for these markers and ~ 20% expression for CHAT. Interestingly, PR+ showed the lower expression of all the markers in comparison to M+, suggesting that the controlled release of the morphogens within the 3D printed constructs is

an efficient way to differentiate and mature neural tissues, achieving the presence of the cell types in the CNS that are important for maintaining homeostasis and neurotransmission.

The membrane potentials of the matured MNs were analyzed on days 30 and 45 to characterize the electrical properties as an indicator of maturity for our bioprinted tissues. As suggested by Robinson *et al.* the FLIPR blue dye is a voltage sensitive dye that can be used as a robust method for determining the electrical activity of cells in *in vitro* [243]. In order to gauge the level of maturation of our bioprinted NPCs, we bioprinted mature hiPSC-derived SMNs to compare their membrane potential on days 0, 1, and 7. The resting membrane potential of mature neurons lies at -70 mV [18]. An action potential occurs when there is an increase in the electrical charge of the membrane that occurs as an all-or-nothing event once the threshold at -50mV has been reached [243]. The resting membrane potential of our bioprinted and matured PR+ and M+ tissues was below 7 mV on day 30. Interestingly, U+ showed the lowest resting membrane potential. Furthermore, in spite of the differentiated tissues not showing a resting membrane potential at -70 mV, the SMNs resting potential on day 0 was ~9 mV and increased for days 1 and 7. The resting membrane potential of our bioprinted constructs remained below 7 mv after day 45 for all groups. This behavior could be attributed to the lack of full maturation of our bioprinted NPCs and possibly a period of acclimation of the cells (SMNs) in our neuro-bioink.

Given that MNs are cholinergic, we stimulated with the neurotransmitter Ach in order analyze their responsiveness as an indication of maturation. By day 30, all groups showed to be responsive upon exposure to Ach. The M+ group showed the most significant differences after stimulation reaching an average membrane potential of 21.8 mV in comparison with the rest of the groups. The SMNs showed a higher increase in the membrane potential reaching an average of 25

mV on day 0. These results correlate with Robinson *et al.* where characterizing the resting membrane potential of mature MNs in 2D showed it to be below ~10 mV and the MNs displayed an average of ~ 20 mV upon stimulation with Ach. This experiment was repeated again on day 45 for our bioprinted constructs with the additional test of exposure to the inhibitory neurotransmitter GABA after stimulation in order to analyze their capability to respond to different neurotransmitters [244]. On day 45, we saw similar levels resting membrane potential, below 6 mV, followed by increase after stimulation with Ach and decrease in membrane potential after exposure to GABA. All groups but M+ showed statistical differences after exposure with each neurotransmitter. This could be explained by the large standard deviation in these readings that could be attributed to the nature of the membrane potential.

GABA is one of the major neurotransmitters in the CNS and it's responsible for the 40% of the inhibitory processes [250]. In the past, it has been observed that the exposure of non-active or immature neurons to GABA can cause depolarization rather than hyperpolarization as a result of an increased Cl^- efflux [244,251]. In this study, inhibition with GABA for all groups led to a lower membrane potential than the initial readings at rest. These results suggest that cells in all groups have effectively differentiated and matured into MNs and are electrophysiologically active as observed by an increase in the average membrane potential upon stimulation with Ach and reversed when adding the inhibitory neurotransmitter.

4.6. Conclusions

In this study, we have shown the successful bioprinting and differentiation of hiPSC-derived neural tissues using small molecule releasing microspheres. To our knowledge, we are the first group to bioprint small molecule releasing microspheres for the derivation of neural tissues.

Our drug-loaded microspheres were homogeneously distributed within the bioink and promoted an efficient differentiation and maturation of MNs. Our tissues also showed the expression of other cells in the CNS such as astrocytes as observed by the expression of GFAP and oligodendrocytes that are actively producing myelin as observed by the expression of O4 and myelin. Furthermore, our matured MNs were shown to be electrophysiologically active upon stimulation with Ach, followed by inhibition with GABA and showed similar behavior to bioprinted mature human SMNs. In the future, our studies will focus on the localization of drug delivery within a single construct, as well as the creation of concentration gradients to fully differentiate different cell types and obtain a more complex environment in our neural tissues in a 3D environment.

Chapter 5 Discussion and conclusion

The overall focus of this research was to develop novel strategies for engineering neural tissue and exploring the differentiation of hiPSCs using drug releasing microspheres and 3D environments. Different scenarios have been explored in which the hiPSCs were exposed to a slow release of morphogens and analyzed their levels of differentiation. The studies presented here address this statement in three specific ways:

5.1. Discussion and conclusion of research aim 1

Research aim 1 was to encapsulate the small molecule puro in PCL to create drug-loaded microspheres and characterize their controlled release and morphology. Puro is a small molecule that activates the SHH pathway and promotes differentiation of hiPSCs into MNs. RA is another small molecule important during neurogenesis and crucial in the development of the CNS. Given the importance of both molecules in the development of neural tissues, both RA- and puro-loaded microspheres were combined with hiPSC-derived NAs and the level of differentiation was determined.

In Chapter 2 we demonstrate that puro can be encapsulated in PCL using a single emulsion, oil-in-water, process and has a controlled release of the drug over 46 days given the release studies. Choosing a polymer that is slowly biodegradable was crucial when encapsulating drugs for the differentiation of neural tissues as it can take about four weeks to obtain neuronal subtypes from hiPSCs. PCL was the polymer of choice as it would degrade slowly to deliver the morphogens needed for differentiation in a controlled and sustained manner for long periods of time. The fabrication of these drug-loaded microspheres was tailored in order to get a high EE of the drug given the amount of PCL used. Additionally, the fabricated microspheres have an average size of

3.4 µm which is appropriate considering the individual cell size (~10 µm), larger microspheres can block the cellular interactions and connections, preventing them from surviving and differentiating. As well, smaller microspheres could be taken up by the individual cells via phagocytosis. Furthermore, the presence of the microspheres within the NAs overcame the challenges of drug degradation when the morphogens are added to the cell culture media.

Given that the microspheres are incorporated throughout each NA, the individual cells have a consistent and sustained exposure to the drug that promotes their differentiation into neural lineages. The effectiveness of the controlled drug release from the microspheres in promoting differentiation was shown in Chapter 2 with the extensive neurite outgrowth and expression of multiple neural markers. The controlled release of the drug from the microspheres provided similar levels of differentiation in comparison with the addition of the drugs to the media, however the overall amount of drug released was significantly smaller, while still being effective, than the soluble drug treatment, making this option more cost effective for further studies.

Furthermore, the incorporation of drug releasing microspheres provides an autonomous way for delivering morphogens to the neural tissues, providing a step towards the production of neural tissues as a drug screening tool in a high-throughput manner.

5.2. Discussion and conclusion of research aim 2

Research aim 2 was to engineer neural tissues from hiPSC-derived NPCs in a 3D environment using a hydrogel bioink and bioprinting technologies. Hydrogel biomaterials swell extensively in the presence of water and are suitable scaffold materials for modeling soft tissues like neural tissues. The suspension of NPCs in within the hydrogel provides a 3D structure for

tissues. The combination of biomaterials in the bioink must meet the characteristics needed for neural tissues to develop and differentiate.

In Chapter 3 we used a fibrin-based bioink and LOP™ technology to bioprint neural tissues in a reproducible way. Fibrin is an important component in the process of wound healing and has been shown to be a suitable component for the development of neural tissues. Alginate is another biomaterial used in this bioink in order to provide the viscosity needed for the fibrin to be bioprinted using the RXI bioprinter. Chitosan was used to provide immediate stability to the bioprinted tissues due to the ionic interactions with alginate. In this study, the macro-architecture chosen was a cylinder and the tissues were bioprinted with concentric fibers smaller than 200 µm in diameter providing an intricate micro-architecture. The NPCs were homogeneously distributed within the crosslinked fibers after bioprinting, during differentiation and maturation. The survival of the cells during the stressful process of bioprinting is crucial for the creation of neural tissues as neural cells are not able to replicate once matured into post-mitotic neuronal subtypes. The LOP™ technology, with its fiber sheathing, was able to protect the cells from shear-stress and maintained cell viability as observed by the high numbers of viable cells observed in all treatments. Furthermore, the biomaterials degraded slowly during the process of maturation and after 30 days, most of the scaffold was gone. However, the cells remained in the cell culture dishes suggesting that the biomaterials provided a suitable environment for the cells to produce their own ECM and form neural tissues.

5.3. Discussion and conclusion of research aim 3

In chapter 4, we hypothesized that the combination of drug releasing microspheres and bioprinting technologies could serve as an effective way to engineer neural tissues. We showed

for the first time that drug-loaded microspheres can be bioprinted and be homogeneously distributed within the whole construct. This remains truthful when bioprinting fluorescent and/or drug loaded microspheres in combination with hiPSC-derived NPCs. Furthermore, we show that the drug loaded microspheres are capable of slowly releasing the drug and supporting NPC differentiation using significantly less drug than adding the soluble drug to the media.

Cellular viability post-printing is one of the major challenges faced in the field of bioprinting when using extrusion-based systems. This is a major concern specifically when bioprinting neural tissues as the cells become post-mitotic once they have matured into neuronal subtypes. In order to analyze the effect of the bioprinting technologies used in this study, we quantified cell viability of the bioprinted hiPSCs-derived NPCs as well as mature post-mitotic SMNs. Our results showed high levels (~80%) of cellular viability post printing for both cell types, proving that the current bioprinting method is appropriate for bioprinting neural-derived tissues.

In chapter 4, we also analyzed differentiation, maturation and responsive profiles of the bioprinted tissues when combined with puro- and RA-loaded microspheres. We show for the first time that our bioprinted tissues can be cultured *in vitro* for up to 45 days. Additionally, the differentiated tissues contained a combination of neurons, astrocytes, and oligodendrocytes, which are the main cellular components in the CNS. The levels of expression of each cell type were larger in our drug-loaded microsphere group in comparison with the soluble drug-treated group suggesting that the controlled release of puro and RA is an effective way for differentiation *in situ* of the bioprinted stem cell derived tissues. The presence of neurons, astrocytes and oligodendrocytes is crucial for the proper functioning and support of neural tissues and it brings us one step closer to creating physiological relevant tissues for drug screening purposes.

Functionality of the neural tissues is another relevant metric for the validation of neural tissues. In this study we analyzed the membrane potentials of our bioprinted hiPSC-derived neural tissues and the mature SMNs in order to compare their functionality. All of the bioprinted tissues showed to be responsive after stimulation with Ach and GABA. This brings us to the conclusion that the bioprinted-hiPSC derived tissues were indeed neural types and that the bioink used effectively supported the differentiation and maturation of neural tissues.

5.4. Overall conclusion and future work

The combination of the engineered strategies explored in this work contributes to the field of neural TE as it brings us one step closer to the development of physiologically relevant tissues with defined micro-architectures, structure, and differentiation cues. We have addressed several limitations which previously existed in the field such as i) the controlled release of morphogens for effective differentiation of hiPSCs, ii) development of a printable and biocompatible bioink that will support the growth of neural tissues, iii) the use of an effective technology to ensure viability of the bioprinted tissues, iv) effective maturation and functionality of the neural tissues. Moreover, the combination of drug-loaded microspheres with bioprinting hiPSC-derived tissues opens up a field of research in TE in which patient specific tissues can be effectively engineered in order to contribute to the development of new therapies for diseases and disorders in the CNS.

Future work will involve the use of drug releasing microspheres to produce concentration gradients or be strategically placed within the fibers of the construct in order to promote differentiation into different cells present in the CNS. Conjointly, using more than one cells type to bioprint neural tissues such as OPCs that promote myelination, astrocytes and endothelial cells which are the cells present in the BSCB will be a good strategy for mimicking the complexity of

the CNS. Encapsulation of the small molecules CHIR, SB, and LDN in microspheres could be useful for the effective and differentiation of the NPCs in a more standardized. Different polymers with faster degradation properties can be explored for the encapsulation of such small molecules as they are only required during the first week of differentiation. In addition, the incorporation of the soluble drug or drug-loaded microspheres of the molecule Aprotinin can provide slower degradation of the fibrin-based scaffolds which might be required when using more than one cell type as more cells present in the bioprinted constructs could speed up the degradation of the scaffolds.

The exposure of the engineered tissues to the molecules present after a SCI in addition to reactive astrocytes will be an essential step towards the creation of the hostile environment present in SCI. Treatments currently used for SCI such as Oxycyte and Minocycline can be used for drug screening and correlate the outcome with the literature published using animal studies. Furthermore, a model created with OPCs can be used to explore the degree of myelination obtained given the cell therapy and compare with the ongoing clinical trial from Asterias Biotherapeutics as a way to better explain the effects of OPCs in a humanized SC model.

Bibliography

1. Saltzman WM. Tissue Engineering : Engineering Principles for the Design of Replacement Organs and Tissues. In: Central PE, ed. 2004 ed.: Oxford University Press, 2004; 2004.
2. Gomes ME RM, Domingues RMA, Reis RL. Tissue Engineering and Regenerative Medicine: New Trends and Directions-A Year in Review. *Tissue Eng Part B Rev.* 2017 Jun;23(3):211-224.
3. Olson JL, Atala A, Yoo JJ. Tissue engineering: current strategies and future directions. *Chonnam Med J.* 2011;47(1):1-13.
4. Willerth S. *Engineering Neural Tissue from Stem Cells.* Academic Press; 2017.
5. Kozloski J, Wagner J. An Ultrascalable Solution to Large-scale Neural Tissue Simulation. *Front Neuroinform.* 2011;5.
6. Lu Y, Belin S, He Z. Signaling regulations of neuronal regenerative ability. *Current opinion in neurobiology.* 2014;27:135-142.
7. Schmidt CE, Leach JB. Neural tissue engineering: strategies for repair and regeneration. *Annu Rev Biomed Eng.* 2003;5:293-347.
8. Stephanie Knowlton SA, Twisha Shah, Savas Tasoglu. Bioprinting for Neural Tissue Engineering. *Trends in Neurosciences.* 2018 Jan;Volume 41(Issue 1):Pages 31-46.
9. Muoio V, Persson PB, Sendeski MM. The neurovascular unit - concept review. *Acta Physiol (Oxf).* 2014;210(4):790-798.
10. Potjewyd G, Moxon S, Wang T, Domingos M, Hooper NM. Tissue Engineering 3D Neurovascular Units: A Biomaterials and Bioprinting Perspective. *Trends Biotechnol.* 2018;36(4):457-472.
11. Willerth SM, Sakiyama-Elbert SE. Combining stem cells and biomaterial scaffolds for constructing tissues and cell delivery. 2008.
12. Inoue H, Nagata N, Kurokawa H, Yamanaka S. iPS cells: a game changer for future medicine. *EMBO J.* 2014.
13. Wang A, Tang Z, Park IH, et al. Induced pluripotent stem cells for neural tissue engineering. *Biomaterials.* 2011;32(22):5023-5032.
14. Thomas M, Willerth SM. 3-D Bioprinting of Neural Tissue for Applications in Cell Therapy and Drug Screening. *Frontiers in bioengineering and biotechnology.* 2017;5:69.
15. Clarke DL, Johansson CB, Wilbertz J, et al. Generalized potential of adult neural stem cells. *Science.* 2000;288(5471):1660-1663.
16. Khorshidi S, Solouk A, Mirzadeh H, et al. A review of key challenges of electrospun scaffolds for tissue-engineering applications. *Journal of Tissue Engineering and Regenerative Medicine.* 2016;10(9):715-738.
17. Kim I-Y, Seo S-J, Moon H-S, et al. Chitosan and its derivatives for tissue engineering applications. *Biotechnology advances.* 2008;26(1):1-21.
18. Hudspeth AJ, Jessell TM, Kandel ER, Schwartz JH, Siegelbaum SA. *Principles of neural science.* McGraw-Hill, Health Professions Division; 2013.

19. Przedborski S, Vila M, Jackson-Lewis V. Neurodegeneration: what is it and where are we? *J Clin Invest.* 2003;111(1):3-10.
20. Wilems TS, Pardieck J, Iyer N, Sakiyama-Elbert SE. Combination therapy of stem cell derived neural progenitors and drug delivery of anti-inhibitory molecules for spinal cord injury. *Acta Biomaterialia.* 2015;28:23-32.
21. Karin S. Straley CWPF, and Sarah C. Heilshorn. Biomaterial Design Strategies for the Treatment of Spinal Cord Injuries. *Journal of Neurotrama.* 2010.
22. Magdalini Tsintou KD, Alexander Marcus Seifalian. Advances in regenerative therapies for spinal cord injury: a biomaterials approach. *Neural Regeneration Research.* 2015;10(5):726–742.
23. Mohtaram NK, Ko J, King C, et al. Electrospun biomaterial scaffolds with varied topographies for neuronal differentiation of human-induced pluripotent stem cells. *Journal of biomedical materials research Part A.* 2015;103(8):2591-2601.
24. Silva NA, Sousa N, Reis RL, Salgado AJ. From basics to clinical: A comprehensive review on spinal cord injury. *Progress in Neurobiology.* 2014;114:25-57.
25. Khaing ZZ, Thomas RC, Geissler SA, Schmidt CE. Advanced biomaterials for repairing the nervous system: what can hydrogels do for the brain? *Materials Today.* 2014;17(7):332-340.
26. Nagoshi N, Okano H. Applications of induced pluripotent stem cell technologies in spinal cord injury. *J Neurochem.* 2017;141(6):848-860.
27. Prabhakaran MPV, Jayarama Reddy; Ramakrishna, Seeram. Mesenchymal stem cell differentiation to neuronal cells on electrospun nanofibrous substrates for nerve tissue engineering. *Biomaterials.* 2009;30(28):4996-5003.
28. Hiroshi Nomura TZ, Howard Kim, Yusuke Katayama, Iris Kulbatski, Cindi M. Morshead, Molly S. Shoichet, and Charles H. Tator. Extramedullary Chitosan Channels Promote Survival of Transplanted Neural Stem and Progenitor Cells and Create a Tissue Bridge After Complete Spinal Cord Transection. *Tissue engineering part A.* 2008;14(8):649-665.
29. Adams B AN, Atkinson R. A Trillion-Dollar Opportunity: How Brain Research Can Drive Health and Prosperity. 2016. https://itif.org/publications/2016/07/11/brain-disorders-and-diseases-cost-us-economy-15-trillion-underscoring-scale. Accessed March 14th 2017.
30. NSCISC. *Spinal Cord Injury Facts and Figures at a Glance* 2018.
31. Wilems TS, Sakiyama-Elbert SE. Sustained dual drug delivery of anti-inhibitory molecules for treatment of spinal cord injury. *Journal of Controlled Release.* 2015;213:103-111.
32. Sertkaya A, Wong H-H, Jessup A, Beleche T. Key cost drivers of pharmaceutical clinical trials in the United States. *Clinical Trials.* 2016;13(2):117-126.
33. Craven R. The risky business of drug development in neurology. *The Lancet Neurology.* 2011;10(2):116-117.
34. Shanks N, Greek R, Greek J. Are animal models predictive for humans? *Philosophy, ethics, and humanities in medicine.* 2009;4(1):2.
35. Vickers AEM, Fisher RL. Organ slices for the evaluation of human drug toxicity. *Chemico-Biological Interactions.* 2004;150(1):87-96.

36. Kapałczyńska M, Kolenda T, Przybyła W, et al. 2D and 3D cell cultures - a comparison of different types of cancer cell cultures. *Arch Med Sci.* 2018;14(4):910-919.
37. Laura de la Vega KK, Stephanie Willerth. Engineering Neural Tissue from Human Pluripotent Stem Cells Using Novel Small Molecule Releasing Microspheres. *Advanced Biosystems* 2018.
38. NIH. What are the treatments for spinal cord injury (SCI)? 2016; https://www.nichd.nih.gov/health/topics/spinalinjury/conditioninfo/treatments.
39. Kim Y-H, Ha K-Y, Kim S-I. Spinal Cord Injury and Related Clinical Trials. *Clinics in Orthopedic Surgery.* 2017;9(1):1-9.
40. Assinck P, Duncan GJ, Hilton BJ, Plemel JR, Tetzlaff W. Cell transplantation therapy for spinal cord injury. *Nature Neuroscience.* 2017;20:637.
41. Tate KM, Munson JM. Assessing drug response in engineered brain microenvironments. *Brain research bulletin.* 2019.
42. Asterias Biotherapeutics Announces Dosing of First Patient in New SCiSTAR Clinical Trial Cohort Testing AST-OPC1 in an Expanded Cervical Spinal Cord Injury Patient Population [press release]. Asteriasbiotherapuetics.com, September 27 2016 2016.
43. Biotherapeutics A. Asterias Provides Top Line 12 Month Data Update for its OPC1 Phase 1/2a Clinical Trial in Severe Spinal Cord Injury. 2019. https://www.globenewswire.com/news-release/2019/01/24/1704757/0/en/Asterias-Provides-Top-Line-12-Month-Data-Update-for-its-OPC1-Phase-1-2a-Clinical-Trial-in-Severe-Spinal-Cord-Injury.html.
44. BioTime. OPC1. 2019; https://www.biotimeinc.com/products-pipeline/opc1/. Accessed July 26th 2019, 2019.
45. Driscoll D, Farnia S, Kefalas P, Maziarz RT. Concise Review: The High Cost of High Tech Medicine: Planning Ahead for Market Access. *STEM CELLS Translational Medicine.* 2017;6(8):1723-1729.
46. Hay AE, Cheung MC. CAR T-cells: costs, comparisons, and commentary. *Journal of Medical Economics.* 2019;22(7):613-615.
47. NICE. *Axicabtagene ciloleucel for treating diffuse large B-cell lymphoma and primary mediastinal B-cell lymphoma after 2 or more systemic therapies.* August 2018 2018.
48. Takahashi K, Tanabe K, Ohnuki M, et al. Induction of Pluripotent Stem Cells from Adult Human Fibroblasts by Defined Factors. *Cell.* 2007;131(5):861-872.
49. Shi Y. Induced pluripotent stem cells, new tools for drug discovery and new hope for stem cell therapies. *Current molecular pharmacology.* 2009;2(1):15-18.
50. Willerth SM. Bioprinting neural tissues using stem cells as a tool for screening drug targets for Alzheimer's disease. In: Future Medicine; 2018.
51. Hu B-Y, Weick JP, Yu J, et al. Neural differentiation of human induced pluripotent stem cells follows developmental principles but with variable potency. *Proceedings of the National Academy of Sciences.* 2010;107(9):4335.
52. Chandrasekaran A, Avci HX, Ochalek A, et al. Comparison of 2D and 3D neural induction methods for the generation of neural progenitor cells from human induced pluripotent stem cells. *Stem Cell Research.* 2017;25:139-151.

53. Sathananthan AH. Neural Stem Cells in Neurospheres, Embryoid Bodies, and Central Nervous System of Human Embryos. *Microscopy and Microanalysis.* 2011;17(4):520-527.
54. Carpenedo RL, Bratt-Leal AM, Marklein RA, et al. Homogeneous and organized differentiation within embryoid bodies induced by microsphere-mediated delivery of small molecules. *Biomaterials.* 2009;30(13):2507-2515.
55. Bratt-Leal AM, Carpenedo RL, McDevitt TC. Engineering the embryoid body microenvironment to direct embryonic stem cell differentiation. *Biotechnology Progress.* 2009;25(1):43-51.
56. Aflaki E, Borger DK, Moaven N, et al. A new glucocerebrosidase chaperone reduces α-synuclein and glycolipid levels in iPSC-derived dopaminergic neurons from patients with Gaucher disease and parkinsonism. *Journal of Neuroscience.* 2016;36(28):7441-7452.
57. Sun Y, Florer J, Mayhew CN, et al. Properties of neurons derived from induced pluripotent stem cells of Gaucher disease type 2 patient fibroblasts: potential role in neuropathology. *PLoS One.* 2015;10(3):e0118771.
58. Agbay A, De La Vega L, Nixon G, Willerth S. Guggulsterone-releasing microspheres direct the differentiation of human induced pluripotent stem cells into neural phenotypes. *Biomedical Materials.* 2018;13(3):034104.
59. Yan Y, Sart S, Li Y. Differentiation of neural progenitor cells from pluripotent stem cells in artificial niches. *Int J Stem Cell Res Transplant.* 2013;1(04):22-27.
60. Xia G, Santostefano K, Hamazaki T, et al. Generation of human induced pluripotent stem cells to model spinocerebellar ataxia type 2 in vitro. *Journal of molecular neuroscience : MN.* 2013;51(2):237-248.
61. Topol A, Tran NN, Brennand KJ. A Guide to Generating and Using hiPSC Derived NPCs for the Study of Neurological Diseases. *Journal of Visualized Experiments : JoVE.* 2015(96):52495.
62. Wilson PG, Stice SS. Development and differentiation of neural rosettes derived from human embryonic stem cells. *Stem cell reviews.* 2006;2(1):67-77.
63. NCBI. *SMAD1 SMAD family member 1 [Homo sapiens (human)].* NCBI July 8th 2019 2018.
64. Sinha S, Chen JK. Purmorphamine activates the Hedgehog pathway by targeting Smoothened. *Nature chemical biology.* 2006;2(1):29.
65. Hu B-Y, Zhang S-C. Differentiation of spinal motor neurons from pluripotent human stem cells. *Nature protocols.* 2009;4(9):1295-1304.
66. Du Z-W, Chen H, Liu H, et al. Generation and expansion of highly pure motor neuron progenitors from human pluripotent stem cells. *Nature communications.* 2015;6:6626.
67. El-Akabawy G, Medina LM, Jeffries A, Price J, Modo M. Purmorphamine increases DARPP-32 differentiation in human striatal neural stem cells through the Hedgehog pathway. *Stem cells and development.* 2011;20(11):1873-1887.
68. Lu B, Atala A. Chapter 6 - Small Molecules: Controlling Cell Fate and Function. In: Lee SJ, Yoo JJ, Atala A, eds. *In Situ Tissue Regeneration.* Boston: Academic Press; 2016:87-110.

69. Sun H, Kawaguchi R. The membrane receptor for plasma retinol-binding protein, a new type of cell-surface receptor. In: *International review of cell and molecular biology.* Vol 288. Elsevier; 2011:1-41.
70. Duester G. Retinoic Acid Synthesis and Signaling during Early Organogenesis. *Cell.* 2008;134(6):921-931.
71. De la Vega L, Lee C, Sharma R, Amereh M, Willerth SM. 3D bioprinting models of neural tissues: The current state of the field and future directions. *Brain Research Bulletin.* 2019;150:240-249.
72. Budday S, Nay R, de Rooij R, et al. Mechanical properties of gray and white matter brain tissue by indentation. *Journal of the mechanical behavior of biomedical materials.* 2015;46:318-330.
73. Leipzig ND, Shoichet MS. The effect of substrate stiffness on adult neural stem cell behavior. *Biomaterials.* 2009;30(36):6867-6878.
74. Elisseeff J. Hydrogels: Structure starts to gel. *Nat Mater.* 2008;7(4):271-273.
75. Banerjee A, Arha M, Choudhary S, et al. The Influence of Hydrogel Modulus on the Proliferation and Differentiation of Encapsulated Neural Stem Cells. *Biomaterials.* 2009;30(27):4695-4699.
76. Bellis SL. Advantages of RGD peptides for directing cell association with biomaterials. *Biomaterials.* 2011;32(18):4205-4210.
77. Patel R, Santhosh M, Dash JK, et al. Ile-Lys-Val-ala-Val (IKVAV) peptide for neuronal tissue engineering. *Polymers for Advanced Technologies.* 2019;30(1):4-12.
78. Cui GS, S.; Yang, J. Designer Self-Assemble Peptides Maximize the Therapeutic Benefits of Neural Stem Cell Transplantation for Alzheimer's Disease via Enhancing Neuron Differentiation and Paracrine Action. *Molecular Neurobiology.* 2016;53(2):1108-1123.
79. Abelseth E, Abelseth L, De la Vega L, Beyer ST, Wadsworth SJ, Willerth SM. 3D printing of neural tissues derived from human induced pluripotent stem cells using a fibrin-based bioink. *ACS Biomaterials Science & Engineering.* 2018;5(1):234-243.
80. Willerth SM, Arendas KJ, Gottlieb DI, Sakiyama-Elbert SE. Optimization of fibrin scaffolds for differentiation of murine embryonic stem cells into neural lineage cells. *Biomaterials.* 2006;27(36):5990-6003.
81. Weisel JW, Litvinov RI. Mechanisms of fibrin polymerization and clinical implications. *Blood.* 2013;121(10):1712-1719.
82. Kolehmainen K, Willerth SM. Preparation of 3D Fibrin Scaffolds for Stem Cell Culture Applications. *Journal of Visualized Experiments : JoVE.* 2012(61):3641.
83. Catelas I, Sese N, Wu BM, Dunn JCY, Helgerson SAM, Tawil B. Human mesenchymal stem cell proliferation and osteogenic differentiation in fibrin gels in vitro. *Tissue engineering.* 2006;12(8):2385-2396.
84. Willerth SM, Faxel TE, Gottlieb DI, Sakiyama-Elbert SE. The Effects of Soluble Growth Factors on Embryonic Stem Cell Differentiation Inside of Fibrin Scaffolds. *Stem cells (Dayton, Ohio).* 2007;25(9):2235-2244.
85. Cui X, Boland T. Human microvasculature fabrication using thermal inkjet printing technology. *Biomaterials.* 2009;30(31):6221-6227.

86. Lee Y-B, Polio S, Lee W, et al. Bio-printing of collagen and VEGF-releasing fibrin gel scaffolds for neural stem cell culture. *Exp Neurol.* 2010;223(2):645-652.
87. Robinson M, Douglas S, Michelle Willerth S. Mechanically stable fibrin scaffolds promote viability and induce neurite outgrowth in neural aggregates derived from human induced pluripotent stem cells. *Sci Rep-Uk.* 2017;7(1):6250.
88. Butler MF, Ng YF, Pudney PDA. Mechanism and kinetics of the crosslinking reaction between biopolymers containing primary amine groups and genipin. *Journal of Polymer Science Part A: Polymer Chemistry.* 2003;41(24):3941-3953.
89. Lee KY, Mooney DJ. Alginate: properties and biomedical applications. *Progress in polymer science.* 2012;37(1):106-126.
90. Purcell EK, Singh A, Kipke DR. Alginate Composition Effects on a Neural Stem Cell–Seeded Scaffold. *Tissue Engineering Part C, Methods.* 2009;15(4):541-550.
91. Duan B, Hockaday LA, Kang KH, Butcher JT. 3D Bioprinting of heterogeneous aortic valve conduits with alginate/gelatin hydrogels. *Journal of Biomedical Materials Research Part A.* 2013;101A(5):1255-1264.
92. Markstedt K, Mantas A, Tournier I, Martínez Ávila H, Hägg D, Gatenholm P. 3D Bioprinting Human Chondrocytes with Nanocellulose–Alginate Bioink for Cartilage Tissue Engineering Applications. *Biomacromolecules.* 2015;16(5):1489-1496.
93. Drury JL, Dennis RG, Mooney DJ. The tensile properties of alginate hydrogels. *Biomaterials.* 2004;25(16):3187-3199.
94. Kim B-S, Nikolovski J, Bonadio J, Mooney DJ. Cyclic mechanical strain regulates the development of engineered smooth muscle tissue. *Nature biotechnology.* 1999;17(10):979.
95. Paige KT, Cima LG, Yaremchuk MJ, Vacanti JP, Vacanti CA. Injectable cartilage. *Plastic and reconstructive surgery.* 1995;96(6):1390-1398.
96. Chang SCN, Rowley JA, Tobias G, et al. Injection molding of chondrocyte/alginate constructs in the shape of facial implants. *Journal of Biomedical Materials Research: An Official Journal of The Society for Biomaterials, The Japanese Society for Biomaterials, and The Australian Society for Biomaterials and the Korean Society for Biomaterials.* 2001;55(4):503-511.
97. Alsberg E, Anderson KW, Albeiruti A, Franceschi RT, Mooney DJ. Cell-interactive alginate hydrogels for bone tissue engineering. *Journal of dental research.* 2001;80(11):2025-2029.
98. Suzuki Y, Tanihara M, Suzuki K, Saitou A, Sufan W, Nishimura Y. Alginate hydrogel linked with synthetic oligopeptide derived from BMP-2 allows ectopic osteoinduction in vivo. *Journal of Biomedical Materials Research: An Official Journal of The Society for Biomaterials, The Japanese Society for Biomaterials, and The Australian Society for Biomaterials and the Korean Society for Biomaterials.* 2000;50(3):405-409.
99. Rowley JA, Mooney DJ. Alginate type and RGD density control myoblast phenotype. *Journal of Biomedical Materials Research: An Official Journal of The Society for Biomaterials, The Japanese Society for Biomaterials, and The Australian Society for Biomaterials and the Korean Society for Biomaterials.* 2002;60(2):217-223.

100. Frampton JP, Hynd MR, Shuler ML, Shain W. Fabrication and optimization of alginate hydrogel constructs for use in 3D neural cell culture. *Biomedical Materials.* 2011;6(1):015002.
101. Li L, Davidovich AE, Schloss JM, et al. Neural lineage differentiation of embryonic stem cells within alginate microbeads. *Biomaterials.* 2011;32(20):4489-4497.
102. Laura de la Vega DARG, Emily Abelseth, Laila Abelseth,, Victor Allisson da Silva aSMW. 3D Bioprinting Human Induced Pluripotent Stem Cell-Derived Neural Tissues Using a Novel Lab-on-a-Printer Technology. *Applied Sciences.* 2018;8(2414).
103. Abelseth E, Abelseth L, De la Vega L, Beyer ST, Wadsworth SJ, Willerth SM. 3D printing of neural tissues derived from human induced pluripotent stem cells using a fibrin-based bioink. *ACS Biomaterials Science & Engineering.* 2018.
104. De S, Robinson D. Polymer relationships during preparation of chitosan–alginate and poly-l-lysine–alginate nanospheres. *Journal of Controlled Release.* 2003;89(1):101-112.
105. Gu Q, Tomaskovic-Crook E, Wallace GG, Crook JM. 3D bioprinting human induced pluripotent stem cell constructs for in situ cell proliferation and successive multilineage differentiation. *Advanced healthcare materials.* 2017;6(17):1700175.
106. Dai X, Ma C, Lan Q, Xu T. 3D bioprinted glioma stem cells for brain tumor model and applications of drug susceptibility. *Biofabrication.* 2016;8(4):045005.
107. Di Martino A, Sittinger M, Risbud MV. Chitosan: a versatile biopolymer for orthopaedic tissue-engineering. *Biomaterials.* 2005;26(30):5983-5990.
108. Monaghan RL, Eveleigh DE, Tewari RP, Reese ET. Chitosanase, a Novel Enzyme. *Nature New Biology.* 1973;245:78.
109. Madihally SV, Matthew HWT. Porous chitosan scaffolds for tissue engineering. *Biomaterials.* 1999;20(12):1133-1142.
110. Huei CR, Hwa H-D. Effect of molecular weight of chitosan with the same degree of deacetylation on the thermal, mechanical, and permeability properties of the prepared membrane. *Carbohydrate polymers.* 1996;29(4):353-358.
111. Szekely G, Didaskalou C. 7 - Biomimics of Metalloenzymes via Imprinting. In: Li S, Cao S, Piletsky SA, Turner APF, eds. *Molecularly Imprinted Catalysts.* Amsterdam: Elsevier; 2016:121-158.
112. Alberts B, Bray D, Hopkin K, et al. *Essential cell biology.* Garland Science; 2013.
113. Hirano S, Tsuchida H, Nagao N. N-acetylation in chitosan and the rate of its enzymic hydrolysis. *Biomaterials.* 1989;10(8):574-576.
114. Skaugrud Ø, Hagen A, Borgersen B, Dornish M. Biomedical and pharmaceutical applications of alginate and chitosan. *Biotechnology and genetic engineering reviews.* 1999;16(1):23-40.
115. Polk A, Amsden B, De Yao K, Peng T, Goosen MFA. Controlled release of albumin from chitosan—alginate microcapsules. *Journal of Pharmaceutical Sciences.* 1994;83(2):178-185.
116. Chenite A, Chaput C, Wang D, et al. Novel injectable neutral solutions of chitosan form biodegradable gels in situ. *Biomaterials.* 2000;21(2155):2161.
117. Prashanth KVH, Tharanathan RN. Crosslinked chitosan—preparation and characterization. *Carbohydrate research.* 2006;341(1):169-173.

118. Sharon Wilbur CH, Eugene Demchuk, Susan Zells Ingber, ATSDR. *Toxicological Profile for Glutaraldehyde* U.S. Department of Health and Human Services: Agency for Toxic Substances and Disease Registry;2017.
119. Muzzarelli RAA. Genipin-crosslinked chitosan hydrogels as biomedical and pharmaceutical aids. *Carbohydrate Polymers.* 2009;77(1):1-9.
120. Ma J, Wang H, He B, Chen J. A preliminary in vitro study on the fabrication and tissue engineering applications of a novel chitosan bilayer material as a scaffold of human neofetal dermal fibroblasts. *Biomaterials.* 2001;22(4):331-336.
121. Lu JX, Prudhommeaux F, Meunier A, Sedel L, Guillemin G. Effects of chitosan on rat knee cartilages. *Biomaterials.* 1999;20(20):1937-1944.
122. Mori T, Irie Y, Nishimura SI, et al. Endothelial cell responses to chitin and its derivatives. *Journal of biomedical materials research.* 1998;43(4):469-472.
123. Wang X, Yan Y, Lin F, et al. Preparation and characterization of a collagen/chitosan/heparin matrix for an implantable bioartificial liver. *Journal of Biomaterials Science, Polymer Edition.* 2005;16(9):1063-1080.
124. Haipeng G, Yinghui Z, Jianchun L, Yandao G, Nanming Z, Xiufang Z. Studies on nerve cell affinity of chitosan-derived materials. *Journal of biomedical materials research.* 2000;52(2):285-295.
125. Yang Z DH, Mo L, Qiao H, Li X. The effect of the dosage of NT3/chitosan carriers on the proliferation and differentiation of neural stem cells. *Biomaterials.* 2010;31(18):4846-4854.
126. Skop NB, Calderon F, Levison SW, Gandhi CD, Cho CH. Heparin crosslinked chitosan microspheres for the delivery of neural stem cells and growth factors for central nervous system repair. *Acta Biomaterialia.* 2013;9(6):6834-6843.
127. Gu Q, Tomaskovic-Crook E, Lozano R, et al. Functional 3D neural mini-tissues from printed gel-based bioink and human neural stem cells. *Advanced healthcare materials.* 2016;5(12):1429-1438.
128. Kim KK, Pack DW. Microspheres for Drug Delivery. In: Ferrari M, Lee AP, Lee LJ, eds. *BioMEMS and Biomedical Nanotechnology: Volume I Biological and Biomedical Nanotechnology.* Boston, MA: Springer US; 2006:19-50.
129. Gomez JC, Edgar JM, Agbay AM, et al. Incorporation of Retinoic Acid Releasing Microspheres into Pluripotent Stem Cell Aggregates for Inducing Neuronal Differentiation. *Cellular and Molecular Bioengineering.* 2015;8(3):307-319.
130. Agbay A, Mohtaram NK, Willerth SM. Controlled release of glial cell line-derived neurotrophic factor from poly (ε-caprolactone) microspheres. *Drug delivery and translational research.* 2014;4(2):159-170.
131. Khademhosseini A, Langer R. A decade of progress in tissue engineering. *Nature Protocols.* 2016;11:1775.
132. Hirenkumar K. Makadia and Steven J. Siegel. Poly Lactic-co-Glycolic Acid (PLGA) as Biodegradable Controlled Drug Delivery Carrier. 2011.
133. Kumari A, Yadav SK, Yadav SC. Biodegradable polymeric nanoparticles based drug delivery systems. *Colloids and Surfaces B: Biointerfaces.* 2010;75(1):1-18.
134. Dasgupta S, Auth T, Gompper G. Nano-and microparticles at fluid and biological interfaces. *Journal of Physics: Condensed Matter.* 2017;29(37):373003.
135. Tiwari G, Tiwari R, Sriwastawa B, et al. Drug delivery systems: An updated review. *International Journal of Pharmaceutical Investigation.* 2012;2(1):2-11.

136. Tasnim N, De la Vega L, Anil Kumar S, et al. 3D Bioprinting Stem Cell Derived Tissues. *Cellular and Molecular Bioengineering.* 2018;11(4):219-240.
137. Guillotin B, Guillemot F. Cell patterning technologies for organotypic tissue fabrication. *Trends in Biotechnology.* 2011;29(4):183-190.
138. Laura de la Vega CL, Ruchi Sharma, Meitham Amereh, Stephanie, Willerth M. 3D bioprinting models of neural tissues: the current state of the field and future directions: a Review article. 2018. Located at: Brain Research Bulletin.
139. Mandrycky C, Wang Z, Kim K, Kim D-H. 3D bioprinting for engineering complex tissues. *Biotechnology advances.* 2016;34(4):422-434.
140. Tasoglu S, Demirci U. Bioprinting for stem cell research. *Trends in Biotechnology.* 2013;31(1):10-19.
141. Nair K, Gandhi M, Khalil S, et al. Characterization of cell viability during bioprinting processes. *Biotechnology Journal: Healthcare Nutrition Technology.* 2009;4(8):1168-1177.
142. Faulkner-Jones A, Fyfe C, Cornelissen D-J, et al. Bioprinting of human pluripotent stem cells and their directed differentiation into hepatocyte-like cells for the generation of mini-livers in 3D. *Biofabrication.* 2015;7(4):044102.
143. Chang R, Nam J, Sun W. Effects of dispensing pressure and nozzle diameter on cell survival from solid freeform fabrication–based direct cell writing. *Tissue Engineering Part A.* 2008;14(1):41-48.
144. Bsoul A, Pan S, Cretu E, Stoeber B, Walus K. Design, microfabrication, and characterization of a moulded PDMS/SU-8 inkjet dispenser for a Lab-on-a-Printer platform technology with disposable microfluidic chip. *Lab on a Chip.* 2016;16(17):3351-3361.
145. AspectBiosystems. Lab-on-a-Printer™ Bioprinting Technology. 2015; http://aspectbiosystems.com/, 2017.
146. Frade JM, Ovejero-Benito MC. Neuronal cell cycle: the neuron itself and its circumstances. *Cell Cycle.* 2015;14(5):712-720.
147. Murphy SV, Atala A. 3D bioprinting of tissues and organs. *Nat Biotech.* 2014;32(8):773-785.
148. Hsieh F-Y, Lin H-H, Hsu S-h. 3D bioprinting of neural stem cell-laden thermoresponsive biodegradable polyurethane hydrogel and potential in central nervous system repair. *Biomaterials.* 2015;71:48-57.
149. Lee W, Pinckney J, Lee V, et al. Three-dimensional bioprinting of rat embryonic neural cells. *Neuroreport.* 2009;20(8):798-803.
150. Tuby H, Maltz L, Oron U. Low-level laser irradiation (LLLI) promotes proliferation of mesenchymal and cardiac stem cells in culture. *Lasers in Surgery and Medicine: The Official Journal of the American Society for Laser Medicine and Surgery.* 2007;39(4):373-378.
151. Lee S-J, Nowicki M, Harris B, Zhang LG. Fabrication of a highly aligned neural scaffold via a table top stereolithography 3D printing and electrospinning. *Tissue Engineering Part A.* 2017;23(11-12):491-502.
152. Bracken MB, Shepard MJ, Hellenbrand KG, et al. Methylprednisolone and neurological function 1 year after spinal cord injury: results of the National Acute Spinal Cord Injury Study. *Journal of neurosurgery.* 1985;63(5):704-713.

153. Hurlbert RJ, Hadley MN, Walters BC, et al. Pharmacological therapy for acute spinal cord injury. *Neurosurgery.* 2015;76(suppl_1):S71-S83.
154. Bose B, Osterholm JL, Kalia M. Ganglioside-induced regeneration and reestablishment of axonal continuity in spinal cord-transected rats. *Neuroscience letters.* 1986;63(2):165-169.
155. Ha K-Y, Carragee E, Cheng I, Kwon S-E, Kim Y-H. Pregabalin as a neuroprotector after spinal cord injury in rats: biochemical analysis and effect on glial cells. *Journal of Korean medical science.* 2011;26(3):404-411.
156. Qu Q, Li D, Louis KR, et al. High-efficiency motor neuron differentiation from human pluripotent stem cells and the function of Islet-1. *Nature communications.* 2014;5:3449.
157. Schwartz MP, Hou Z, Propson NE, et al. Human pluripotent stem cell-derived neural constructs for predicting neural toxicity. *Proceedings of the National Academy of Sciences.* 2015;112(40):12516-12521.
158. Khazaei M, Ahuja CS, Fehlings MG. Induced Pluripotent Stem Cells for Traumatic Spinal Cord Injury. *Front Cell Dev Biol.* 2016;4:152.
159. Bahmad H, Hadadeh O, Chamaa F, et al. Modeling Human Neurological and Neurodegenerative Diseases: From Induced Pluripotent Stem Cells to Neuronal Differentiation and Its Applications in Neurotrauma. *Front Mol Neurosci.* 2017;10:50.
160. Lancaster MA, Renner M, Martin CA, et al. Cerebral organoids model human brain development and microcephaly. *Nature.* 2013;501(7467):373-379.
161. Conley BJ, Young JC, Trounson AO, Mollard R. Derivation, propagation and differentiation of human embryonic stem cells. *Int J Biochem Cell Biol.* 2004;36(4):555-567.
162. Kurosawa H. Methods for inducing embryoid body formation: in vitro differentiation system of embryonic stem cells. *Journal of Bioscience and Bioengineering.* 2007;103(5):389-398.
163. Bratt-Leal AM, Carpenedo RL, McDevitt TC. Engineering the embryoid body microenvironment to direct embryonic stem cell differentiation. *Biotechnol Prog.* 2009;25(1):43-51.
164. Van Winkle AP, Gates ID, Kallos MS. Mass Transfer Limitations in Embryoid Bodies during Human Embryonic Stem Cell Differentiation. *Cells Tissues Organs.* 2012;196(1):34-47.
165. Carpenedo Richard L, Sargent Carolyn Y, McDevitt Todd C. Rotary Suspension Culture Enhances the Efficiency, Yield, and Homogeneity of Embryoid Body Differentiation. *Stem Cells.* 2009;25(9):2224-2234.
166. Karp JM, Yeh J, Eng G, et al. Controlling size, shape and homogeneity of embryoid bodies using poly(ethylene glycol) microwells. *Lab on a Chip.* 2007;7(6):786-794.
167. Ogawa D, Okada Y, Nakamura M, et al. Evaluation of human fetal neural stem/progenitor cells as a source for cell replacement therapy for neurological disorders: Properties and tumorigenicity after long-term in vitro maintenance. *J Neurosci Res.* 2009;87(2):307-317.
168. Makadia HK, Siegel SJ. Poly lactic-co-glycolic acid (PLGA) as biodegradable controlled drug delivery carrier. *Polymers.* 2011;3(3):1377-1397.

169. Bratt-Leal AM, Nguyen AH, Hammersmith KA, Singh A, McDevitt TC. A microparticle approach to morphogen delivery within pluripotent stem cell aggregates. *Biomaterials.* 2013;34(30):7227-7235.
170. Qutachi O, Shakesheff KM, Buttery LD. Delivery of definable number of drug or growth factor loaded poly(DL-lactic acid-co-glycolic acid) microparticles within human embryonic stem cell derived aggregates. *J Control Release.* 2013;168(1):18-27.
171. Gomez J, Edgar, J., Agbay, A., Bibault E., Montgomery, A., Mohtaram, N., Willerth, S. Incorporation of retinoic acid releasing microspheres into pluripotent stem cell aggregates for inducing neuronal differentiation. *Cellular and Molecular Bioengineering.* 2015;8(3):307-319.
172. Dulin JN, Lu P. Bridging the injured spinal cord with neural stem cells. *Neural Regeneration Research.* 2014;9(3):229-231.
173. Silva NA, Sousa N, Reis RL, Salgado AJ. From basics to clinical: a comprehensive review on spinal cord injury. *Prog Neurobiol.* 2014;114:25-57.
174. Stys PK. Anoxic and ischemic injury of myelinated axons in CNS white matter: from mechanistic concepts to therapeutics. *Journal of Cerebral Blood Flow & Metabolism.* 1998;18(1):2-25.
175. Yuan YM, He C. The glial scar in spinal cord injury and repair. *Neurosci Bull.* 2013;29(4):421-435.
176. Yan Y, Bejoy J, Xia J, Guan J, Zhou Y, Li Y. Neural patterning of human induced pluripotent stem cells in 3-D cultures for studying biomolecule-directed differential cellular responses. *Acta Biomater.* 2016;42:114-126.
177. Sinha VR, Bansal K, Kaushik R, Kumria R, Trehan A. Poly-epsilon-caprolactone microspheres and nanospheres: an overview. *Int J Pharm.* 2004;278(1):1-23.
178. C. Changyong SYC, N. Jae-Won. Thermosensitive poly(N-isopropylacrylamide)-b-poly(ε-caprolactone) nanoparticles for efficient drug delivery system. *Polymer.* 2006;47:4571.
179. Shenoy DB, Amiji MM. Poly (ethylene oxide)-modified poly (ε-caprolactone) nanoparticles for targeted delivery of tamoxifen in breast cancer. *International journal of pharmaceutics.* 2005;293(1-2):261-270.
180. Hu BY, Zhang SC. Differentiation of spinal motor neurons from pluripotent human stem cells. *Nat Protoc.* 2009;4(9):1295-1304.
181. Liggins RT, D'Amours S, Demetrick JS, Machan LS, Burt HM. Paclitaxel loaded poly(l-lactic acid) microspheres for the prevention of intraperitoneal carcinomatosis after a surgical repair and tumor cell spill. *Biomaterials.* 2000;21(19):1959-1969.
182. Woo BH, Kostanski JW, Gebrekidan S, Dani BA, Thanoo BC, DeLuca PP. Preparation, characterization and in vivo evaluation of 120-day poly(d,l-lactide) leuprolide microspheres. *Journal of Controlled Release.* 2001;75(3):307-315.
183. Edgar JM, Robinson M, Willerth SM. Fibrin hydrogels induce mixed dorsal/ventral spinal neuron identities during differentiation of human induced pluripotent stem cells. *Acta Biomaterialia.* 2017;51:237-245.
184. Pevny LH, Nicolis SK. Sox2 roles in neural stem cells. *The international journal of biochemistry & cell biology.* 2010;42(3):421-424.

185. Tang X, Zhou L, Wagner AM, et al. Astroglial cells regulate the developmental timeline of human neurons differentiated from induced pluripotent stem cells. *Stem cell research.* 2013;11(2):743-757.
186. Jha BS, Rao M, Malik N. Motor neuron differentiation from pluripotent stem cells and other intermediate proliferative precursors that can be discriminated by lineage specific reporters. *Stem Cell Rev.* 2015;11(1):194-204.
187. Shin S XH, Mattson MP, Rao MS. Stage-dependent Olig2 expression in motor neurons and oligodendrocytes differentiated from embryonic stem cells. *Stem Cells Dev.* 2007;16(1):131-141.
188. Thiel G. Synapsin I, synapsin II, and synaptophysin: marker proteins of synaptic vesicles. *Brain Pathology.* 1993;3(1):87-95.
189. Ebert AD, Yu J, Rose Jr FF, et al. Induced pluripotent stem cells from a spinal muscular atrophy patient. *Nature.* 2009;457(7227):277.
190. Ronaghi M, Erceg S, Moreno-Manzano V, Stojkovic M. Challenges of Stem Cell Therapy for Spinal Cord Injury: Human Embryonic Stem Cells, Endogenous Neural Stem Cells, or Induced Pluripotent Stem Cells? *Stem Cells.* 2009;28(1):93-99.
191. Rowland JW, Hawryluk GWJ, Kwon B, Fehlings MG. Current status of acute spinal cord injury pathophysiology and emerging therapies: promise on the horizon. *Neurosurgical Focus.* 2008;25(5):E2.
192. Zhao T, Zhang Z-n, Westenskow PD, et al. Humanized Mice Reveal Differential Immunogenicity of Cells Derived from Autologous Induced Pluripotent Stem Cells. *Cell stem cell.* 2015;17(3):353-359.
193. Robinson M, Yau S-y, Sun L, et al. Optimizing Differentiation Protocols for Producing Dopaminergic Neurons from Human Induced Pluripotent Stem Cells for Tissue Engineering Applications: Supplementary Issue: Stem Cell Biology. *Biomarker insights.* 2015;10:BMI-S20064.
194. Robinson J, Lu P. Optimization of trophic support for neural stem cell grafts in sites of spinal cord injury. *Exp Neurol.* 2017;291:87-97.
195. Maitin IB, Cruz E. *Current Diagnosis & Treatment: Physical Medicine & Rehabilitation.* McGraw-Hill Education; 2015.
196. WHO. Spinal Cord Injury. 2013; http://www.who.int/news-room/fact-sheets/detail/spinal-cord-injury, 2018.
197. Fehlings MG, Vaccaro AR, Ditunno J, Vaccaro AR, Rossignol S, Burns A. *Essentials of Spinal Cord Injury : Basic Research to Clinical Practice.* New York, UNITED STATES: Thieme Medical Publishers, Incorporated; 2012.
198. Pal R, Singh M, Kumar K, et al. Understanding the Presentations and Patterns of Traumatic Spinal Cord Injuries to Develop the Data Collection Format. *Indian Journal Of Neurotrauma [serial online].* 2017;14:135-141.
199. Lin C-W, Huang Y-P, Pan S-L. Spinal Cord Injury Is Related to an Increased Risk of Multiple Sclerosis: A Population-Based, Propensity Score-Matched, Longitudinal Follow-Up Study. *Journal of Neurotrauma.* 2015;32(9):655-659.
200. Cox A, Varma A, Banik N. Recent Advances in the Pharmacologic Treatment of Spinal Cord Injury. *Metabolic brain disease.* 2015;30(2):473-482.
201. Temenoff JS, Mikos AG. *Biomaterials: the intersection of biology and materials science.* Vol 1. Upper Saddle River, N.J: Pearson/Prentice Hall; 2008.

202. Thomas M, Willerth SM. 3-D Bioprinting of Neural Tissue for Applications in Cell Therapy and Drug Screening. *Frontiers in Bioengineering and Biotechnology.* 2017;5(69).
203. Wang M, Zhai P, Chen X, Schreyer DJ, Sun X, Cui F. Bioengineered Scaffolds for Spinal Cord Repair. *Tissue Engineering Part B: Reviews.* 2011;17(3):177-194.
204. Gao G, Cui X. Three-dimensional bioprinting in tissue engineering and regenerative medicine. *Biotechnology letters.* 2016;38(2):203-211.
205. Mothe AJ, Tator CH. Advances in stem cell therapy for spinal cord injury. *J Clin Invest.* 2012;122(11):3824-3834.
206. Nandoe Tewarie RS, Hurtado A, Bartels RH, Grotenhuis A, Oudega M. Stem Cell-Based Therapies for Spinal Cord Injury. *The Journal of Spinal Cord Medicine.* 2009;32(2):105-114.
207. Hu B-Y, Weick JP, Yu J, et al. Neural differentiation of human induced pluripotent stem cells follows developmental principles but with variable potency. *Proceedings of the National Academy of Sciences of the United States of America.* 2010;107(9):4335-4340.
208. Hospodiuk M, Dey M, Sosnoski D, Ozbolat IT. The bioink: A comprehensive review on bioprintable materials. *Biotechnology Advances.* 2017;35(2):217-239.
209. Robinson M, Douglas S, Michelle Willerth S. Mechanically stable fibrin scaffolds promote viability and induce neurite outgrowth in neural aggregates derived from human induced pluripotent stem cells. *Sci Rep-Uk.* 2017;7:6250.
210. Tasnim N, De la Vega L, Kumar SA, et al. 3D Bioprinting Stem Cell Derived Tissues. *Cellular and Molecular Bioengineering.* 2018;11(4):219-240.
211. Bsoul A, Cretu E, Walus K. Lab-on-a-printer platform technology. 19th International Conference on Miniaturized Systems for Chemistry and Life Sciences; 2015; Gyeongju, KOREA.
212. Biosystems A. Lab-On-A-Printer. https://www.aspectbiosystems.com/technology. Accessed September 20th, 2018.
213. Takazawa T, Croft GF, Amoroso MW, Studer L, Wichterle H, MacDermott AB. Maturation of Spinal Motor Neurons Derived from Human Embryonic Stem Cells. *PLoS ONE.* 2012;7(7):e40154.
214. Neely MD, Litt MJ, Tidball AM, et al. DMH1, a Highly Selective Small Molecule BMP Inhibitor Promotes Neurogenesis of hiPSCs: Comparison of PAX6 and SOX1 Expression during Neural Induction. *ACS chemical neuroscience.* 2012;3(6):482-491.
215. Hu B-Y, Zhang S-C. Differentiation of spinal motor neurons from pluripotent human stem cells. *Nature Protocols.* 2009;4:1295.
216. De la Vega L, Karmirian K, Willerth SM. Engineering Neural Tissue from Human Pluripotent Stem Cells Using Novel Small Molecule Releasing Microspheres. *Advanced Biosystems.* 2018;0(0):1800133.
217. Thomas AM, Kubilius MB, Holland SJ, et al. Channel density and porosity of degradable bridging scaffolds on axon growth after spinal injury. *Biomaterials.* 2013;34(9):2213-2220.
218. Ghasemi-Mobarakeh L, Prabhakaran MP, Morshed M, Nasr-Esfahani M-H, Ramakrishna S. Electrospun poly (ε-caprolactone)/gelatin nanofibrous scaffolds for nerve tissue engineering. *Biomaterials.* 2008;29(34):4532-4539.

219. Joung D, Truong V, Neitzke CC, et al. 3D Printed Stem-Cell Derived Neural Progenitors Generate Spinal Cord Scaffolds. *Advanced Functional Materials.* 2018;28(39):1801850.
220. Derakhshanfar S, Mbeleck R, Xu K, Zhang X, Zhong W, Xing M. 3D bioprinting for biomedical devices and tissue engineering: A review of recent trends and advances. *Bioactive Materials.* 2018;3(2):144-156.
221. Skardal A, Mack D, Kapetanovic E, et al. Bioprinted Amniotic Fluid-Derived Stem Cells Accelerate Healing of Large Skin Wounds. *STEM CELLS Translational Medicine.* 2012;1(11):792-802.
222. Jia W, Gungor-Ozkerim PS, Zhang YS, et al. Direct 3D bioprinting of perfusable vascular constructs using a blend bioink. *Biomaterials.* 2016;106:58-68.
223. Zhou X, Cui H, Nowicki M, et al. Three-Dimensional-Bioprinted Dopamine-Based Matrix for Promoting Neural Regeneration. *ACS applied materials & interfaces.* 2018;10(10):8993-9001.
224. Romanazzo S, Nemec S, Roohani I. iPSC Bioprinting: Where are We at? *Materials.* 2019;12(15):2453.
225. Jung JW, Lee H, Hong JM, et al. A new method of fabricating a blend scaffold using an indirect three-dimensional printing technique. *Biofabrication.* 2015;7(4):045003.
226. Weickenmeier J, Kurt M, Ozkaya E, et al. Brain stiffens post mortem. *Journal of the mechanical behavior of biomedical materials.* 2018;84:88-98.
227. Christ AF, Franze K, Gautier H, et al. Mechanical difference between white and gray matter in the rat cerebellum measured by scanning force microscopy. *Journal of biomechanics.* 2010;43(15):2986-2992.
228. Zhuang P, An J, Tan LP, Chua CK. The current status of 3D bioprinting for neural tissue models. 2018.
229. Lee C, Abelseth E, de la Vega L, Willerth SM. Bioprinting a novel glioblastoma tumor model using a fibrin-based bioink for drug screening. *Materials Today Chemistry.* 2019;12:78-84.
230. Kim H, Cooke MJ, Shoichet MS. Creating permissive microenvironments for stem cell transplantation into the central nervous system. *Trends in Biotechnology.* 2012;30(1):55-63.
231. Xiong Y, Zhu J-X, Fang Z-Y, et al. Coseeded Schwann cells myelinate neurites from differentiated neural stem cells in neurotrophin-3-loaded PLGA carriers. *International journal of nanomedicine.* 2012;7:1977.
232. Nampoothiri KM, Nair NR, John RP. An overview of the recent developments in polylactide (PLA) research. *Bioresource technology.* 2010;101(22):8493-8501.
233. Gu Q, Tomaskovic-Crook E, Lozano R, et al. Functional 3D Neural Mini-Tissues from Printed Gel-Based Bioink and Human Neural Stem Cells. *Advanced Healthcare Materials.* 2016;5(12):1429-1438.
234. Li Y, Jiang X, Li L, et al. 3D printing human induced pluripotent stem cells with novel hydroxypropyl chitin bioink: scalable expansion and uniform aggregation. *Biofabrication.* 2018;10(4):044101.
235. Dillon GP, Yu X, Sridharan A, Ranieri JP, Bellamkonda RV. The influence of physical structure and charge on neurite extension in a 3D hydrogel scaffold. *Journal of Biomaterials Science, Polymer Edition.* 1998;9(10):1049-1069.

236. Liu Y, Zheng Y, Li S, et al. Human neural progenitors derived from integration-free iPSCs for SCI therapy. *Stem cell research.* 2017;19:55-64.
237. 2 - Modification of drug release. In: Bruschi ML, ed. *Strategies to Modify the Drug Release from Pharmaceutical Systems.* Woodhead Publishing; 2015:15-28.
238. De la Vega L, Rosas Gomez D, Abelseth E, Abelseth L, Alisson da Silva V, Willerth SM. 3D bioprinting human induced pluripotent stem cell-derived neural tissues using a novel Lab-on-a-Printer technology. . *Applied Science* 2018 In press.
239. Chambers SM, Qi Y, Mica Y, et al. Combined small-molecule inhibition accelerates developmental timing and converts human pluripotent stem cells into nociceptors. *Nature Biotechnology.* 2012;30:715.
240. Chambers SM, Fasano CA, Papapetrou EP, Tomishima M, Sadelain M, Studer L. Highly efficient neural conversion of human ES and iPS cells by dual inhibition of SMAD signaling. *Nature Biotechnology.* 2009;27:275.
241. BrainXell. Cryopreserved Human Motor Neurons (BX-0100). https://static1.squarespace.com/static/5936c50fbe6594d92e8321a2/t/5afc50498a922d0d384f020f/1526485119468/CP+MN+v4.2. Accessed July 11th, 2019, 2019.
242. MACS MB. Neural Tissue Dissociation Kits. 2019; Order no: 130-092-628. Available at: https://www.miltenyibiotec.com/CA-en/products/macs-sample-preparation/tissue-dissociation-kits/neural-tissue-dissociation-kits.html#130-092-628, 2019.
243. Robinson M, Valente KP, Willerth SM. A Novel Toolkit for Characterizing the Mechanical and Electrical Properties of Engineered Neural Tissues. *Biosensors.* 2019;9(2):51.
244. Fairless R, Beck A, Kravchenko M, et al. Membrane potential measurements of isolated neurons using a voltage-sensitive dye. *PloS one.* 2013;8(3):e58260.
245. Sawkins MJ, Mistry P, Brown BN, Shakesheff KM, Bonassar LJ, Yang J. Cell and protein compatible 3D bioprinting of mechanically strong constructs for bone repair. *Biofabrication.* 2015;7(3):035004.
246. Poldervaart MT, Wang H, van der Stok J, et al. Sustained release of BMP-2 in bioprinted alginate for osteogenicity in mice and rats. *PloS one.* 2013;8(8):e72610.
247. Luo Y, Luo G, Gelinsky M, Huang P, Ruan C. 3D bioprinting scaffold using alginate/polyvinyl alcohol bioinks. *Materials Letters.* 2017;189:295-298.
248. Madl CM, LeSavage BL, Dewi RE, et al. Maintenance of neural progenitor cell stemness in 3D hydrogels requires matrix remodelling. *Nature materials.* 2017;16(12):1233.
249. Hendrickson ML, Rao AJ, Demerdash ONA, Kalil RE. Expression of nestin by neural cells in the adult rat and human brain. *PloS one.* 2011;6(4):e18535.
250. Melcangic M, Bowery NG. GABA and its receptors in the spinal cord. *Trends in pharmacological sciences.* 1996;17(12):457-462.
251. Ben-Ari Y, Gaiarsa J-L, Tyzio R, Khazipov R. GABA: a pioneer transmitter that excites immature neurons and generates primitive oscillations. *Physiological reviews.* 2007;87(4):1215-1284.
252. Bracken MB, Shepard MJ, Collins WF, et al. A Randomized, Controlled Trial of Methylprednisolone or Naloxone in the Treatment of Acute Spinal-Cord Injury. *New England Journal of Medicine.* 1990;322(20):1405-1411.

253. Bracken MB, Shepard MJ, Holford TR, et al. Administration of methylprednisolone for 24 or 48 hours or tirilazad mesylate for 48 hours in the treatment of acute spinal cord injury: results of the Third National Acute Spinal Cord Injury Randomized Controlled Trial. *Jama.* 1997;277(20):1597-1604.
254. Geisler FH, Dorsey FC, Coleman WP. Recovery of motor function after spinal-cord injury—a randomized, placebo-controlled trial with GM-1 ganglioside. *New England Journal of Medicine.* 1991;324(26):1829-1838.
255. Geisler FH, Dorsey FC, Coleman WP. GM-1 ganglioside and motor recovery following human spinal cord injury. *Journal of Emergency Medicine.* 1993;11:49-49.
256. Ha K-Y, Kim Y-H, Rhyu K-W, Kwon S-E. Pregabalin as a neuroprotector after spinal cord injury in rats. *European Spine Journal.* 2008;17(6):864-872.
257. Wrathall JR, Teng YD, Choiniere D. Amelioration of functional deficits from spinal cord trauma with systemically administered NBQX, an antagonist of non-N-methyl-D-aspartate receptors. *Exp Neurol.* 1996;137(1):119-126.
258. Wrathall JR, Teng YD, Marriott R. Delayed antagonism of AMPA/kainate receptors reduces long-term functional deficits resulting from spinal cord trauma. *Exp Neurol.* 1997;145(2):565-573.
259. Boran BO, Colak A, Kutlay M. Erythropoietin enhances neurological recovery after experimental spinal cord injury. *Restorative neurology and neuroscience.* 2005;23(5, 6):341-345.
260. King VR, Averill SA, Hewazy D, Priestley JV, Torup L, Michael-Titus AT. Erythropoietin and carbamylated erythropoietin are neuroprotective following spinal cord hemisection in the rat. *European Journal of Neuroscience.* 2007;26(1):90-100.
261. Fehlings MG, Tator CH, Linden RD. The effect of nimodipine and dextran on axonal function and blood flow following experimental spinal cord injury. *Journal of neurosurgery.* 1989;71(3):403-416.
262. Hugenholtz H, Cass DE, Dvorak MF, et al. High-dose methylprednisolone for acute closed spinal cord injury-only a treatment option. *Canadian journal of neurological sciences.* 2002;29(3):227-235.
263. Cardenas DD, Ditunno J, Graziani V, et al. Phase 2 trial of sustained-release fampridine in chronic spinal cord injury. *Spinal cord.* 2007;45(2):158.
264. Yune TY, Lee JY, Jung GY, et al. Minocycline alleviates death of oligodendrocytes by inhibiting pro-nerve growth factor production in microglia after spinal cord injury. *Journal of Neuroscience.* 2007;27(29):7751-7761.
265. Casha S, Zygun D, McGowan MD, Bains I, Yong VW, John Hurlbert R. Results of a phase II placebo-controlled randomized trial of minocycline in acute spinal cord injury. *Brain.* 2012;135(4):1224-1236.
266. Ok J-H, Kim Y-H, Ha K-Y. Neuroprotective effects of hypothermia after spinal cord injury in rats: comparative study between epidural hypothermia and systemic hypothermia. *Spine.* 2012;37(25):E1551-E1559.
267. Ha K-Y, Kim Y-H. Neuroprotective effect of moderate epidural hypothermia after spinal cord injury in rats. *Spine.* 2008;33(19):2059-2065.

268. Biernaskie J, Sparling JS, Liu J, et al. Skin-derived precursors generate myelinating Schwann cells that promote remyelination and functional recovery after contusion spinal cord injury. *Journal of Neuroscience.* 2007;27(36):9545-9559.
269. Sparling JS, Bretzner F, Biernaskie J, et al. Schwann cells generated from neonatal skin-derived precursors or neonatal peripheral nerve improve functional recovery after acute transplantation into the partially injured cervical spinal cord of the rat. *Journal of Neuroscience.* 2015;35(17):6714-6730.
270. Xu XM, Guénard V, Kleitman N, Bunge MB. Axonal regeneration into Schwann cell-seeded guidance channels grafted into transected adult rat spinal cord. *Journal of Comparative Neurology.* 1995;351(1):145-160.
271. Fouad K, Schnell L, Bunge MB, Schwab ME, Liebscher T, Pearse DD. Combining Schwann cell bridges and olfactory-ensheathing glia grafts with chondroitinase promotes locomotor recovery after complete transection of the spinal cord. *Journal of Neuroscience.* 2005;25(5):1169-1178.
272. Barbour HR, Plant CD, Harvey AR, Plant GW. Tissue sparing, behavioral recovery, supraspinal axonal sparing/regeneration following sub-acute glial transplantation in a model of spinal cord contusion. *BMC neuroscience.* 2013;14(1):106.
273. López-Vales R, García-Alías G, Forés J, Navarro X, Verdú E. Increased expression of cyclo-oxygenase 2 and vascular endothelial growth factor in lesioned spinal cord by transplanted olfactory ensheathing cells. *Journal of neurotrauma.* 2004;21(8):1031-1043.
274. Richter MW, Fletcher PA, Liu J, Tetzlaff W, Roskams AJ. Lamina propria and olfactory bulb ensheathing cells exhibit differential integration and migration and promote differential axon sprouting in the lesioned spinal cord. *Journal of Neuroscience.* 2005;25(46):10700-10711.
275. Ramer LM, Au E, Richter MW, Liu J, Tetzlaff W, Roskams AJ. Peripheral olfactory ensheathing cells reduce scar and cavity formation and promote regeneration after spinal cord injury. *Journal of Comparative Neurology.* 2004;473(1):1-15.
276. Gu W, Zhang F, Xue Q, Ma Z, Lu P, Yu B. Transplantation of bone marrow mesenchymal stem cells reduces lesion volume and induces axonal regrowth of injured spinal cord. *Neuropathology.* 2010;30(3):205-217.
277. Ritfeld GJ, Patel A, Chou A, et al. The role of brain-derived neurotrophic factor in bone marrow stromal cell-mediated spinal cord repair. *Cell transplantation.* 2015;24(11):2209-2220.
278. Abrams MB, Dominguez C, Pernold K, et al. Multipotent mesenchymal stromal cells attenuate chronic inflammation and injury-induced sensitivity to mechanical stimuli in experimental spinal cord injury. *Restorative neurology and neuroscience.* 2009;27(4):307-321.
279. Hawryluk GWJ, Mothe A, Wang J, Wang S, Tator C, Fehlings MG. An in vivo characterization of trophic factor production following neural precursor cell or bone marrow stromal cell transplantation for spinal cord injury. *Stem cells and development.* 2011;21(12):2222-2238.
280. Lu P, Blesch A, Graham L, et al. Motor axonal regeneration after partial and complete spinal cord transection. *Journal of Neuroscience.* 2012;32(24):8208-8218.

281. Nakajima H, Uchida K, Guerrero AR, et al. Transplantation of mesenchymal stem cells promotes an alternative pathway of macrophage activation and functional recovery after spinal cord injury. *Journal of neurotrauma.* 2012;29(8):1614-1625.
282. DePaul MA, Palmer M, Lang BT, et al. Intravenous multipotent adult progenitor cell treatment decreases inflammation leading to functional recovery following spinal cord injury. *Sci Rep-Uk.* 2015;5:16795.
283. Cao Q, Xu X-M, DeVries WH, et al. Functional recovery in traumatic spinal cord injury after transplantation of multineurotrophin-expressing glial-restricted precursor cells. *Journal of Neuroscience.* 2005;25(30):6947-6957.
284. Cao Q, He Q, Wang Y, et al. Transplantation of ciliary neurotrophic factor-expressing adult oligodendrocyte precursor cells promotes remyelination and functional recovery after spinalcord injury. *Journal of Neuroscience.* 2010;30(8):2989-3001.
285. Hofstetter CP, Holmström NAV, Lilja JA, et al. Allodynia limits the usefulness of intraspinal neural stem cell grafts; directed differentiation improves outcome. *Nature neuroscience.* 2005;8(3):346.
286. Hawryluk GWJ, Spano S, Chew D, et al. An examination of the mechanisms by which neural precursors augment recovery following spinal cord injury: a key role for remyelination. *Cell transplantation.* 2014;23(3):365-380.
287. Yasuda A, Tsuji O, Shibata S, et al. Significance of remyelination by neural stem/progenitor cells transplanted into the injured spinal cord. *Stem Cells.* 2011;29(12):1983-1994.
288. Keirstead HS, Nistor G, Bernal G, et al. Human embryonic stem cell-derived oligodendrocyte progenitor cell transplants remyelinate and restore locomotion after spinal cord injury. *Journal of Neuroscience.* 2005;25(19):4694-4705.
289. Lu P, Wang Y, Graham L, et al. Long-distance growth and connectivity of neural stem cells after severe spinal cord injury. *Cell.* 2012;150(6):1264-1273.
290. Nori S, Okada Y, Nishimura S, et al. Long-term safety issues of iPSC-based cell therapy in a spinal cord injury model: oncogenic transformation with epithelial-mesenchymal transition. *Stem Cell Reports.* 2015;4(3):360-373.
291. Kobayashi Y, Okada Y, Itakura G, et al. Pre-evaluated safe human iPSC-derived neural stem cells promote functional recovery after spinal cord injury in common marmoset without tumorigenicity. *PloS one.* 2012;7(12):e52787.
292. Lu P, Woodruff G, Wang Y, et al. Long-distance axonal growth from human induced pluripotent stem cells after spinal cord injury. *Neuron.* 2014;83(4):789-796.
293. Kadoya K, Lu P, Nguyen K, et al. Spinal cord reconstitution with homologous neural grafts enables robust corticospinal regeneration. *Nature medicine.* 2016;22(5):479.
294. All AH, Gharibani P, Gupta S, et al. Early intervention for spinal cord injury with human induced pluripotent stem cells oligodendrocyte progenitors. *PLoS One.* 2015;10(1):e0116933.

Chapter 6 Appendices

6.1. Appendix A

Appendix A contains Table 6.1 and Table 6.2 from chapter one.

Approach	Type of therapy	Result	Conclusion	Reference
Methylprednisolone	Chemical	Reduction of cytokine expression	Results inconsistent and absence of significant improvement	152,153,252,253
GM-1 ganglioside	Chemical	Induction of neurotrophic factors, anti-excitotoxic effects and promotion of neurite growth. Recovery of motor, bowel/bladder function.	No follow up studies to confirm or refute such results.	154,254,255
Excitatory neurotransmitter antagonist	Chemical	Anti-apoptotic and anti-inflammatory effects and decreased proliferation of astrocytes were reported	Studies 12 months after treatment failed to show a long-term benefit in this trial	155,256-258
Erythropoietin (EPO)	Chemical	neurogenesis and neuronal differentiation were noted in an animal study.	Clinical trial for this drug has not been performed yet. Concerns about stimulation of EPO activity and possible thrombosis.	259,260
Calcium channel blockade	Chemical	Prevention of ionic over-influx that causes neuronal and glial cell death.	1-year follow up showed no significant differences compared to control	261,262

Potassium channel blockade	Chemical	Improvement in impression scores and spasticity in chronic SCI patients with use of a low dose.	Adverse side effects with higher doses.	263
Minocycline	Chemical	Anti-inflammatory, anti-apoptotic effects, decrease in the activation of microglia	Significant ASIA score improvement in patients after 1 year.	256,264,265
Hypothermia	Physical	15/35 patients with cervical SCI improved at least one neurological grade (ISNCSCI) at 10-month follow-up	Not enough evidence available in favor or against the practice of therapeutic hypothermia	153,266,267

Table 6.1. Neuroprotective approaches for SCI.
Adapted from 40.

Type of cell	Function	Host	Mechanism	Reference
Schwann cells	Myelination of peripheral nervous system	Rat or mouse	Neuroprotection, axonal regeneration and sprouting, myelination	268-271
OECs	Glial cells that support axonal growth in the olfactory bulb	Rat or mouse	Neuroprotection, axon regeneration and sprouting	272-275
MSCs and multipotent adult progenitor cells (MAPCs)	Located in bone marrow	Rat	Neuroprotection, immunomodulation, axonal regeneration and sprouting	276-280
Pelvic bone marrow	MAPCs	Human	Neuroprotection and immunomodulation	281,282
Neural stem progenitor cells (NPSCs)	From SC or brain, transplanted as grafts	Rat, mouse, human	Neuroprotection, immunomodulation, axonal regeneration and sprouting, myelinogenesis, relay information	283-287
ESCs	Cells derived from	Human	Neuroprotection, immunomodulation, axonal regeneration	288,289

	immortalized cell lines		and sprouting, myelinogenesis, relay information	
Induced pluripotent stem cells	Fibroblasts differentiated into NPCs	Human	Neuroprotection, axon regeneration and sprouting, relay information	290-293
Peripheral blood monocytes, fetal lung fibroblasts or bone marrow stem cells	Differentiated into OPCs	Mouse	Neuroprotection, myelinogenesis	294

Table 6.2 Cell transplantation approaches and proposed mechanism of action. Adapted from 40.

6.2. Appendix B

Appendix B contains Figure 6.1 and Figure 6.2 which are supplemental information available from the original publication [1].

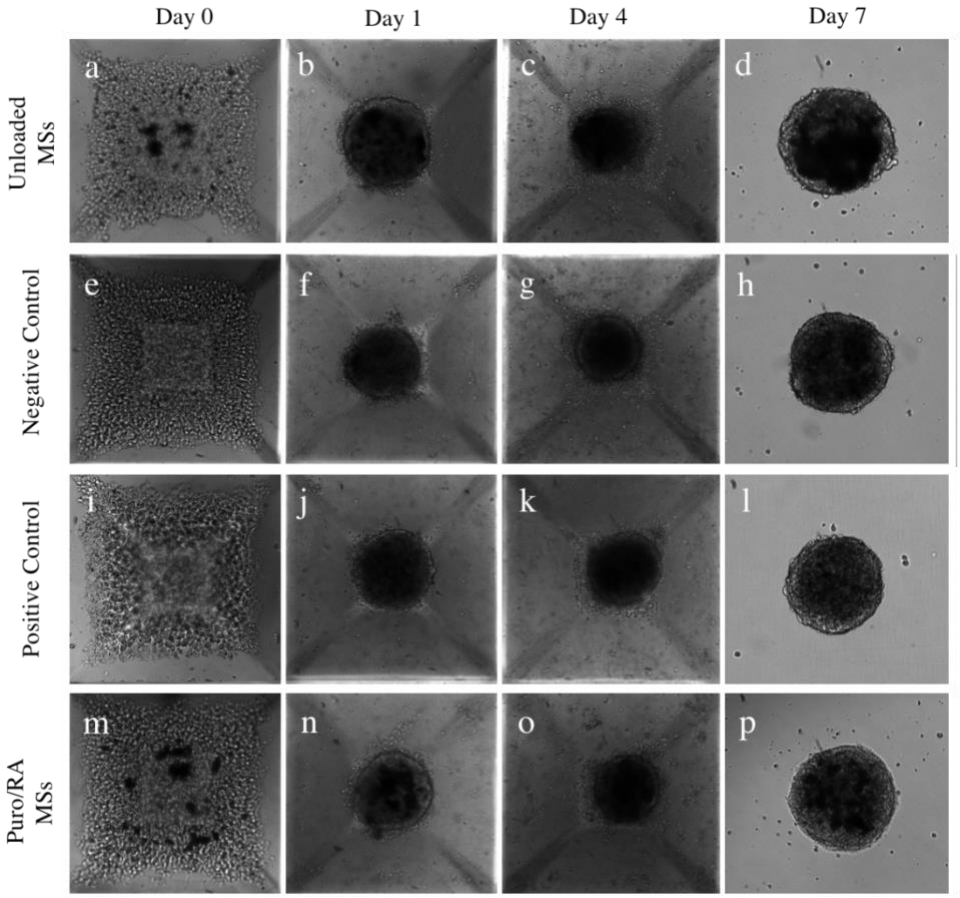

Figure 6.6.1 Phase contrast imaging (10x magnification) of embryoid bodies formation during 7 days in Aggrewell plates.

Phase contrast imaging (10x magnification) of embryoid bodies formation during 7 days in Aggrewell plates. a-d) Cell aggregates combined with unloaded microspheres, e-h) negative control (N - untreated), i-l) positive control (P - soluble puro/RA), and m-p) engineered neural tissues containing puro/RA loaded-microspheres (M). Images of day 7

[1] From: De la Vega L, Karmirian K, Willerth SM. **Engineering Neural Tissue from Human Pluripotent Stem Cells Using Novel Small Molecule Releasing Microspheres.** Advanced Biosystems 2018.

(d, h, l, p) were captured just after transferring to PLO-laminin plate. Scale bar represents (300 μm).

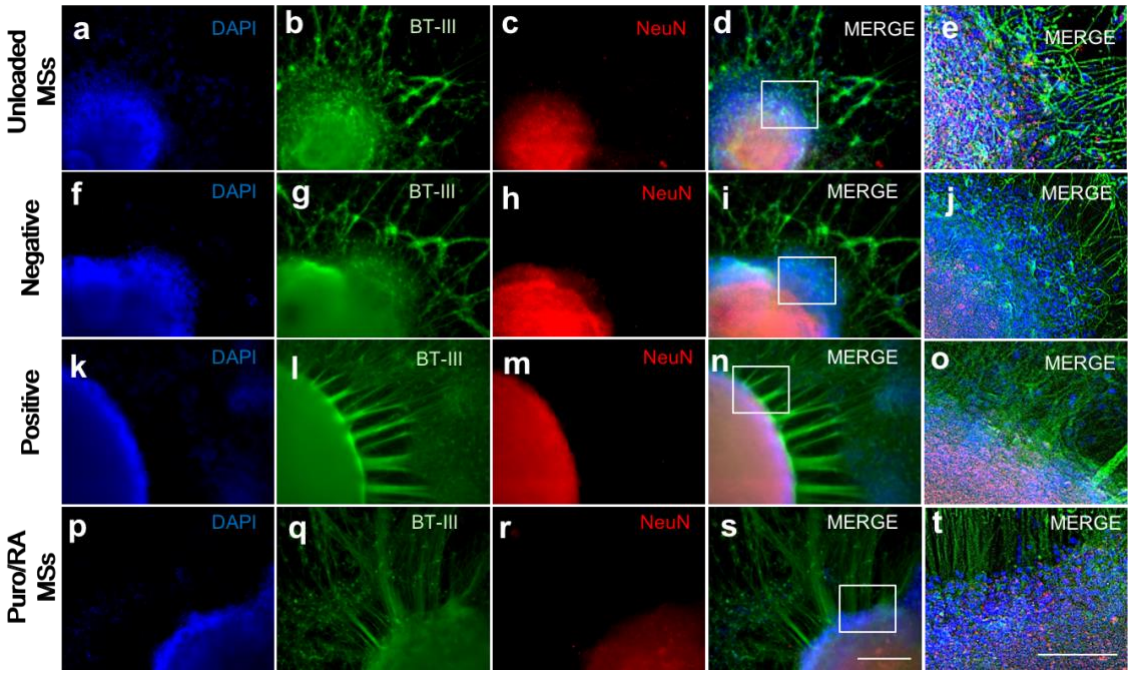

Figure 6.6.2 Analysis of neural cell cultures and engineered neural tissues after 28 days of differentiation in vitro.

All groups (n=3) were stained for βT-III (green), NeuN (neuronal nuclei marker, red), and DAPI (blue). a-e) Cell aggregates combined with unloaded microspheres (U), f-j) negative control (untreated - N), k-o) positive control (soluble puro/RA - P), and p-t) engineered neural tissues containing puro/RA loaded-microspheres (M). Scale bar for a-d, f-i, k-n, and p-s represents 300 μm. Scale bar for e, j, o, and t represents 50μm.